UNIVERSIDAD DE COSTA RICA
SISTEMA DE ESTUDIOS DE POSGRADO

DEVELOPMENT AND VALIDATION OF FLUORESCENCE LIVE-CELL IMAGING APPROACHES TO STUDY FLAVIVIRUS INFECTION KINETICS IN ANIMAL CELLS

Tesis sometida a la consideración de la Comisión del Programa de Doctorado en Ciencias para optar al grado y título de Doctorado Académico en Ciencias

JORGE LUIS ARIAS ARIAS

Ciudad Universitaria Rodrigo Facio, Costa Rica
2021

Dedicatoria

A mi madre, por su ejemplo, empatía y amor incondicional

A mis hermanas por el apoyo constante

Al destino por traerlas a mi vida

Agradecimientos

Mi más sincero agradecimiento al Centro de Investigación en Enfermedades Tropicales y a la Facultad de Microbiología de la Universidad de Costa Rica por abrirme las puertas para realizar labores de investigación con infinita libertad y confianza. A todo el personal docente y administrativo de dichas instancias que con su valiosa labor posibilitan el trabajo de investigación, en especial a Teresita Solano Díaz, Erick López Sánchez, Norman Rojas Campos, Erick Guerrero Torres y Susan Chavarría Montenegro.

A mi tutor Rodrigo Mora Rodríguez por su invaluable consejo científico, apoyo con herramientas biocomputacionales y en la consecución de fondos que posibilitaron este trabajo. Su perspectiva desde la investigación en cáncer me permitió amalgamar la biología celular con la virología de una manera más armoniosa y moderna.

A la profesora Jeanne A. Hardy del Departamento de Química de la Universidad de Massachusetts, Amherst por recibirme en su laboratorio y permitirme trabajar con entera libertad conceptual y financiera durante la fructífera colaboración establecida.

A Francisco Vega Aguilar por su amistad y valiosísimo consejo metodológico que hicieron posible esta investigación.

A Eugenia Corrales Aguilar, Carlos Chacón Díaz, Steve Quirós Barrantes, Cesar Rodríguez Sánchez y Esteban Chaves Olarte por la camaradería, consejo científico, apoyo emocional y aliento durante este proceso.

A Gilbert David Loría Masís por la perspectiva científica brindada durante la primera etapa de este proceso.

A Jose María Gutiérrez Gutiérrez por la revisión crítica y constructiva del primer artículo publicado durante esta investigación.

A Laya Hun Opfer, Sandra Silva de la Fuente y Marielos Mora López por la confianza depositada en mi persona y por creer en mi trabajo en los buenos y malos momentos.

A los todos aquellos estudiantes y compañeros que me brindaron su apoyo en distintas etapas de este proceso, en especial a Marvin Durán Delgado, Ana Laura Rodríguez Hidalgo, Víctor González Calderón, Vanessa López Li, Sofía Herrera Agüero, Beatriz Aragón Chamberlain, Katherine Benavides Mayorga, Juan Diego Romero Carpio, Catalina Porras Silesky, Norman Brenes Cordero, David Vargas Díaz, Jose Arturo Molina Mora, Iveth Jiménez Badilla, Ramezi Araya Rivera, Isaac Quirós Fernández, Silvia Elena Molina Castro, Dayana Jiménez Araya, Claudio Soto Garita, Shirley Camacho Vargas, María Carolina Castro Peña, Javier Mora Rodríguez, Alonso Saavedra Coles y Ginger Monge Jiménez.

A Mayra Lizeth Taylor Castillo (ł) que en espíritu siempre estuvo presente acompañándome y motivándome durante las largas jornadas de trabajo.

"Esta tesis fue aceptada por la Comisión del Programa de Doctorado en Ciencias de la Universidad de Costa Rica, como requisito parcial para optar al grado y título de Doctorado Académico en Ciencias"

JAVIER FRANCISCO MORA RODRIGUEZ (FIRMA)

Firmado digitalmente por JAVIER FRANCISCO MORA RODRIGUEZ (FIRMA)
Fecha: 2021.10.26 14:11:05 -06'00'

Dr. Javier Mora Rodríguez
Representante del Decano
Sistema de Estudios de Posgrado

RODRIGO MORA RODRIGUEZ (FIRMA)

Firmado digitalmente por RODRIGO MORA RODRIGUEZ (FIRMA)
Fecha: 2021.10.23 11:32:14 +02'00'

Dr. Rodrigo Mora Rodríguez
Profesor Guía

STEVE QUIROS BARRANTES (FIRMA)
PERSONA FISICA, CPF-01-1060-0117.
Fecha declarada: 25/10/2021 05:13:13 PM
Esta representación visual no es fuente de confianza. Valide siempre la firma.

Dr. Steve Quirós Barrantes
Lector

EUGENIA CORRALES AGUILAR (FIRMA)

Firmado digitalmente por EUGENIA CORRALES AGUILAR (FIRMA)
Fecha: 2021.10.25 16:28:14 -06'00'

Dra. Eugenia Corrales Aguilar
Lectora

ESTEBAN RICARDO CHAVES OLARTE (FIRMA)

ESTEBAN RICARDO CHAVES OLARTE (FIRMA)
2021.11.01 15:44:17 -06'00'

Dr. Esteban Chaves Olarte
Representante de la Directora
Programa de Doctorado en Ciencias

JORGE LUIS ARIAS ARIAS (FIRMA)

Firmado digitalmente por JORGE LUIS ARIAS ARIAS (FIRMA)
Fecha: 2021.10.21 14:43:55 -06'00'

Jorge Luis Arias Arias
Sustentante

Tabla de contenidos

Resumen

El género *Flavivirus* de la familia Flaviviridae incluye muchos virus de importancia médica, como el virus del dengue (DENV), el virus Zika (ZIKV) y el virus de la fiebre amarilla (YFV). La búsqueda de blancos terapéuticos para combatir las afecciones causadas por flavivirus requiere un mejor entendimiento de la cinética de interacción virus-célula durante las infecciones con cepas virales silvestres. Sin embargo, esto se ve obstaculizado por las limitaciones de los sistemas celulares actuales para monitorear la infección por flavivirus mediante imagenología de células vivas. La presente tesis describe el desarrollo y validación de sensores fluorescentes activables para detectar la actividad de la serin proteasa flaviviral NS2B-NS3 en células vivas. El sistema consta de reporteros basados en la proteína verde fluorescente (GFP) que activan la fluorescencia al ser cortados por proteasas recombinantes de DENV-2/ZIKV *in vitro*. Tras la infección por DENV-2/ZIKV, una versión de este sensor que contiene el sitio de corte interno de la proteína NS3 de flavivirus (AAQRRGRIG) reportó la mayor activación de fluorescencia en células de mamífero transducidas de manera estable. La activación de la fluorescencia correlacionó con la actividad de la proteasa viral. Además, una versión de color rojo lejano de este sensor de flavivirus presentó la mejor relación señal/ruido en un ensayo de placas de Dulbecco fluorescentes, lo que llevó a la construcción de una plataforma multireportero que combina el sensor de flavivirus con sondas fluorescentes de intercalado en el ADN para la detección de condensación de cromatina y muerte celular inducida por el virus (marcaje del efecto citopático). Esto permitió realizar estudios de formación de placas virales con resolución a nivel de células individuales. Dicho abordaje para el marcaje del efecto citopático fue conceptualizado y validado durante el presente trabajo. Finalmente, la aplicación de la plataforma multireportero también posibilitó el estudio de la cinética de infección a nivel de subpoblaciones celulares, así como de la inducción del efecto citopático por DENV-2, ZIKV y YFV. Anticipamos que estudios futuros de la cinética de infección viral con nuestros sistemas reporteros permitirán investigaciones básicas de la interacción virus-célula huésped y facilitarán el tamizaje de fármacos antivirales para controlar las infecciones por flavivirus.

Abstract

The genus *Flavivirus* in the family Flaviviridae comprises many clinically important viruses, such as dengue virus (DENV), Zika virus (ZIKV), and yellow fever virus (YFV). The quest for therapeutic targets to combat flavivirus infections requires a better understanding of the kinetics of the virus-cell interplay during infections with wild-type viral strains. Nevertheless, this is hindered by limitations of the current cell-based systems for monitoring flavivirus infection by live-cell imaging. The present dissertation describes the development and validation of fluorescence-activatable sensors to detect the activity of flavivirus NS2B-NS3 serine proteases in living cells. The system consists of green fluorescent protein (GFP)-based reporters that become fluorescent upon cleavage by recombinant DENV-2/ZIKV proteases *in vitro*. A version of this sensor containing the flavivirus internal NS3 cleavage site linker (AAQRRGRIG) reported the highest fluorescence activation in stably transduced mammalian cells upon DENV-2/ZIKV infection. The onset of fluorescence correlated with viral protease activity. Moreover, a far-red version of this flavivirus sensor presented the best signal-to-noise ratio in a fluorescent Dulbecco's plaque assay, leading to the construction of a multireporter platform combining the flavivirus sensor with DNA fluorescent dyes for the detection of virus-induced chromatin condensation and cell death (cytophatic effect labeling). This enabled studies of viral plaque formation with a single-cell resolution. This cytopathic effect labeling approach was conceptualized and validated during the present work. Finally, the application of the multireporter platform also enabled the study of kinetics of infection and cytophatic effect induction by DENV-2, ZIKV, and YFV in cell-subpopulations. We anticipate that future studies of viral infection kinetics with our reporter systems will enable basic investigations of virus-host cell interactions and will also facilitate the screening of antiviral drugs to manage flavivirus infections.

List of figures

UNIVERSIDAD DE COSTA RICA

SEP Sistema de Estudios de Posgrado

Autorización para digitalización y comunicación pública de Trabajos Finales de Graduación del Sistema de Estudios de Posgrado en el Repositorio Institucional de la Universidad de Costa Rica.

Yo, Jorge Luis Arias Arias, con cédula de identidad, 2-0604-0936 en mi condición de autor del TFG titulado Development and Validation of Fluorescence Live-Cell Imaging Approaches to Study Flavivirus Infection Kinetics in Animal Cells

---

Autorizo a la Universidad de Costa Rica para digitalizar y hacer divulgación pública de forma gratuita de dicho TFG a través del Repositorio Institucional u otro medio electrónico, para ser puesto a disposición del público según lo que establezca el Sistema de Estudios de Posgrado. **SI** [X] **NO** *[ ]

***En caso de la negativa favor indicar el tiempo de restricción:_____año (s).**

Este Trabajo Final de Graduación será publicado en formato PDF, o en el formato que en el momento se establezca, de tal forma que el acceso al mismo sea libre, con el fin de permitir la consulta e impresión, pero no su modificación.

Manifiesto que mi Trabajo Final de Graduación fue debidamente subido al sistema digital Kerwá y su contenido corresponde al documento original que sirvió para la obtención de mi título, y que su información no infringe ni violenta ningún derecho a terceros. El TFG además cuenta con el visto bueno de mi Director (a) de Tesis o Tutor (a) y cumplió con lo establecido en la revisión del Formato por parte del Sistema de Estudios de Posgrado.

INFORMACIÓN DEL ESTUDIANTE:

Nombre Completo: Jorge Luis Arias Arias.

Número de Carné: A30449 Número de cédula: 2-0640-0936.

Correo Electrónico: jorgeluis.arias@ucr.ac.cr.

Fecha: 12/10/2021. Número de teléfono: 8515-0440.

Nombre del Director (a) de Tesis o Tutor (a): Rodrigo Mora Rodríguez.

JORGE LUIS ARIAS ARIAS (FIRMA)

Firmado digitalmente por JORGE LUIS ARIAS ARIAS (FIRMA)
Fecha: 2021.10.21 14:46:01 -06'00'

FIRMA ESTUDIANTE

Nota: El presente documento constituye una declaración jurada, cuyos alcances aseguran a la Universidad, que su contenido sea tomado como cierto. Su importancia radica en que permite abreviar procedimientos administrativos, y al mismo tiempo genera una responsabilidad legal para que quien declare contrario a la verdad de lo que manifiesta, puede como consecuencia, enfrentar un proceso penal por delito de perjurio, tipificado en el artículo 318 de nuestro Código Penal. Lo anterior implica que el estudiante se vea forzado a realizar su mayor esfuerzo para que no sólo incluya información veraz en la Licencia de Publicación, sino que también realice diligentemente la gestión de subir el documento correcto en la plataforma digital Kerwá.

Aims

General

To develop and validate fluorescence live-cell imaging approaches to study flavivirus infection kinetics in animal cells.

Specific

To evaluate and validate the usage of DNA fluorescent dyes to label and monitor the kinetics of flavivirus-induced cytopathic effect by live-cell imaging in single animal cells.

To develop and validate a kinetic flavivirus plaque assay to track the cytopathic effect by fluorescent labeling and live-cell imaging.

To design, elaborate and biochemically validate a genetic construct codifying for a fluorescence-activatable reporter of flavivirus NS2B-NS3 protease activity.

To establish a stable animal cell line expressing homogenous levels of a genetic construct codifying for a fluorescence-activatable reporter of flavivirus NS2B-NS3 protease activity and validate its performance to monitor flavivirus infection in single cells.

To establish a multireporter fluorescent plaque assay combining a fluorescence-activatable reporter of flaviviral NS2B-NS3 protease activity and DNA fluorescent dyes to monitor flavivirus replication and cytopathic effect by live-cell imaging and validate it against standard virological methods.

Hypothesis

The kinetics of flavivirus infection in animal cells can be studied and monitored by the application of live-cell imaging approaches based on molecular reporters of the viral NS2B-NS3 protease activity and/or the fluorescent labeling of virus-induced cytopathic effect.

Prologue

The present dissertation is divided in three chapters. Chapter 1 serves as an introduction to the fluorescence imaging techniques applied in flavivirus research and also address our previous work in the field that guided us into the live-cell imaging methodologies. Chapter 2 represents the core of the work in the form of a research article with a detail description about the development and validation of two cell-based molecular approaches for the study of flavivirus infection kinetics by live-cell imaging. Finally, chapter 3 contains a deep description of the protocols for live-cell imaging of flavivirus infection that were developed during the present research work.

Chapter 1

An overview of the fluorescence imaging approaches in flavivirus research

Summary

The genus *Flavivirus* within the family *Flaviviridae* contains many arthropod-borne infectious agents of medical relevance such as dengue virus (DENV), Zika virus (ZIKV), and West Nile virus (WNV), among others, that can cause epidemics of hemorrhagic fevers and encephalitis for which there are no antiviral treatments and effective vaccines yet available. Fluorescence imaging is a powerful and versatile research tool for the study of flaviviral diseases. This tool can be complemented with biochemical and molecular methods to gain insight into the mechanisms of flavivirus infection and immunity, in order to develop feasible prophylactic and therapeutic interventions to lower these viruses impact on public health. The present introductory chapter addresses the basic aspects of the fluorescence imaging techniques currently employed in flavivirus research, including immunofluorescence assay (IFA), fluorescence *in situ* hybridization (FISH), fluorescence-labeled viral particles, fluorescent labeling of cytopathic effect (CPE), subgenomic reporter replicons (SRRs) / reporter virus particles (RVPs), and cell-based molecular reporters (CBMRs). This chapter also includes a published article (Arias-Arias et al., 2018), where we developed and applied a rapid IFA protocol for DENV that can be easily adapted to other flaviviruses. This protocol is described in detail at the end of the chapter as its validation was our starting point in the field of flavivirus fluorescence imaging.

Background

The genus *Flavivirus* within the family *Flaviviridae* contains more than 70 species of arthropod-borne viruses, transmitted to animals and humans by the bite of infected

mosquitoes or ticks, including the clinically relevant species DENV, ZIKV, YFV, WNV, JEV, TBEV, and SLEV, among others (Gould and Solomon, 2008).

Flaviviruses possess small enveloped icosahedral particles of about 50 nm in diameter, which harbor a positive sense RNA genome of approximately 11 kb in length. This genome encodes three structural proteins: capsid (C), membrane precursor (prM), and envelope (E), and seven nonstructural proteins: NS1, NS2A, NS2B, NS3, NS4A, NS4B, and NS5, that form a precursor polyprotein (Figure 3A) which must be cleaved by both cellular and viral proteases in order to generate the individual viral proteins (Lindenbach et al., 2007).

During the last seven decades, flaviviruses have continuously emerged and re-emerged, constituting a global threat as causes of epidemics of hemorrhagic fevers and encephalitis for which there are no specific treatments more than life support upon hospitalization. This highlights the critical need for a detailed understanding of the biology of flavivirus, the interplay between the virus and the host cell, and the immunological responses elicited, in order to develop feasible prophylactic and therapeutic approaches to lower their impact on public health (Lindenbach et al., 2007; Pierson and Diamond, 2020).

In this scenario, fluorescence imaging techniques represent powerful and versatile research tools for visualization and study of flavivirus infected cells, that can be complemented with biochemical and molecular methods in order to gain knowledge about the mechanisms of infection and to test candidate antiviral drugs and vaccines to combat flaviviral diseases (Chong et al., 2014)**.** Among them**,** immunofluorescence assay (IFA), fluorescence *in situ* hybridization (FISH), fluorescent labeling of cytopathic effect (CPE), fluorescence-labeled viral particles, subgenomic reporter replicons (SRRs) / reporter virus particles (RVPs), and cell-based molecular reporters (CBMRs), have been applied in flavivirus research and will be individually discussed in the present introductory chapter.

Immunofluorescence assay (IFA)

IFA is the most popular and widely applied fluorescence imaging approach for flaviviruses, since this method has been used in diagnostics and research of flaviviral infections for more than 50 years (Atchison et al., 1966). Indeed, virus presence and cellular localization can be visualized inside infected cells by means of fluorophore-tagged antibodies directed against either structural or non-structural flavivirus antigens (Chong et al., 2014). Zuza and collaborators observed a perinuclear localization of the SLEV proteins upon immuno-labeling of infected astrocytes with a polyclonal ascitic fluid from immunized mice (Zuza et al., 2016). Likewise, Miorin and collaborators reported that the TBEV E, prM, and NS1 proteins were localized at the perinuclear region and within irregularly shaped foci of infected BHK-21 cells (Miorin et al., 2013). This is a common fluorescence pattern observed among other members of the genus, including DENV 1-4, ZIKV, YFV, JEV, and WNV (Ledizet et al., 2007; Ricciardi-Jorge et al., 2017; Slon Campos et al., 2017), since flaviviruses replication and assembly occurs on the cytosolic side of the endoplasmic reticulum (ER) membrane (Rothan and Kumar, 2019).

IFA also remains as an excellent method to evaluate and visualize the permissiveness of cell lineages to flavivirus infection. Růžek and collaborators tested the susceptibility of different human neural cell lines and the TBEV-induced cytopathic effect using an anti-E antibody (Růžek et al., 2009). In our work, we applied immunostaining of E and NS3 proteins as part of our experiments to demonstrate the permissiveness of primary human umbilical artery smooth muscle cells (HUASMC) to clinical isolates of both DENV-2 and DENV-3 (Figure 1C) (Arias-Arias et al., 2018). Others also employed immunolabeling to evaluate the susceptibility of JEG-3 and hCMEC/D3 cell lines, as well as Sertoli cells in mouse testis to ZIKV infection (Chiu et al., 2020; Sheng et al., 2017).

IFA also enables the study of colocalization as a first screening approach of protein-protein interactions by the combination of different antibodies directed against both host and viral antigens, as these interactions play important roles during flavivirus infection. Hung and

collaborators employed IFA colocalization of host secreted heat-shock protein 90 beta (Hsp90β) and viral E protein during JEV infection (Hung et al., 2011). They performed a subsequent validation with sucrose-density fractionation and Western blot analysis to demonstrate that this interaction is required for JEV infectivity in BHK-21 cells. In addition, using IFA and cryoimmunoelectron microscopy colocalization with monospecific antibodies, NS3 and NS2B proteins were found to be present in WNV-induced membrane structures in Vero cells (Westaway et al., 1997).

One of the greatest methodological advantages of applying IFA in flavivirus research, is the wide commercial availability of group cross-reactive and type-specific antibodies. This is based on the fact that some flaviviral proteins possess both conserved and variable antigens, e.g., the fusion loop at the extremity of domain II of protein E carries the flavivirus group conserved epitopes, whereas domains I and III contain the variable antigens (Lai et al., 2008). This observation guided the *in vitro* production of the hybridoma clone D1-4G2-4-15, which produces the most popular flavivirus group monoclonal antibody (4G2), used in diagnostics for the screening of viral isolates from clinical samples and in research for the monitoring of the infection by agents like DENV, WNV, JEV, YFV, and ZIKV (Garg et al., 2020; Göertz et al., 2017; Lai et al., 2008; Martins et al., 2019), among other flaviviruses.

At the end of this chapter, I describe in detail an IFA protocol for the immunostaining of DENV/ZIKV with commercial antibodies, that was applied in the first published article from this dissertation (Arias-Arias et al., 2018, attached article) and for the generation of the images depicted in Figure 1.

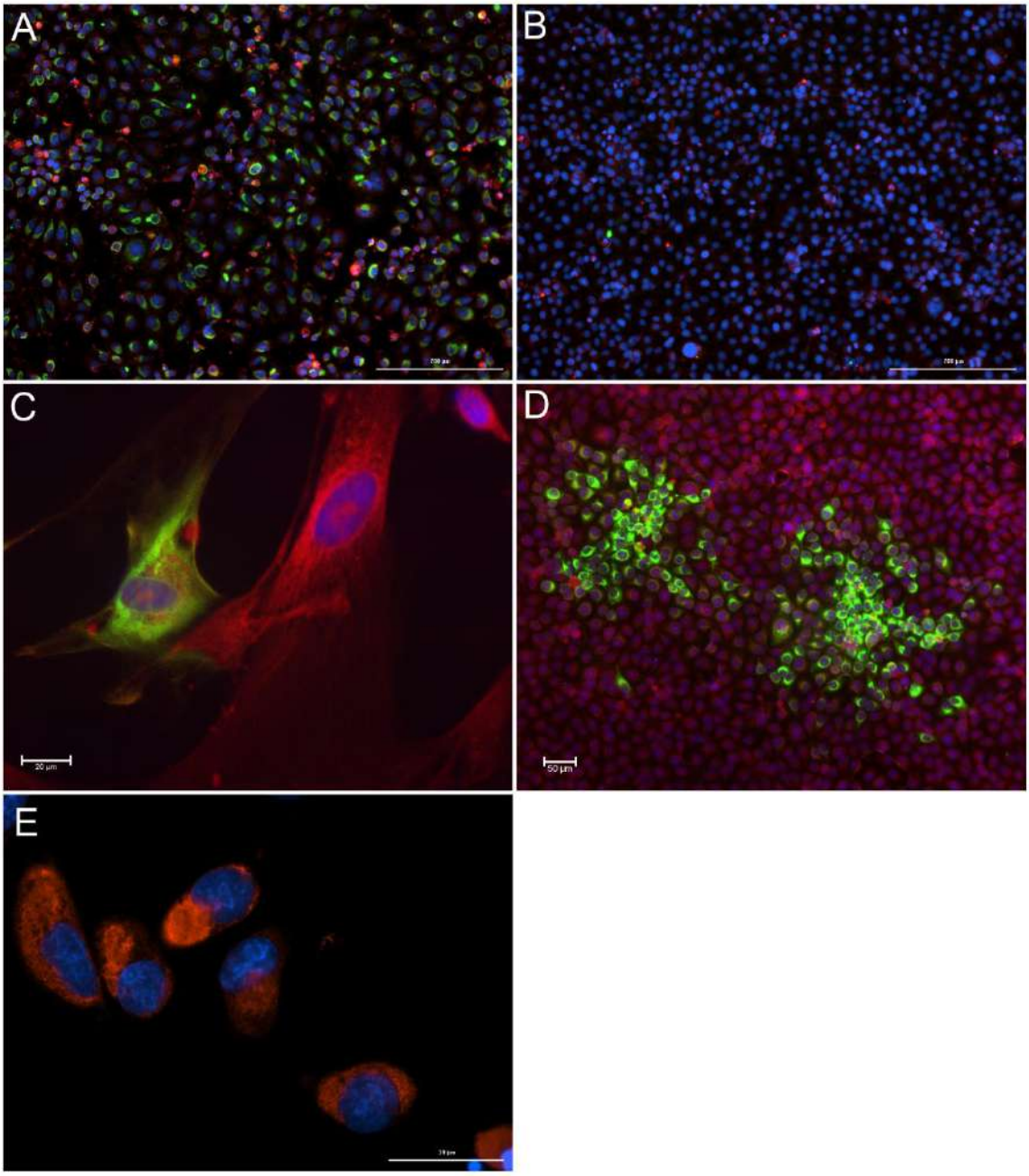

Figure 1. Immunofluorescence assay (IFA) in DENV/ZIKV-infected cell cultures. Epifluorescence images of ZIKV-infected (A) and mock-infected (B) Vero cells after immunostaining with an anti-ZIKV E protein monoclonal antibody (green) and cytoplasmic (Evans blue, red) - nuclear (Hoechst 33342, blue) counterstains (total magnification of 100 X; scale bar = 200 µm). DENV-infected HUASMC (C) and LLC-MK2 (B) cells immunostained with an anti-DENV 1-4 E protein monoclonal antibody (green) and counterstained with

cytoplasmic (Evans blue, red) and nuclear (Hoechst 33342, blue) fluorescent dyes (total magnification of 400 X and 100 X; scale bars = 20 µm and 50 µm, respectively). Immunolabeling of DENV in BHK-21 cell with an anti-DENV NS3 protein polyclonal antibody (orange) and a nuclear counterstain (Hoechst 33342, blue, total magnification of 600 X; scale bar = 30 µm). Images by Jorge L. Arias-Arias, Universidad de Costa Rica.

Fluorescence *in situ* hybridization (FISH)

FISH is a classical cytogenetic technique used to detect both RNA and DNA within tissues and cells by the application of fluorochrome-labelled probes that are complementary to the sequence of interest, with their subsequent visualization by fluorescence microscopy (Rudkin and Stollar, 1977). One of the mayor goals in RNA viruses research is the understanding of the coordination of the intracellular trafficking of viral RNA and proteins during the assembly of virions, as well as the deciphering of the involved interactions between the viral genome and other components of the host and the virus itself (Vyboh et al., 2012). A combination of FISH with other cellular and molecular techniques has been applied in recent years to tackle the above-mentioned challenges in flavivirus infection research.

FISH is the method of choice to visualize the localization, transcription, and replication of flavivirus RNA inside infected cells. Raquin and collaborators developed a set of highly specific oligonucleotide probes that hybridize to the viral RNA from a broad range of DENV isolates including all the four serotypes, but not to the closely related YFV and WNV genomes. They used those probes to label DENV RNA *in vitro* on infected C6/36 cells and *in vivo* with dissected salivary glands from infected *Aedes albopictus* specimens (Raquin et al., 2012). Similar FISH approaches have been used for the observation of ZIKV (Hou et al., 2017; Liu et al., 2019; Martinez-Lopez et al., 2019) and YFV genome replication (Sinigaglia et al., 2018), and for the visualization of WNV noncoding RNAs (Roby et al., 2014), among other flaviviruses.

When combined with IF, FISH serves as a useful starting point to study protein-viral RNA interactions. Hirano and collaborators applied FISH/IF and immunoprecipitation/RT-PCR to demonstrate that neuronal granules, involved in the transportation and local translation of dendritic mRNAs, also transport the TBEV genomic RNA (Hirano et al., 2017). Viral RNA interacts with a RNA-binding protein present in the neuronal granules and impairs the transport of dendritic mRNAs, which seems to be involved in the neuropathogenesis of the TBEV infection. Also, Hou and collaborators observed co-localization of ZIKV E protein with its own viral RNA by FISH/IF and demonstrated its interaction via an RNA chromatin immunoprecipitation (RNA-ChIP) assay, implying that the E protein may have a role in ZIKV replication (Hou et al., 2017).

The availability of online bioinformatic tools and databases assisting probe design (e.g., https://www.arb-silva.de/fish-probes/probe-design/), together with the custom probe synthesis services offered by many biotech companies, is increasing the feasible application of RNA FISH in the field of virology, including flavivirus research. For a detailed and versatile FISH protocol specially standardized for RNA viruses, please refer to the work of Lindquist and Schmaljohn (Lindquist and Schmaljohn, 2018).

Fluorescence-labeled viral particles

In recent years, with the improvements in confocal and super-resolution fluorescence microscopy, several researchers have exploited the direct labeling of virions for the visualization of the early events in virus-cell interactions, even at a single particle level (Sakin et al., 2016). To assess viral membrane fusion, the use of lipophilic dyes that get inserted into the lipid bilayer membrane of virions and are released in the endosomal membrane after the fusion event, have been reported for some flaviviruses (Hoffmann et al., 2018). Nour and collaborators applied octadecyl rhodamine B chloride (R18) labeling of JEV and YFV particles to study the kinetics of viral membrane fusion and nucleocapsid delivery into the cytoplasm (Nour et al., 2013). Moreover, labeling of virions with 1,1'-dioctadecyl-3,3,3',3'-tetramethylindodicarbocyanine, 4-chlorobenzenesulfonate salt (DiD) was used to

analyze the cellular entry of WNV (Makino et al., 2014) and to demonstrate the involvement of the autophagy machinery during the early stages of DENV infection (Chu, 2013).

Furthermore, Zhang and collaborators developed a simple and efficient method to covalently tag the amino free groups of DENV E protein with the dye Alexa Fluor 594 succinimidyl ester, a useful labeling approach employed to monitor virus binding, uptake, and intracellular trafficking (Zhang et al., 2010). A similar procedure was used to label ZIKV particles with the dye Atto647N-NHS ester, which enabled the visualization of viral transcytosis through both the placental and the blood brain barriers (Chiu et al., 2020).

Labeling of virions is an advantageous technique since the above-mentioned dyes show bright fluorescence, high photostability, are suitable to be applied in both fixed and live-cell imaging protocols, and exist in a broad range of colors over the ultraviolet-visible spectrum (Hoffmann et al., 2018). The work of Zhang and collaborators describes a detailed protocol for the fluorescence-labeling of flavivirus particles (Zhang et al., 2011). A comprehensive description of labeling procedures applied to a broader repertory of viruses is discussed by Hoffmann and collaborators (Hoffmann et al., 2018).

Fluorescent labeling of cytopathic effect (CPE)

Detection of CPE as an indirect way to monitor viral infections has been largely exploited since the early days of virology and constitutes a fundamental part of the principle behind classical virological methods such as Dulbecco plaque assay (Dulbecco, 1952). For example, monitoring the morphological changes on flavivirus infected cells is generally accomplished by bright-field light microscopy, directly on living cells or after fixation and staining with conventional dyes as crystal violet or hematoxylin-eosin (Bakonyi et al., 2005; Chong et al., 2014).

Taking into account that in many cases the CPE is a result of virus–cell interactions leading to cell demise by host-encoded programs like programmed necrosis and apoptosis (Agol,

2012), during the present research work we envisaged a simple but effective way to label and monitor CPE in real-time by fluorescence live-cell imaging (chapter 2). Using fluorescent DNA dyes commonly employed in cell biology and cancer research such as nuclei stains (Hoechst 33342) and cell dead markers (propidium iodide, SYTOX green, TO-PRO-3 iodide), we were able to visualize early (chromatin condensation) and late (membrane permeabilization) events of the virus elicited CPE correlating with cell damage and cell death, respectively.

We successfully applied the above-mentioned approach to perform kinetics of CPE detection and real-time plaque assays on living cells infected with DENV, ZIKV, and YFV (Figure 2). This allowed us to analyze the viral plaques growth over time at a single-cell level using an image analysis software, as exposed in the second published article from this thesis (Arias-Arias et al., 2020, attached in chapter 2). A detailed protocol for kinetic CPE labeling and monitoring in flavivirus infected cells is described in chapter 3.

Subgenomic reporter replicons (SRRs) and reporter virus particles (RVPs)

Flaviviruses harbor positive strand RNA genomes that are *per se* infectious. Thus, transfection of RNA produced by *in vitro* transcription from a cDNA clone containing the reverse transcribed full-length flavivirus genome results in the production of infectious recombinant viral particles (Figure 3A). In contrast, flavivirus subgenomic replicons possess all the essential genetic elements for self- replication and production of nonstructural proteins, but lack the complete encoding sequences of the structural C-prM-E proteins (Figure 3B) and consequently do not allow the generation of virions. Using such replicons as templates, SRRs are established by the introduction of reporter genes that code for bioluminescent or fluorescent proteins in the position of the deleted structural genes (Figure 3C) (Kümmerer, 2018). This enables the easy tracking of the replication/translation of subgenomic replicons and the screening of antiviral compounds by the direct visualization and measurement of the signal produced by the reporter proteins (Kato and Hishiki, 2016). Flavivirus SRRs have been developed and validated for YFV (Jones et al.,

2005), JEV (Li et al., 2013), WNV (Shi et al., 2002), ZIKV (Mutso et al., 2017), and DENV (Pang et al., 2001; Usme-Ciro et al., 2017), among others.

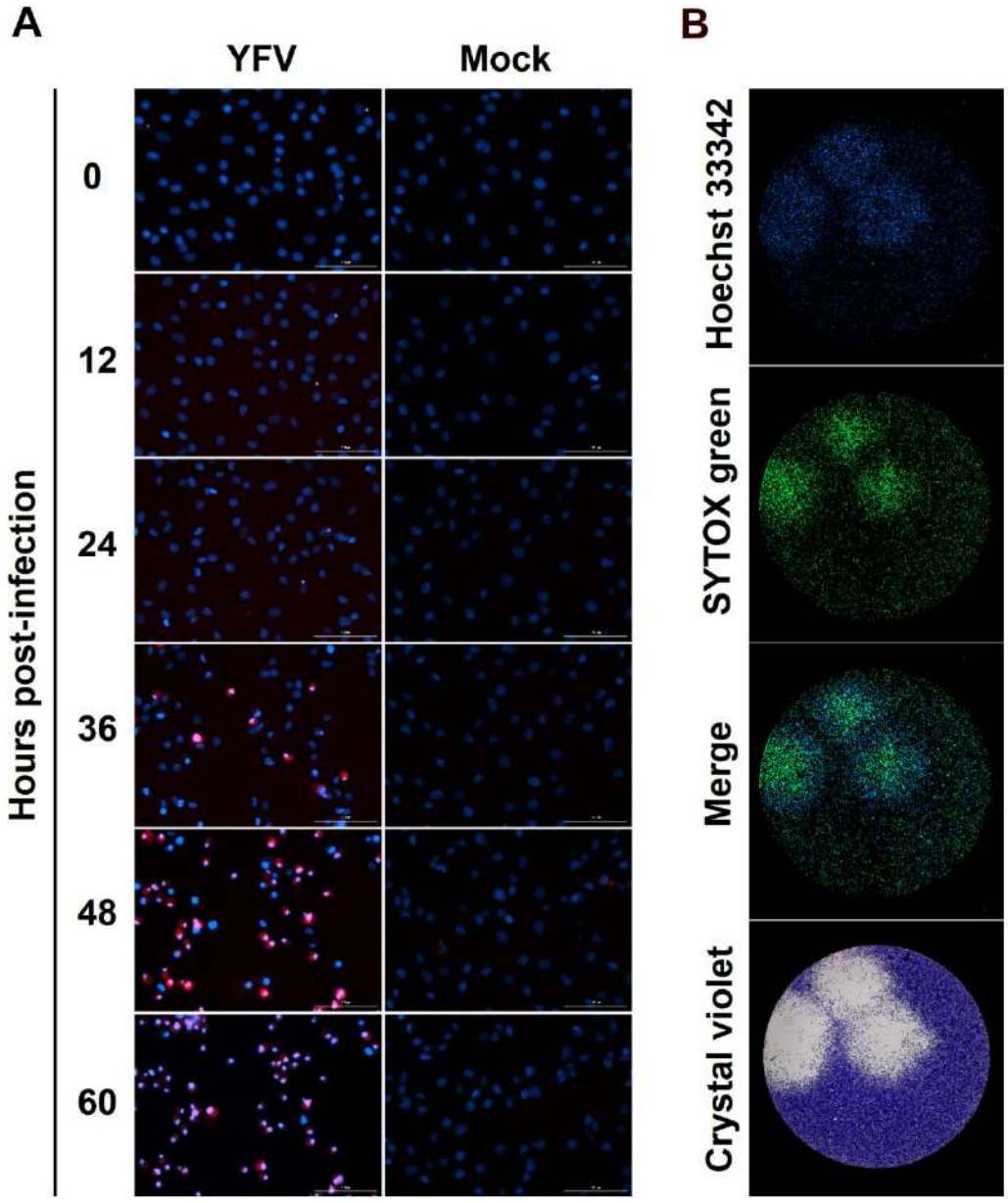

Figure 2. Fluorescent labeling of cytopathic effect (CPE) in flavivirus-infected cell cultures. A. CPE imaging kinetics in YFV-infected BHK-21 cells with the DNA staining dyes Hoechst 33342 (cells with condensed chromatin, saturated blue) and TO-PRO-3 iodide (dead cells, red) at a total magnification of 200 X (scale bar = 100 µm). B. Dulbecco's plaque assay on unfixed Vero cells by CPE labeling with the nucleic acid dyes Hoechst 33342 (DNA/chromatin

condensation, blue) and SYTOX green (cell death, green), at 96 hours post-infection with ZIKV (total magnification of 40 X; scale bar = 1000 µm). Images by Jorge L. Arias-Arias, Universidad de Costa Rica.

SRRs are also used for the generation of single-round infectious RVPs, by providing the deleted C-prM-E genes *in trans* with another genetic construct (Figure 3D). Such single-round RVPs are extremely useful as surrogate pseudoviruses in studies of BSL3-handling of flaviviruses such as JEV (Lu et al., 2017) and WNV (Li et al., 2017; Velado Fernández et al., 2014). Single-round infectious RVPs have also been used on the development of easy fluorescent neutralization assays for the detection of flavivirus-specific antibodies in the serum of individuals and the assessment of the humoral immune response elicited by candidate vaccines, as shown for DENV (Mattia et al., 2011), TBEV (Yoshii et al., 2009), ZIKV (Garg et al., 2017), and WNV (Pierson et al., 2006).

However, SRRs and single-round infectious RVPs cannot be used to study the pathogenesis, transmission, and dynamics of the complete virus replication cycle, as well as for the screening of antivirals targeting the structural proteins (Kato and Hishiki, 2016). For such applications, whole genome RVPs have been engineered by the insertion of reporter genes into full-length flavivirus cDNA clones (full-length reporter cDNA clone, Figure 3E), as described for JEV (Jia et al., 2016), DENV (Schmid et al., 2015; Schoggins et al., 2012; Suphatrakul et al., 2018), WNV (Pierson et al., 2005), and ZIKV (Gadea et al., 2016), among others. As an example, Schmid and collaborators developed and characterized a far-red DENV-2 reporter virion that allows the monitoring of the viral infection kinetics in animal cells by live imaging (Schmid et al., 2015).

For further details, the work by Kümmerer describes in detail the molecular genetics, development and applications of flavivirus subgenomic and full-length replicons (Kümmerer, 2018).

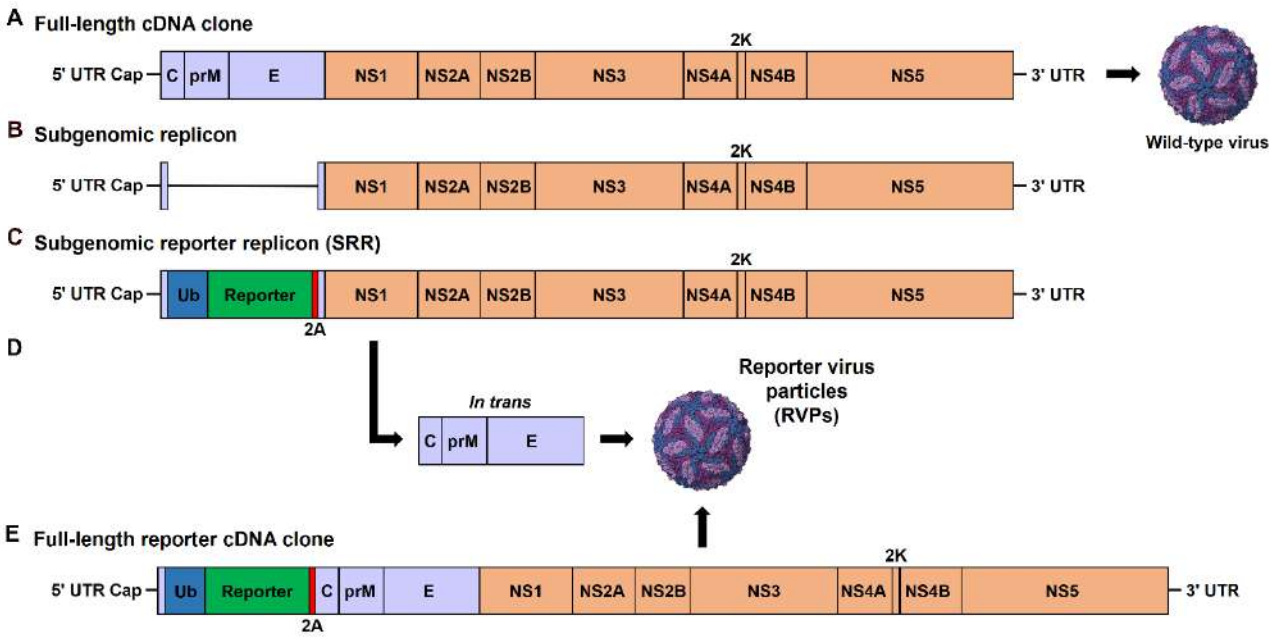

Figure 3. Schematic presentation of genetic constructs encoding flavivirus full-length cDNA clones (A), subgenomic replicons (B), subgenomic reporter replicons (SRRs, C), and full-length reporter cDNA clones (E), which enable the production of reporter virus particles (RVPs, D). UTR: untranslated region; Ub: ubiquitin coding sequence; 2A: ribosomal skipping 2A peptide. Modified and adapted from Kümmerer, 2018.

Cell-based molecular reporters (CBMRs)

SRRs and RVPs are valuable tools to perform kinetic studies by live-cell imaging, but their development is expensive, time consuming, and limited only to the pre-selected molecular clones derived from specific flavivirus strains, which precludes the direct work with clinical isolates and wild-type virus strains. To overcome this limitation, in recent years a few articles have outlined the use of CBMRs as an alternative to carry out kinetics of infection with wild-type flaviviruses in living cells (Arias-Arias et al., 2020).

So far, all the published flavivirus CBMRs are based on the monitoring of the proteolytic activity of the flaviviral NS2B-NS3 serine protease. Medin and collaborators devised a DENV 1-4 plasmid-based reporter system containing the cleavage site between the NS4B and NS5

proteins attached to an EGFP by a nuclear localization sequence (NLS) (Medin et al., 2015). Upon cleavage the EGFP relocalizes from the cytoplasm to the nucleus of infected cells. The same principle was adapted by McFadden and collaborators for imaging ZIKV infection in living Huh7 cells (McFadden et al., 2018). In addition, a modification of this approach by Hsieh and collaborators exploited the DENV NS3 cleavage between NS4B/NS5 to activate a Cre recombinase-based nuclear reporter (Hsieh et al., 2017). This system showed superior performance than traditional methods for DENV 1-4 titration.

Moreover, during the present research work we developed a fluorescence-activatable reporter of flavivirus infection by the modification of previously published caspase 7 reporters (Wu et al., 2013). Instead of the caspase 7 cleavage sequence, we inserted the internal NS3 cleavage site (conserved among many members of the *Flavivirus* genus) between a fluorescent protein and a quenching peptide (QP, Figure 4A). This reporter system was used to generate a BHK-21 reporter cell line suitable for monitoring the kinetics of infection by DENV, ZIKV, and YFV both in viral plaques and at a single-cell level using live-cell imaging (Figure 4B) (Arias-Arias et al., 2020).

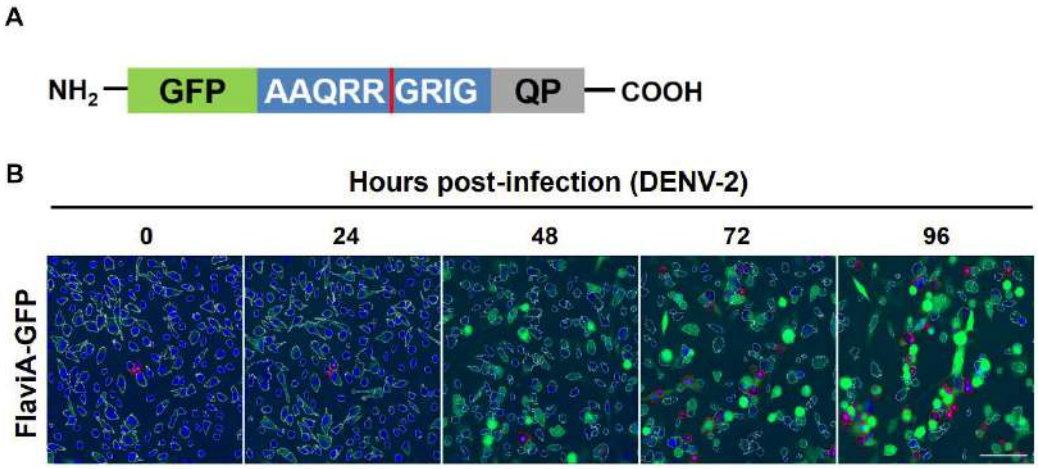

Figure 4. The flavivirus cell-based molecular reporter. A. The flavivirus-activatable GFP reporter (FlaviA-GFP) contains a GFP with a C-terminal quenching peptide (QP) joined by a linker composed by a cleavage site of the flaviviral NS3 protease. When the protease cuts

the linker, the quenching peptide is removed, and the GFP adopts the fluorescent conformation. B. DENV-2 infection kinetics in BHK-21 reporter cells. An automated image analysis protocol was programmed in CellProfiler 2.0 for the quantification of activated FlaviA-GFP fluorescent cells (green), live cells (white outline) and dead cells (red outline). Total magnification of 200 X; scale bar = 100 µm. Adapted from Arias-Arias et al., 2020.

The details about the development and validation of our flaviviral CBMR system are addressed in chapter 2 and the exact protocol for the generation of the above-mentioned reporter cell line is described in the third published article from this dissertation (Arias-Arias et al., 2021, attached in chapter 3).

Published article

Arias-Arias, J.L., Vega-Aguilar, F., Corrales-Aguilar, E., Hun, L., Loría, G.D., Mora-Rodríguez, R., 2018. *Dengue virus infection of primary human smooth muscle cells*. Am. J. Trop. Med. Hyg. 99, 1451–1457. https://doi.org/10.4269/ajtmh.18-0175

Am. J. Trop. Med. Hyg., 99(6), 2018, pp. 1451–1457
doi:10.4269/ajtmh.18-0175

Dengue Virus Infection of Primary Human Smooth Muscle Cells

Jorge L. Arias-Arias, Francisco Vega-Aguilar, Eugenia Corrales-Aguilar, Laya Hun, Gilbert D. Loría, and Rodrigo Mora-Rodríguez*
Centro de Investigación en Enfermedades Tropicales (CIET), Facultad de Microbiología, Universidad de Costa Rica, San José, Costa Rica

Abstract. Dengue virus (DENV) infection of humans is presently the most important arthropod-borne viral global threat, for which no suitable or reliable animal model exists. Reports addressing the effect of DENV on vascular components other than endothelial cells are lacking. Dengue virus infection of vascular smooth muscle cells, which play a physiological compensatory response to hypotension in arteries and arterioles, has not been characterized, thus precluding our understanding of the role of these vascular components in dengue pathogenesis. Therefore, we studied the permissiveness of primary human umbilical artery smooth muscle cells (HUASMC) to DENV 1–4 infection and compared with the infection in the previously reported primary human umbilical vein endothelial cells (HUVEC) and the classically used, non-transformed, and highly permissive Lilly Laboratories Cell-Monkey Kidney 2 cells. Our results show that HUASMC are susceptible and productive to infection with the four DENV serotypes, although to a lesser extent when compared with the other cell lines. This is the first report of DENV permissiveness in human smooth muscle cells, which might represent an unexplored pathophysiological contributor to the vascular collapse observed in severe human dengue infection.

INTRODUCTION

Dengue virus (DENV) is a member of the genus *Flavivirus* within the Flaviviridae family, for which five serotypes have been described (DENV 1–5).[1] The virion comprises an enveloped spherical particle that harbors a positive single-stranded RNA genome.[2] Dengue virus is transmitted by mosquito vectors, mainly *Aedes aegypti*, and is considered the most important arthropod-borne viral disease worldwide.[3]

Dengue virus represents a global threat, for which there is no specific treatment available. Although a tetravalent, live-attenuated, dengue vaccine was recently approved,[4] safety concerns[5] have highlighted the urgent need for antiviral drugs to treat DENV infections. However, the development of an antiviral drug targeting viral factors of all DENV serotypes has been problematic. New promising approaches rely on the targeting of host factors to achieve antiviral activity.[6] Nevertheless, this strategy requires an in-depth understanding of the pathogenesis of dengue disease, including the identification of the key cellular targets involved in severe infections.

The determinants of dengue disease severity are complex and multifactorial, and although several models have been developed over the years to bridge translation from in vitro to human observational studies, no laboratory animals (wild-type or genetically modified) develop all of the clinical manifestations of severe dengue disease in humans.[7] Dengue virus infects many animal cell lines such as the highly permissive baby hamster kidney cells (BHK-21), C6/36, Vero and LLC-MK2 (macaque kidney cells), and human cell lines such as HepG2, U937, and HEK-293, with varying degrees of permissiveness.[8–10] However, the question remains as to whether those cells types represent relevant targets of DENV infection in vivo. Therefore, most conclusions regarding the in vivo situation in humans rely on postmortem studies or on the in vitro permissiveness of primary cells such as human umbilical vein endothelial cells (HUVEC) and peripheral blood mononuclear cells to DENV.[8,11]

Postmortem studies depend on the detection of DENV antigens in tissues. The most specific marker of DENV infection in vivo is the nonstructural protein 3 (NS3) because it does not enter the secretory pathway, and thus demonstrating exclusively intracellular localization.[11,12] However, localization of NS3 protein in tissues varies depending on which host species is analyzed. In mice, NS3 was detected in phagocytes of the spleen and lymph nodes, as well as in hepatocytes and myeloid cells in the bone marrow.[11] In human postmortem tissues, the NS3 protein was detected in phagocytes of spleen and lymph nodes, hepatocytes and endothelial cells in spleen, perivascular cells in brain, and alveolar macrophages in lungs of DENV severe cases.[11] Others reported that skeletal and cardiac muscle cells are also infected in vivo.[13,14] In addition, it has been shown that myotubes can also be infected in vitro.[14]

Endothelial cells have long been implicated in the physiopathology of DENV infection. Microvascular and endothelial dysfunctions are associated with the severity of dengue, and this occurs before the appearance of severe clinical manifestations.[15] Indeed, there are tests and treatments to identify and handle various forms of vascular dysfunction that could be applied for the clinical management of patients with severe dengue.[3] It has been reported that endothelial cells are permissive to DENV infection in vitro although they produce low viral titers.[16] Nevertheless, DENV infection of ECV304 human endothelial cells leads to chemokine production and complement activation, suggesting an important role in microvascular dysfunction during DENV physiopathology.[17] Moreover, others have shown the effect of DENV infection on gene expression in HUVEC cells and identified potentially novel mechanisms involved in dengue disease manifestations such as hemostatic disturbances.[18] However, only a small percentage of endothelial cells were productively infected in vitro using the DENV-2 16681 strain.[19] Despite these observations, the importance of endothelial cells as targets of DENV infection in vivo remains a subject of debate.

Reports addressing the effect of DENV on other vascular components such as smooth muscle cells, which play a physiologically relevant role in arteries and arterioles, are lacking. Dengue virus infection of vascular smooth muscle cells has not been characterized, thus precluding our understanding of the role of these vascular components in

* Address correspondence to Rodrigo Mora-Rodríguez, Facultad de Microbiología, Centro de Investigación en Enfermedades Tropicales, Universidad de Costa Rica, Ciudad Universitaria Rodrigo Facio, San Pedro de Montes de Oca, San José 11501-2060, Costa Rica. E-mail: rodrigo.morarodriguez@ucr.ac.cr

dengue pathogenesis. To address this issue, here we worked with human umbilical artery smooth muscle cells (HUASMC), which are primary smooth muscle cells isolated from normal healthy human umbilical arteries. Human umbilical artery smooth muscle cells have been used along HUVEC to study the dynamics, maturation, and effects of toxic stimulus on blood vessels, and constitutes a suitable and well-validated model that could be applied on DENV research.[20,21] This work describes for the first time a DENV-permissive infection of primary arterial smooth muscle cells in vitro, which might represent an unexplored pathophysiological contributor to the reduced vascular reactivity to hypotension observed during dengue shock syndrome and dengue hemorrhagic fever.

MATERIALS AND METHODS

Viruses. Dengue virus-1 Angola (D1/AO/XX/1988) and DENV-4 Dominica (D4/DM/814669/1981) strains were supplied by the Instituto de Medicina Tropical Pedro Kourí, Havana, Cuba. The clinical isolates from Costa Rican patients DENV-2 10066 (D2/CR/10066/2007) and DENV-3 14531 (D3/CR/14531/2007) were provided by the Instituto Costarricense de Investigación y Enseñanza en Nutrición y Salud, Cartago, Costa Rica.[22] Viruses were produced in C6/36 cells from *Aedes albopictus* (ATCC, Manassas, VA) by inoculating cellular monolayers with DENV at a multiplicity of infection (MOI) of 0.01 and incubating for 3 days with Roswell Park Memorial Institute-1640 medium supplemented with 2% fetal bovine serum (FBS) (Gibco, Gaithersburg, MD) at 33°C in an atmosphere of 5% CO_2. Then, culture supernatant was collected and centrifuged at 3,000 × *g* for 10 minutes. Before storage at –80°C, 23% newborn calf serum (Gibco) was added.[9] Culture supernatant from uninfected C6/36 cells was collected and used as negative control (mock control). Viruses were titrated by plaque assay in BHK-21 cells (ATCC) as previously described.[23] Briefly, 10-fold serial dilutions of viruses were added to BHK-21 confluent monolayers. After 2 hours of adsorption, cells were incubated at 37°C in an atmosphere of 5% CO_2 for 5 days with minimum essential medium (MEM) supplemented with 2% FBS (Gibco) and 1% carboxymethylcellulose (Sigma, St. Louis, MO). Plaque numbers were counted after staining with crystal violet.

Cell lines and virus infections. Human umbilical artery smooth muscle cells and HUVEC were purchased and maintained in smooth muscle cell growth medium and endothelial cell growth medium, respectively, according to the manufacturer's instructions (Cell Applications, San Diego, CA). LLC-MK2 cells (ATCC) were grown in MEM supplemented with 10% FBS. Cell monolayers were DENV or mock infected at a MOI of 1 and allowed virus adsorption for 2 hours at 37°C. After three washes with phosphate-buffered saline (PBS), cells were incubated with 2% FBS medium at 37°C in an atmosphere of 5% CO_2 for different times. All experiments were performed with the same number of HUASMC, HUVEC, and LLC-MK2 cells.

Plaque assays for virus quantification. Culture supernatants of HUASMC were collected at 0, 24, 48, and 72 hours postinfection (p.i.) and DENV infectious particles were quantified by plaque assays in BHK-21 cells, as described earlier. Concomitantly, supernatants from HUVEC and LLC-MK2 cell cultures at 72 hours p.i. were titrated.

Real-time reverse transcription-quantitative polymerase chain reaction (RT-qPCR) for genome copies quantification. Culture supernatants of HUASMC cells were collected at 0, 24, 48, and 72 hours p.i. and DENV genomes were quantified by RT-qPCR. Briefly, viral RNA was extracted with the NucleoSpin RNA virus kit (Macherey-Nagel, Düren, Germany) and quantified using the Genesig RT-qPCR advanced kit for dengue virus (Primerdesign, Southampton, United Kingdom) according to the manufacturer's instructions. The reactions were carried out with a StepOne™ real-time PCR system (Applied Biosystems, Carlsbad, CA). Supernatants from HUVEC and LLC-MK2 cell cultures at 72 hours p.i. were also tested.

Indirect immunofluorescence for DENV infected cells quantification. Human umbilical artery smooth muscle cells, HUVEC, and LLC-MK2 cells were cultured on glass coverslips coated with 1% gelatin (Sigma) in 24 well plates seeded with 100,000 cells per well. At 72 hours p.i., cells were fixed with cold acetone for 10 minutes, washed with PBS, and stored at –20°C. Afterward, the slides were treated with 50 mM NH_4Cl for 10 minutes and incubated with a 1:300 dilution of mouse anti-DENV 1, 2, 3 and 4 envelope protein monoclonal antibody (GTX29202; GeneTex, Irvine, CA) or a 1:800 dilution of rabbit anti-DENV NS3 protein polyclonal antibody (GTX124252; GeneTex) for 1 hour at 37°C. After washing, the coverslips were incubated for 30 minutes at 37°C with 1:75 diluted fluorescein isothiocyanate-conjugated goat anti-mouse immunoglobulin G (IgG) (DAKO, Glostrup, Denmark) in 0.02% Evans blue or 1:400 dilution of Alexa Fluor 647 goat anti-rabbit IgG (Invitrogen, CA) in PBS. Stained slides were mounted with Prolong Gold with 4′,6-diamidino-2-phenylindole (DAPI; Invitrogen, Carlsbad, CA) and images were acquired with a Cytation 3 Cell Imaging Multi-Mode Reader (BioTeK, Winooski, VT). Image analysis of the whole coverslip was performed with the software CellProfiler 2.0 (http://www.cellprofiler.org; Broad Institute, Cambridge, MA).

Statistics. Data are expressed as mean ± standard deviation of three independent experiments. Statistical significance of the differences between mean values was determined by using an unpaired Student's *t*-test. The level of significance is denoted in each figure.

RESULTS

All four dengue serotypes are able to replicate in HUASMC cells. To test the permissiveness of HUASMC to DENV infection, confluent cell monolayers where infected at a MOI of 1 with each of the four DENV serotypes. Virions were quantified in culture supernatants every 24 hours for 72 hours. The supernatants of HUASMC monolayers infected with the four DENV serotypes exhibited an increasing number of plaque-forming units (PFU) after 48 hours p.i. (Figure 1A). However, there were significantly higher replication efficiencies of the different DENV serotypes in HUVEC and LLC-MK2 cell line when compared with HUASMC at 72 hours after infection (Figure 1B). These results demonstrate that the HUASMC line is permissive to DENV infection by all four serotypes; however, virion production is lower in these cells than in the frequently used HUVEC and LLC-MK2 cells.

To confirm the permissiveness of HUASMC to DENV infection and estimate the replicative fitness of the virus in this cell line, monolayers were infected at a MOI of 1 with the four DENV serotypes. Dengue virus RNA was quantified from culture supernatants every 24 hours for 72 hours. The supernatants of HUASMC monolayers infected with the four DENV

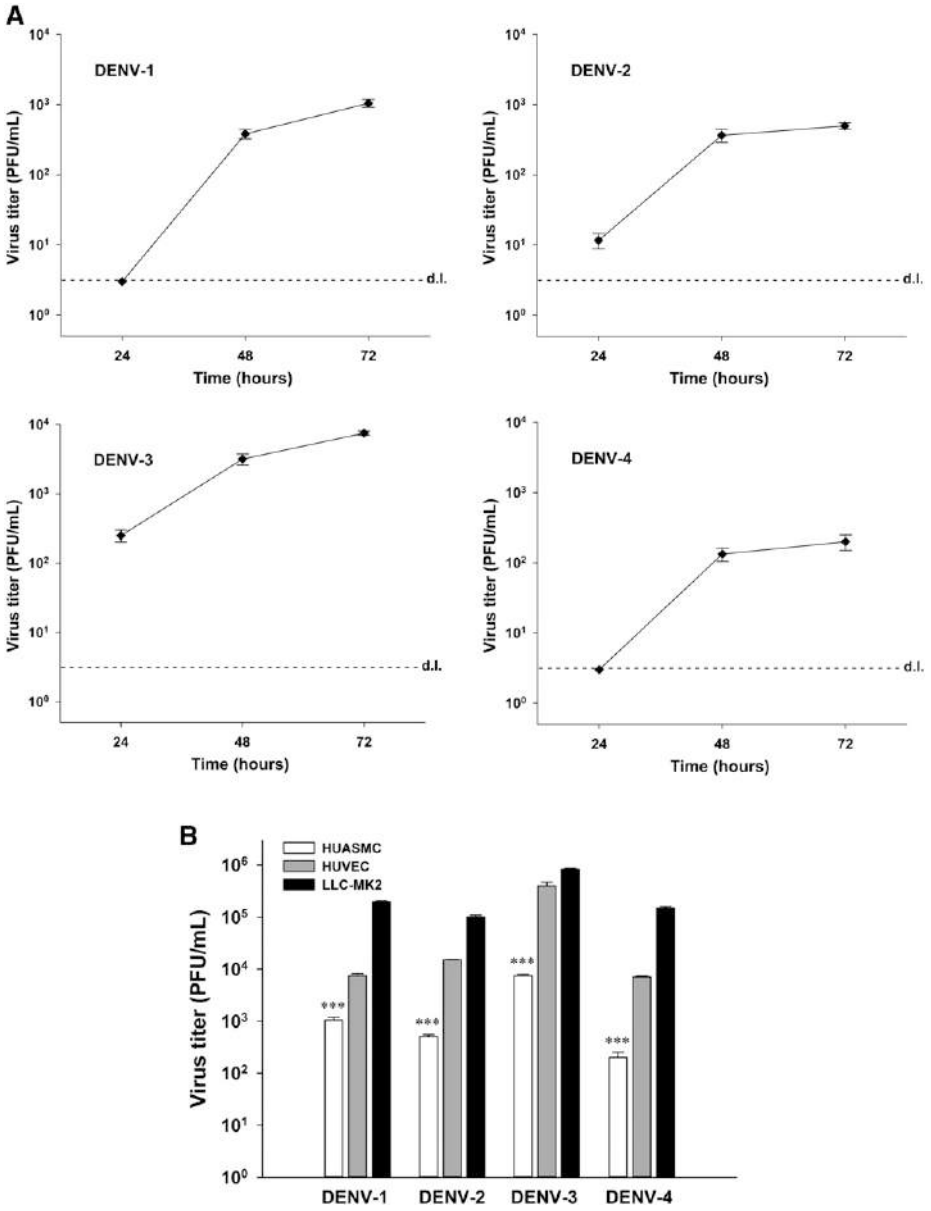

FIGURE 1. Human umbilical artery smooth muscle cells (HUASMC) are permissive to dengue virus (DENV) infection. Virion production and release was quantified by plaque assays of culture supernatants at different time points post-infection (p.i.) of HUASMC, human umbilical vein endothelial cells (HUVEC), and LLC-MK2 (macaque kidney cells) infected with each of the four DENV serotypes (multiplicity of infection:1). (**A**) Infection kinetics of HUASMC cells (24–72 hours p.i.) with DENV 1–4 measured by plaque assays (plaque-forming units [PFU]/mL). (**B**) DENV 1–4 titers in culture supernatants of HUASMC, HUVEC, and LLC-MK2 cells at 72 hours p.i. Data are expressed as the mean ± standard deviation of three independent experiments. ***$P < 0.001$ compared with its HUVEC and LLC-MK2 cells counterparts. (**D**) l. = assay detection limit.

serotypes showed an increase in DENV genomic RNA copies at 48 hours p.i. (Figure 2A). Nevertheless, the production of infectious virions and genomic RNA from the different DENV serotypes was significantly higher in HUVEC and LLC-MK2 cells than in HUASMC cells at 72 hours after infection (Figure 2B). Thus, the replicative fitness of DENV in HUASMC cells was significantly lower than that observed in HUVEC and LLC-MK2 cell lines, based on the genome-to-PFU ratios calculated at 72 hours p.i. (Figure 2C).

Dengue virus antigens are detected by immunofluorescence in HUASMC. Human umbilical artery smooth muscle cells' monolayers infected with the four DENV serotypes were stained by indirect immunofluorescence to quantify cellular infection. After 72 hours of infection, HUASMC, HUVEC, and LLC-MK2 cells were stained with an anti-DENV 1, 2, 3 and 4 envelope protein monoclonal antibody and fluorescence images were analyzed using the software CellProfiler 2.0. In contrast to the mock control (Figure 3A), infected HUASMC showed cytoplasmic green fluorescence staining (Figure 3B and C, white arrows), which was automatically identified by image analysis (Figure 3D, green outlines) to calculate the percentage of infected cells against the total number of identified cellular nuclei (Figure 3D, white outlines). As expected, the LLC-MK2 cell line showed higher percentages of positive cells with all four DENV serotypes compared with HUASMC cells (Figure 3E). By contrast,

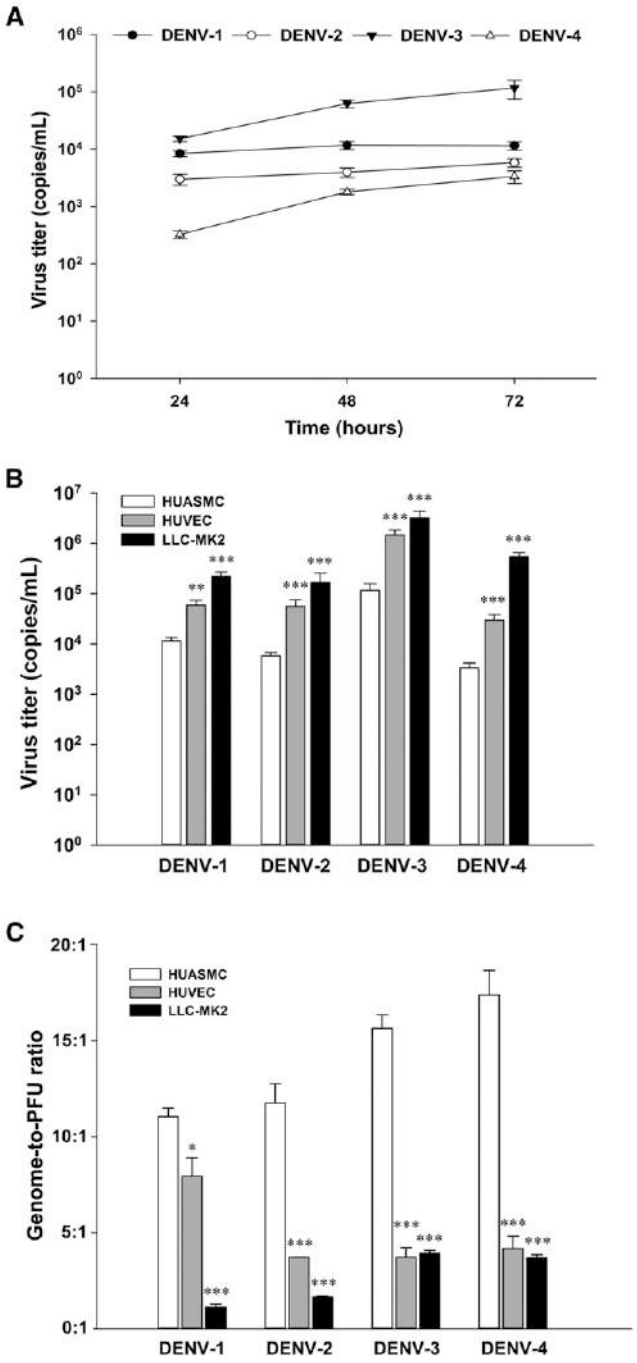

FIGURE 2. Human umbilical artery smooth muscle cells (HUASMC) release dengue virus (DENV) genomes on infection. Dengue virus genomic RNA was quantified by real-time qRT-PCR from cell culture supernatants of HUASMC, human umbilical vein endothelial cells (HUVEC), and LLC-MK2 (macaque kidney cells) infected with DENV (multiplicity of infection:1). (**A**) Dengue virus 1–4 infection kinetics (24–72 hours post-infection [p.i.]) of HUASMC cells measured by real-time genomic qRT-PCR (copies/mL). (**B**) Genome copies present in culture supernatants of HUASMC, HUVEC, and LLC-MK2 cells at 72 hours p.i. with the four DENV serotypes. (**C**) Calculated genome-to-plaque-forming unit (PFU) ratios of HUASMC, HUVEC, and LLC-MK2 cells supernatants at 72 hours p.i. with each DENV serotype. Data are expressed as the mean ± standard deviation of three independent experiments. $^{*}P < 0.05$, $^{**}P < 0.005$, and $^{***}P < 0.001$ calculated to its HUASMC counterpart.

HUASMC displayed a small percentage of cells (5–15%) with positive staining, indicating that this cell line has a low permissiveness to DENV infection with all four serotypes. However, only DENV-2 and DENV-3 led to a higher antigen production in HUVEC cell line compared with HUASMC cells (Figure 3E). Finally, no difference was observed in the identification of HUASMC-infected cells by immunostaining with an anti-DENV 1-4 envelope protein-specific monoclonal antibody and an anti-NS3 polyclonal antibody (Figure 3F), which indicates that the detected antigens are produced de novo during the infection. These results demonstrate that DENV antigens can be detected in HUASMC despite the low permissiveness as shown by the low percentage of infected cells compared with HUVEC and LLC-MK2 cells.

DISCUSSION

Research on DENV pathophysiology has been hampered by the lack of competent animal models for reproducing the in vivo human infection.[7] Therefore, most conclusions regarding the pathophysiological mechanisms of this disease in humans rely on postmortem studies or are extrapolations from the in vitro permissiveness of primary cells to DENV.[8,11] A key remaining question regarding DENV pathophysiology is the role of alterations in the different cellular components of the blood vessel. This has been addressed for endothelial cells because they are the major component of capillary blood vessels, and the microvascular dysfunction is closely associated with the severity of dengue.[15] Our findings confirm that DENV do infect the endothelial cell line HUVEC, as shown previously.[16] Indeed, future work is necessary to assess whether direct dengue viral infection of endothelium is the major cause of the extensive vascular leakage, which has been previously observed in patients with dengue hemorrhagic fever and dengue shock syndrome.[19]

A neglected component of the tissue response to this extensive vascular leakage has to do with the physiological compensatory mechanisms associated with the response of arterioles and particularly with the regulation of vascular diameter by smooth muscle cells present in the arteriolar wall. Significant vascular leakage and the resulting hypovolemia trigger vasoconstriction of arterioles to compensate for hypotension.[24] During hemorrhagic shock, the vascular hyporeactivity is related to a desensitization to calcium and mitochondrial dysfunction in smooth muscle cells in blood vessels.[25,26] In addition, damage to lymphatic smooth muscle cells in collecting lymphatic vessels leads to an impairment in lymph formation and interstitial fluid balance, generating edema and thereby perturbing blood volume recovery.[21] Therefore, the observed effect of DENV infection in smooth muscle cells could play an important role in precipitating the outcome of severe shock due to a deficient compensatory response to hypotension. Our observations in cell culture conditions may thus reveal a hitherto unexplored mechanism of vascular pathology in DENV infection.

In the present work, we compared the permissiveness of primary HUASMC cells, primary HUVEC cells, and the model cell line LLC-MK2 with DENV strains of the four serotypes. The results demonstrate that HUASMC cells are permissive to DENV infection by all four serotypes. However, virus production and replicative fitness are significantly lower in this cell line than in HUVEC and LLC-MK2 cells. Indeed, on infection, HUASMC cells displayed a small percentage of DENV

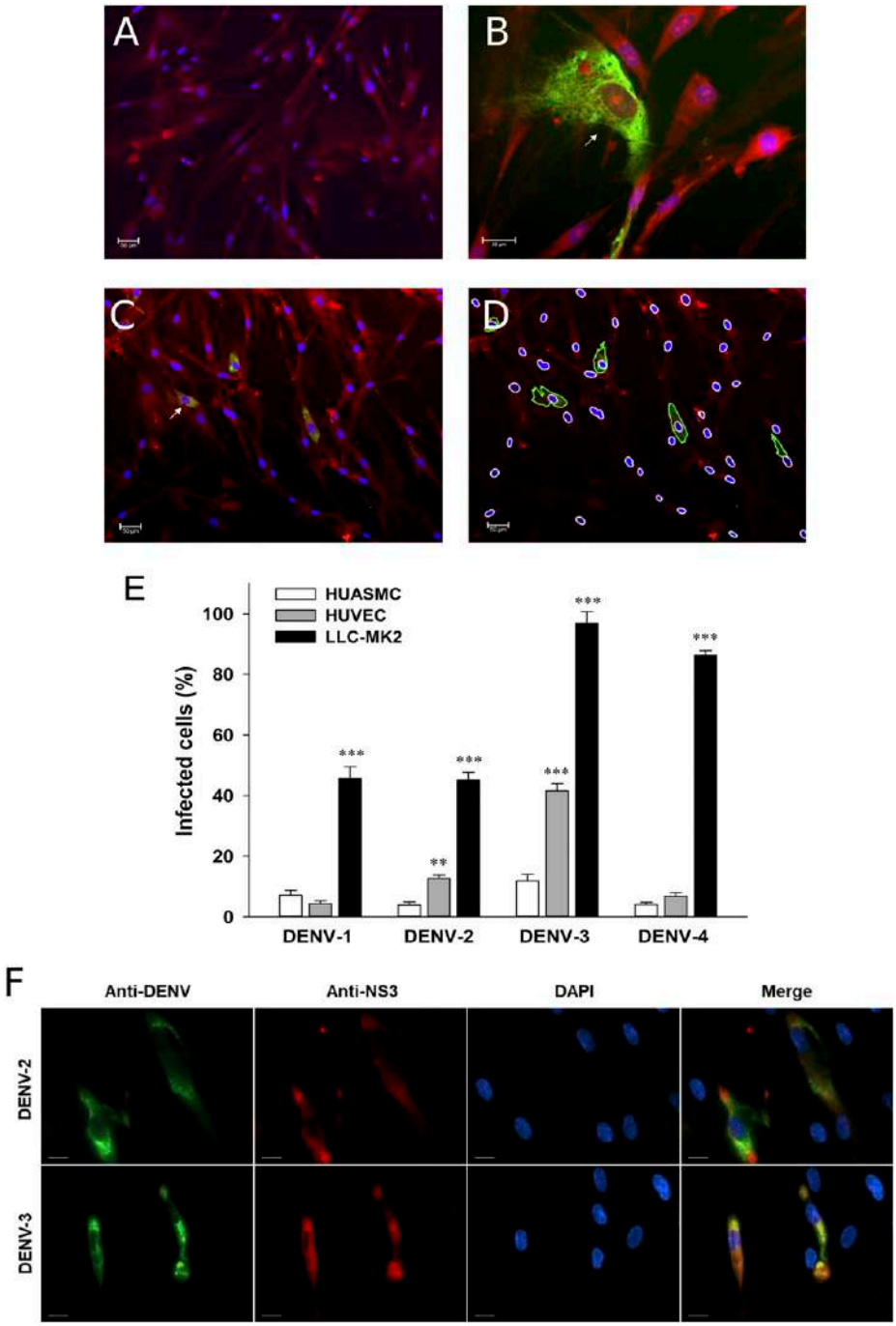

FIGURE 3. Dengue virus (DENV) antigens are detected in human umbilical artery smooth muscle cells (HUASMC). Epifluorescence images of immunostained cells with an anti-DENV 1-4 envelope protein-specific monoclonal antibody (green), and a cytoplasmic (red) and nuclei (blue) counterstains. The images were captured at 72 hours post-infection (p.i.) with each DENV serotype at a multiplicity of infection (MOI) of 1. (**A**) Representative image of mock-infected HUASMC cells at ×100 magnification (scale bar = 50 μm). (**B** and **C**) Representative images of DENV-infected HUASMC (arrows) at ×400 (scale bar = 20 μm) and ×100 (scale bar = 50 μm) magnification, respectively. (**D**) Image analysis for quantifying infected cells (green outline) vs total cell nuclei (white outlines) with the software CellProfiler 2.0. (**E**) Percentages of infected cells in HUASMC, human umbilical vein endothelial cells (HUVEC), and LLC-MK2 (macaque kidney cells) cell lines. (**F**) Comparison of DENV labeling by immunostaining with an anti-DENV 1-4 envelope protein-specific monoclonal antibody (green) and an anti-NS3 polyclonal antibody (red) in HUASMC cells at 72 hours p.i. with DENV-2 and DENV-3 at a MOI of 1. Magnification of ×400 (scale bar = 20 μm). Data are expressed as mean ± standard deviation of three independent experiments. $^{**}P < 0.005$, $^{***}P < 0.001$ calculated to its HUASMC cells counterpart. This figure appears in color at www.ajtmh.org.

antigen-positive cells, indicating that this cell line has a low permissiveness to DENV infection by all four serotypes. Although it is evident that new infectious viral particles were produced by infected HUASMC (Figure 1), the genome copies did not increase (for DENV1 and DENV2) or only increased one log after 48 hours p.i. (for DENV3 and DENV4), as shown in Figure 2. This observation suggests that most of the genomes detected in the supernatant are from defective particles

produced by these cells or genomes released from dead cells, which occlude the expected elevation associated with the increased infectious particles.

In the context of a viral infection with low permissiveness, a possibility to explain this phenomenon arises if the infected cells are able to replicate the viral genomes, but there is a problem with virion assembly or maturation in a high proportion of infected cells. These genomes would be eventually released from the cells, explaining the high genome copies at all-time points assessed. Only the viral particles produced from a subpopulation of infected cells with relatively higher permissiveness would represent the PFUs, which are increasing progressively over time. This is probably due to a viral morphogenesis problem in infected HUASMC cells and, therefore, the viral antigens are detected only in a small proportion of cells. Nevertheless, the immunofluorescence data demonstrate that new viral proteins are produced at least in the subpopulation of cells that produce viable viral particles (Figure 3). Indeed, permissiveness was very similar for HUASMC and HUVEC cells, both of which derive from the umbilical cord, where they form functional blood vessels.[20] Altogether, these results support a model where DENV induces the dysfunction of smooth muscle cells, thereby contributing to the vascular hyporeactivity in vivo.

The compensatory mechanisms to hypovolemia include an early sympathetic response characterized by increased heart rate and systemic increments in vascular resistance, which are mostly mediated by the action of catecholamines, especially noradrenaline, in cardiac muscle and in arteriolar smooth muscle cells.[27,28] In addition, this compensatory vasoconstriction is mediated by thromboxane A2-triggered signaling in smooth muscle cells.[29] It has been demonstrated that plasma levels of thromboxane A2 are significantly lower in dengue shock syndrome patients than in healthy populations and patients with dengue hemorrhagic fever but without shock.[30] This suggests that smooth muscle cells are already hyporeactive during DENV-induced shock. Thus, the infection of those cells by DENV would further contribute to vascular dysfunction in vivo. In support of this contention, work by Balsitis and collaborators displays a splenic artery highly positive for NS3 staining located within the muscular layer in the arterial wall,[11] suggesting that the infection of smooth muscle cells might occur in vivo during the DENV infection in humans.

This is the first report of DENV-permissive infection of smooth muscle cells. Despite the limitations of an in vitro model of infection, our results suggest that the infection of arteriolar, arterial, or lymphatic smooth muscle cells could have important implications for DENV-induced shock. Further work is required to demonstrate the infection and dysfunction of these cells in vivo and to design strategies to protect them for cardiovascular homeostatic mechanisms. This protection may represent a new approach in the treatment of DENV-induced hypotension.

Received February 27, 2018. Accepted for publication August 14, 2018.

Published online November 5, 2018.

Acknowledgments: We thank Carlos Vargas Eduarte for his invaluable technical support and assistance, as well as José María Gutiérrez Gutiérrez from Insituto Clodomiro Picado (Universidad de Costa Rica) for his scientific advice and critical reading of the manuscript. We are also grateful to Christine Carrington (The University of West Indies) for English proofreading of the manuscript.

Financial support: This work was supported by Universidad de Costa Rica (project VI-803-A5-025), Consejo Nacional para Investigaciones Científicas y Tecnológicas (project FI-182-10), and the Florida Ice and Farm Co.

Authors' addresses: Jorge L. Arias-Arias, Francisco Vega-Aguilar, Eugenia Corrales-Aguilar, Laya Hun, Gilbert D. Loría, and Rodrigo Mora-Rodríguez, Facultad de Microbiología, Centro de Investigación en Enfermedades Tropicales, Universidad de Costa Rica, Ciudad Universitaria Rodrigo Facio, San José, Costa Rica, E-mails: jorgeluis.arias@ucr.ac.cr, francisco.vega@ucr.ac.cr, eugenia.corrales@ucr.ac.cr, ruchlia.hun@ucr.ac.cr, gilbert.loria@ucr.ac.cr, and rodrigo.morarodriguez@ucr.ac.cr.

REFERENCES

1. Mustafa MS, Rasotgi V, Jain S, Gupta V, 2015. Discovery of fifth serotype of dengue virus (DENV-5): a new public health dilemma in dengue control. *Med J Armed Forces India 71:* 67–70.
2. Guzman MG et al., 2010. Dengue: a continuing global threat. *Nat Rev Microbiol 8 (12 Suppl):* S7–S16.
3. World Health Organization and Special Programme for Research and Training in Tropical Diseases, 2009. *Dengue: Guidelines for Diagnosis, Treatment, Prevention, and Control*, new edition. Geneva, Switzerland: WHO and Special Programme for Research and Training in Tropical Diseases.
4. Scott LJ, 2016. Tetravalent dengue vaccine: a review in the prevention of dengue disease. *Drugs 76:* 1301–1312.
5. Normile D, 2017. Safety concerns derail dengue vaccination program. *Science 358:* 1514–1515.
6. Acosta EG, Bartenschlager R, 2016. The quest for host targets to combat dengue virus infections. *Curr Opin Virol 20:* 47–54.
7. Chan KW, Watanabe S, Kavishna R, Alonso S, Vasudevan SG, 2015. Animal models for studying dengue pathogenesis and therapy. *Antiviral Res 123:* 5–14.
8. Diamond MS, Edgil D, Roberts TG, Lu B, Harris E, 2000. Infection of human cells by dengue virus is modulated by different cell types and viral strains. *J Virol 74:* 7814–7823.
9. Medina F, Medina JF, Colon C, Vergne E, Santiago GA, Munoz-Jordan JL, 2012. Dengue virus: isolation, propagation, quantification, and storage. *Curr Protoc Microbiol 15D:* 2.1–2.24.
10. Barr KL, Anderson BD, 2013. Dengue viruses exhibit strain-specific infectivity and entry requirements in vitro. *Virus Adapt Treat 5:* 1–9.
11. Balsitis SJ, Coloma J, Castro G, Alava A, Flores D, Beatty R, Harris E, 2008. Tropism of replicating dengue virus in mice and humans defined by viral nonstructural protein 3-specific immunohistochemistry. *Am J Trop Med Hyg 79:* 38.
12. Lindenbach BD, Rice CM, 2007. Flaviviridae: the viruses and their replication. *Fields Virol 2007:* 1101–1151.
13. Paliwal VK, Garg RK, Juyal R, Husain N, Verma R, Sharma PK, Verma R, Singh MK, 2011. Acute dengue virus myositis: a report of seven patients of varying clinical severity including two cases with severe fulminant myositis. *J Neurol Sci 300:* 14–18.
14. Salgado DM et al., 2010. Heart and skeletal muscle are targets of dengue virus infection. *Pediatr Infect Dis J 29:* 238–242.
15. Yacoub S, Wertheim H, Simmons CP, Screaton G, Wills B, 2015. Microvascular and endothelial function for risk prediction in dengue: an observational study. *Lancet 385 (Suppl 1):* S102.
16. Huang YH, Lei HY, Liu HS, Lin YS, Liu CC, Yeh TM, 2000. Dengue virus infects human endothelial cells and induces IL-6 and IL-8 production. *Am J Trop Med Hyg 63:* 71–75.
17. Avirutnan P, Malasit P, Seliger B, Bhakdi S, Husmann M, 1998. Dengue virus infection of human endothelial cells leads to chemokine production, complement activation, and apoptosis. *J Immunol 161:* 6338–6346.
18. Warke RV et al., 2003. Dengue virus induces novel changes in gene expression of human umbilical vein endothelial cells. *J Virol 77:* 11822–11832.
19. Malavige GN, Fernando S, Fernando DJ, Seneviratne SL, 2004. Dengue viral infections. *Postgrad Med J 80:* 588–601.

20. Korff T, Kimmina S, Martiny-Baron G, Augustin HG, 2001. Blood vessel maturation in a 3-dimensional spheroidal coculture model: direct contact with smooth muscle cells regulates endothelial cell quiescence and abrogates VEGF responsiveness. *FASEB J 15:* 447–457.
21. Mora J, Mora R, Lomonte B, Gutiérrez JM, 2008. Effects of bothrops asper snake venom on lymphatic vessels: insights into a hidden aspect of envenomation. *PLoS Negl Trop Dis 2:* e318.
22. Soto-Garita C, Somogyi T, Vicente-Santos A, Corrales-Aguilar E, 2016. Molecular characterization of two major dengue outbreaks in Costa Rica. *Am J Trop Med Hyg 95:* 201–205.
23. Morens DM, Halstead SB, Repik PM, Putvatana R, Raybourne N, 1985. Simplified plaque reduction neutralization assay for dengue viruses by semimicro methods in BHK-21 cells: comparison of the BHK suspension test with standard plaque reduction neutralization. *J Clin Microbiol 22:* 250–254.
24. Gutierrez G, Reines HD, Wulf-Gutierrez ME, 2004. Clinical review: hemorrhagic shock. *Crit Care 8:* 373–381.
25. Li T, Liu L, Xu J, Yang G, Ming J, 2006. Changes of Rho kinase activity after hemorrhagic shock and its role in shock-induced biphasic response of vascular reactivity and calcium sensitivity. *Shock 26:* 504–509.
26. Song R, Bian H, Wang X, Huang X, Zhao K-S, 2011. Mitochondrial injury underlies hyporeactivity of arterial smooth muscle in severe shock. *Am J Hypertens 24:* 45–51.
27. Flint LM, Cryer HM, Simpson CJ, Harris PD, 1984. Microcirculatory norepinephrine constrictor response in hemorrhagic shock. *Surgery 96:* 240–247.
28. Scully CG et al., 2016. Effect of hemorrhage rate on early hemodynamic responses in conscious sheep. *Physiol Rep 4:* 1–15.
29. Dorn GW, Becker MW, 1993. Thromboxane A2 stimulated signal transduction in vascular smooth muscle. *J Pharmacol Exp Ther 265:* 447–456.
30. Preeyasombat C, Treepongkaruna S, Sriphrapradang ACL, 1999. The role of prostacyclin (PGI2) and thromboxane A2 (TXA2) in pathogenesis of dengue hemorrhagic fever (DHF). *J Med Assoc Thai 82 (Suppl 1):* S16–S21.

Protocol. Rapid IFA for labeling DENV/ZIKV structural and nonstructural proteins.

1. Seed and infect the model cells with the DENV/ZIKV strain of interest at the desired multiplicity of infection (MOI), on a µClear black 96-well plate (Greiner Bio-One 655090).
2. Remove the culture media and wash once with 100 µL/well of phosphate-buffered saline (PBS, Gibco 10010023) to remove detached cells and cellular debris.
3. Fix the cell monolayers with 50 µL/well of a 3.5% paraformaldehyde (Sigma 158127) solution in PBS for 15 min at room temperature. Remove the fixative and wash once with 100 µL/well of PBS.
4. Permeabilize cells with 50 µL/well of 70% ethanol in water for 15 min at room temperature. Remove the ethanol and wash once with 100 µL/well of PBS.
5. Incubate for 1 h at 37 °C with 50 µL/well of one of the following primary antibodies diluted in a 0.001% Triton X-100 (Sigma 10789704001) solution in PBS:

- 1:400 dilution of mouse anti-DENV 1-4 E protein monoclonal antibody (GeneTex GTX29202).
- 1:400 dilution of mouse anti-ZIKV E protein monoclonal antibody (GeneTex GTX634157).
- 1:800 dilution of rabbit anti-DENV NS3 protein polyclonal antibody (GeneTex GTX124252).
- 1:400 dilution of rabbit anti-ZIKV NS3 protein polyclonal antibody (GeneTex GTX133309).

6. Wash twice with 100 µL/well of PBS and once with 100 µL/well of 0.001% Triton X-100 solution in PBS.
7. Incubate for 30 min at 37 °C with 50 µL/well of one of the following secondary antibodies (accordingly) diluted in a solution of 0.001% Triton X-100, 0.02% Evans blue (Sigma E2129), and 1 µg/mL Hoechst 33342 (Invitrogen H3570, 1:10 000 dilution) in PBS:

- 1:400 dilution of Alexa Fluor 488 goat anti-mouse IgG, IgM (Invitrogen A-10684), Alexa Fluor 568 goat anti-mouse IgG (Invitrogen A-11031), or Alexa Fluor 647 goat anti-mouse IgG (Invitrogen A-21237).
- 1:400 dilution of Alexa Fluor 488 goat anti-rabbit IgG (Invitrogen A-11034), Alexa Fluor 594 goat anti-rabbit IgG (Invitrogen A-11037), or Alexa Fluor 647 goat anti-rabbit IgG (Invitrogen A-21245).

8. Wash three times with 100 µL/well of PBS, add 100 µL/well of FluoroBrite Dulbecco's modified Eagle's medium (DMEM, Gibco A1896701), and acquire images at the desired magnification with an automated fluorescence microscope (e.g., BioTek Lionheart FX).
9. Analyze the images using an image analysis software (e.g., CellProfiler 3.0, Broad Institute https://www.cellprofiler.org/) to quantify the percentages of infected cells.

Notes: Cells could be also seeded and infected on round glass coverslips into a 24-well plate, stained and mounted in slides to analyze the results with a conventional fluorescence microscope. We have also labeled all the above-mentioned primary antibodies using commercial labeling kits for Alexa Fluor 488 (Invitrogen A20181), Alexa Fluor 568 (Invitrogen A20184), and Alexa Fluor 647 (Invitrogen A20186), facilitating a much faster direct IFA protocol applying dilutions in the range 1:75-1:150, as well as flow cytometry assays with dilutions 1:300-1:400.

Chapter 2

Development and validation of cell-based molecular reporters and cytopathic effect fluorescent labeling approaches for the study of flavivirus infection kinetics in single cells and viral plaques by live-cell imaging

Summary

The identification of therapeutic targets to combat flavivirus infections requires a better understanding of the kinetics of virus-host interactions during infections with wild-type viral strains. However, this is precluded by limitations of current cell-based systems for monitoring flavivirus infection in living cells. This chapter describes the construction of fluorescence-activatable sensors to detect the activities of flavivirus NS2B-NS3 serine proteases in living cells. The system consists of GFP-based reporters that become fluorescent upon cleavage by recombinant DENV-2/ZIKV proteases *in vitro*. A version of this sensor containing the flavivirus internal NS3 cleavage site linker (AAQRRGRIG) presented the highest fluorescence activation in stably transduced mammalian cells upon DENV-2/ZIKV infection. Moreover, the onset of fluorescence correlated with viral protease activity. A far-red version of this flavivirus sensor had the best signal-to-noise ratio in a fluorescent Dulbecco's plaque assay, leading to the construction of a multireporter platform combining the flavivirus sensor with DNA fluorescent dyes for the detection of virus-induced chromatin condensation and cell death (CPE labeling), enabling studies of viral plaque formation with single-cell resolution. Finally, the application of the multireporter platform also enabled the study of cell-population kinetics of infection and CPE induction by DENV-2, ZIKV, and YFV. Such approaches constitute valuable tools for both basic and applied research in flavivirology.

Published articles

Arias-Arias, J.L., MacPherson, D.J., Hill, M.E., Hardy, J.A., Mora-Rodríguez, R., 2020. *A fluorescence-activatable reporter of flavivirus NS2B–NS3 protease activity enables live imaging of infection in single cells and viral plaques*. J. Biol. Chem. 295, 2212–2226. https://doi.org/10.1074/jbc.RA119.011319

Arias-Arias, J.L., Corrales-Aguilar, E., Mora-Rodríguez, R.A., 2021. *A fluorescent real-time plaque assay enables single-cell analysis of virus-induced cytopathic effect by live-cell imaging*. Viruses 13, 1193. https://doi.org/10.3390/v13071193

A fluorescence-activatable reporter of flavivirus NS2B–NS3 protease activity enables live imaging of infection in single cells and viral plaques

Received for publication, October 2, 2019, and in revised form, January 2, 2020 Published, Papers in Press, January 9, 2020, DOI 10.1074/jbc.RA119.011319

Jorge L. Arias-Arias[‡], Derek J. MacPherson[§], Maureen E. Hill[§], Jeanne A. Hardy[§], and Rodrigo Mora-Rodríguez[‡1]

From the [‡]Centro de Investigación en Enfermedades Tropicales, Facultad de Microbiología, Universidad de Costa Rica, San José 11501-2060, Costa Rica and the [§]Department of Chemistry, University of Massachusetts, Amherst, Massachusetts 01003

Edited by Craig E. Cameron

The genus *Flavivirus* in the family Flaviviridae comprises many medically important viruses, such as dengue virus (DENV), Zika virus (ZIKV), and yellow fever virus. The quest for therapeutic targets to combat flavivirus infections requires a better understanding of the kinetics of virus–host interactions during infections with native viral strains. However, this is precluded by limitations of current cell-based systems for monitoring flavivirus infection in living cells. In the present study, we report the construction of fluorescence-activatable sensors to detect the activities of flavivirus NS2B–NS3 serine proteases in living cells. The system consists of GFP-based reporters that become fluorescent upon cleavage by recombinant DENV-2/ZIKV proteases *in vitro*. A version of this sensor containing the flavivirus internal NS3 cleavage site linker reported the highest fluorescence activation in stably transduced mammalian cells upon DENV-2/ZIKV infection. Moreover, the onset of fluorescence correlated with viral protease activity. A far-red version of this flavivirus sensor had the best signal-to-noise ratio in a fluorescent Dulbecco's plaque assay, leading to the construction of a multireporter platform combining the flavivirus sensor with reporter dyes for detection of chromatin condensation and cell death, enabling studies of viral plaque formation with single-cell resolution. Finally, the application of this platform enabled the study of cell-population kinetics of infection and cell death by DENV-2, ZIKV, and yellow fever virus. We anticipate that future studies of viral infection kinetics with this reporter system will enable basic investigations of virus–host interactions and facilitate future applications in antiviral drug research to manage flavivirus infections.

The genus *Flavivirus* in the family *Flaviviridae* comprises more than 70 species of arthropod-borne viruses (arboviruses) that are transmitted to vertebrates by infected mosquitoes or ticks, producing diseases in animals and humans, including many medically important viruses like West Nile virus (WNV),[2] yellow fever virus (YFV), St. Louis encephalitis virus, dengue virus (DENV), Japanese encephalitis virus (JEV), Zika virus (ZIKV), and tick-borne encephalitis virus (TBEV) (1).

The genome of flaviviruses is a positive sense RNA of ~11 kb that encodes three structural proteins, *i.e.* capsid (C), membrane precursor (prM), and envelope (E), and seven nonstructural proteins, *i.e.* NS1, NS2A, NS2B, NS3, NS4A, NS4B, and NS5. These proteins initially form a precursor polyprotein (NH_2-C-prM-E-NS1-NS2A-NS2B-NS3-NS4A-NS4B-NS5-COOH) that is cleaved by both cellular and viral proteases to release the mature viral proteins (2). The flavivirus serine protease NS2B–NS3 consists of the N-terminal domain of the NS3 protein associated with the membrane-resident NS2B cofactor to form an active complex. This viral protease cleaves the precursor polyprotein at the NS2A/NS2B, NS2B/NS3, NS3/NS4A, and NS4B/NS5 junctions, as well as at internal sites within C, NS2A, NS3, and NS4A (3–5).

Flaviviruses have continued to emerge in recent years, and together represent a global threat responsible for pandemics associated with encephalitis and hemorrhagic fever diseases for which there are no specific treatments available other than supportive care upon hospitalization (2). Moreover, the development of successful human vaccines seems to be challenging for some flaviviruses. Although YFV, JEV, and TBEV vaccines are highly effective, the development of vaccines for other flaviviruses like WNV and DENV have presented some drawbacks and safety concerns (6–8) This situation partially arises from the limitations of clinical studies, and although there are established animal models for flaviviruses, they do not faithfully reproduce all the clinical manifestations observed in the human host (9, 10). Therefore, post-mortem studies and cell culture models are still an important approach to study flavivirus diseases (11–13), especially for the quest of novel therapeutic targets to combat these infections, either on the virus or on the host (14, 15).

Currently, the identification of flavivirus-infected cells relies on either immunostaining of viral proteins (12), the application

This work was supported by Universidad de Costa Rica Project VI-803-B9–505 (to J. L. A.-A. and R. M.-R.), National Science Foundation Grant NSF CBET1511367 (to J. A. H.), and International Centre for Genetic Engineering and Biotechnology Grant CRP/CRI18-02 (to R. M.-R). The authors declare that they have no conflicts of interest with the contents of this article.
This article contains Table S1 and Figs. S1–S5.

[1] To whom correspondence should be addressed: Centro de Investigación en Enfermedades Tropicales, Facultad de Microbiología, Universidad de Costa Rica, Ciudad Universitaria Rodrigo Facio, San Pedro de Montes de Oca, San José 11501-2060, Costa Rica. Tel.: 506-2511-8635; E-mail: rodrigo.morarodriguez@ucr.ac.cr.

[2] The abbreviations used are: WNV, West Nile virus; DENV, dengue virus; ZIKV, Zika virus; YFV, yellow fever virus; JEV, Japanese encephalitis virus; TBEV, tick-borne encephalitis virus; CA, caspase-activatable; FlaviA, flavivirus-activatable; MOI, multiplicity of infection; FBS, fetal bovine serum; MEM, minimum essential medium; DMEM, Dulbecco's modified Eagle's medium.

of recombinant reporter replicons or viral genomes (16–20), or the use of cell-based molecular reporters of the NS2B–NS3 activity (21–23). Antibody staining techniques require both fixation and permeabilization because of the lack of flavivirus expressed proteins directly on the cell surface of infected cells as a part of the viral replication cycle (2, 24, 25), which precludes their application for live-cell imaging. Reporter replicons and viral genomes allow kinetic studies in living cells but are limited to molecular clones and thus not suitable to study clinical isolates or native virus strains. In this respect, genetically encoded molecular reporters monitoring the flavivirus NS2B–NS3 proteolytic activity upon infection are an advantageous approach that is suitable for live-cell imaging studies of native flavivirus strains.

Previously, we developed a series of caspase-activatable reporters by fusing, via a linker containing the caspase-3/7 cleavage site DEVD, a hydrophobic quenching peptide to the C terminus of a fluorescent protein (26–28). This quenching peptide inhibits the maturation of the chromophore in the fluorescent protein until it is proteolytically removed by an active caspase, fully restoring the fluorescence (26, 27). In the present study, we developed genetically encoded flavivirus molecular reporters by inserting a flaviviral NS2B–NS3 cleavage site into our caspase-activatable (CA) GFP (26) or CA-mNeptune (28), giving rise to the flavivirus-activatable (FlaviA) GFP and FlaviA-mNeptune reporters, respectively. To our knowledge, this is the first fluorescence-activatable molecular reporter system for live-cell imaging of the infection by both reference and native strains of flaviviruses like DENV, ZIKV, and YFV.

Results

Fluorescence-activatable GFP-based reporters of flavivirus NS2B–NS3 protease activity become fluorescent upon cleavage by recombinant DENV-2/ZIKV proteases in vitro

We based the design of a molecular sensor for flavivirus proteases on our previously reported CA-GFP sensor that comprises GFP, a linker for caspase cleavage and a C-terminal quenching peptide (26–28). However, we encountered several limitations for the development of the new sensor, mainly with the linker sequence for the reporter function. This led us to envisage several alternative designs by changing the linker sequence. Indeed, we generated several variants of the reporter that remained uncleaved and/or nonfluorescent upon DENV-2 NS2B–NS3 protease treatment *in vitro* (Table S1). Therefore, we designed a linker based on previously characterized flavivirus polyprotein cleavage sites (29). After careful analysis and avoiding the formation of cleavage sites for other cellular proteases within the resulting protein sequence of the sensor (http://web.expasy.org/peptide_cutter/),[3] we selected the cleavage sequences that define the linker. Three variants of this reporter were constructed by changing the linker sequence: ZIKVA-GFP (ZIKV polyprotein NS2B/NS3 cleavage site linker), DENV2A-GFP (DENV-2 polyprotein NS2B/NS3 cleavage site linker), and FlaviA-GFP with the internal NS3 cleavage site present in many members of the *Flavivirus* genus (3, 5, 30).

[3] Please note that the JBC is not responsible for the long-term archiving and maintenance of this site or any other third party hosted site.

Using these variants of the reporter, we verified the cleavage *in vitro* by Coomassie Blue–stained SDS-PAGE gels (Fig. 1, *A* and *B*, and Fig. S1) and the fluorescence activation (Fig. 1*C*) to evaluate at the protein level the potential of these linkers to be used within reporters of viral protease activity.

Purified recombinant DENV-2 NS2B–NS3 protease (Fig. 1*A*, *left panels*) or ZIKV NS2B–NS3 protease (Fig. 1*A*, *right panels*) were added to the three purified FlaviA-GFP reporter proteins. The DENV-2 NS2B–NS3 protease band was observed at 25 kDa, and the ZIKV NS2B–NS3 protease was located below 20 kDa, whereas all three full-length reporter proteins appeared above 30 kDa. To determine the location of the cleaved reporters, we generated a truncated variant of the FlaviA-GFP reporter protein (tRep/control) by inserting a stop codon downstream of the cleavage site in the DNA sequence of the linker. The bands of the cleaved reporters appeared between the 25- and 30-kDa markers. The cleavage kinetics of the reporters can be observed over time for the three variants tested (Fig. 1, *A* and *B*).

The intensities of these bands were quantified, and a ratio of the cleaved reporter to the total amount of reporter protein for each time point was calculated. The results are displayed as time-resolved cleavage efficiency (%) to compare among the different variants of the reporter (Fig. 1*B*). The DENV-2 NS2B–NS3 protease has very similar cleavage kinetics for the three variants with some slight differences. Although the FlaviA-GFP reporter showed an earlier increase, the ZIKVA-GFP reporter also reached ~80% of cleavage efficiency. The DENV2A-GFP reached only ~50% efficiency (Fig. 1*B*, *left panel*). On the other hand, striking differences are observed for the cleavage efficiency of the three variants of the reporter by the ZIKV NS2B–NS3 protease. The ZIKVA-GFP reporter had a much earlier increase, reaching almost 100% cleavage by 10 h. In contrast, the FlaviA-GFP and the DENV2A-GFP variants reached only 40% of cleavage efficiency after 20 h (Fig. 1*B*, *right panel*). These results indicate that the reporters are sensitive to flavivirus protease cleavage as designed, although with different efficiencies and kinetics.

To determine whether these cleavage kinetics correlate with fluorescence activation of the reporters, we monitored the fluorescence signal of each reporter as a function of time and normalized it to the background signal for each construct, obtaining thereby a time-resolved signal-to-noise ratio for the fluorescence of the reporters. All three reporters showed an increased in this signal-to-noise ratio for both protease treatments, indicating that the cleavage of the constructs correlates with the fluorescence increase of the GFP. The ZIKVA-GFP reporter showed the highest increase in fluorescence for both protease treatments, followed by the FlaviA-GFP and the DENV2A-GFP. These results indicate that the increase of the signal-to-noise ratio is a sensitive marker of cleavage, especially for the ZIKVA-GFP reporter (Fig. 1*C*).

The FlaviA-GFP sensor reports the highest fluorescence increase in stably transduced mammalian cells upon DENV-2/ZIKV infection

To validate our candidate GFP-based reporters of flavivirus NS2B–NS3 proteases, we generated three BHK-21 stable cell lines expressing each reporter. Upon DENV-2 or ZIKV infec-

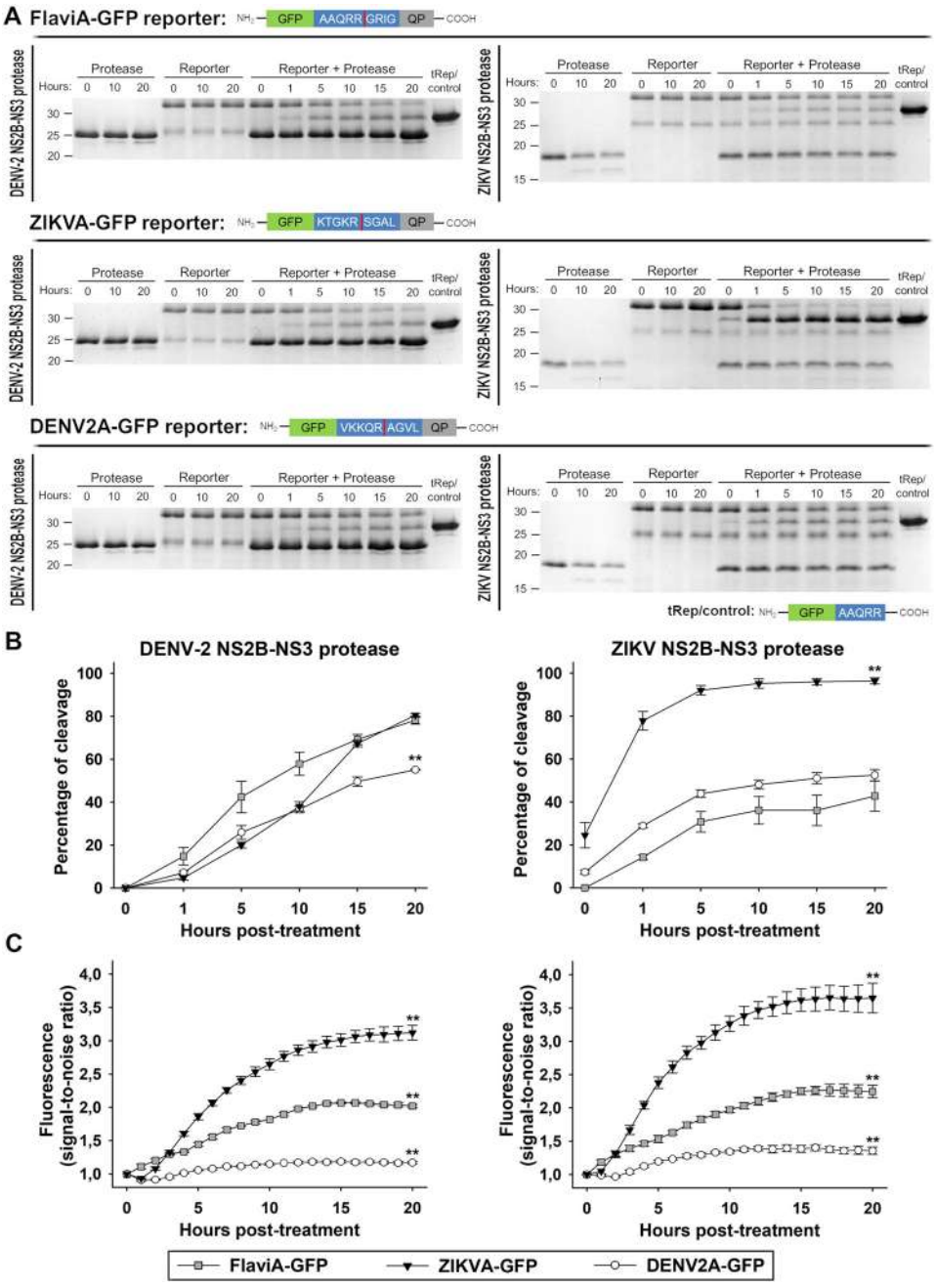

Figure 1. Fluorescence-activatable GFP-based reporters for flavivirus NS2B–NS3 protease activity become fluorescent upon cleavage by DENV-2/ZIKV recombinant proteases *in vitro*. The flavivirus-activatable GFP reporters contain a quenching peptide (*QP*) at the C terminus of GFP joined by a linker consisting of a cleavage site for the flavivirus NS2B–NS3 proteases. When the viral proteases cleave the linker, the quenching peptide is removed, and the GFP adopts a conformation promoting chromophore maturation. Three variants of this reporter were developed by changing the linker sequence: ZIKVA-GFP (ZIKV polyprotein NS2B/NS3 cleavage site linker), DENV2A-GFP (DENV-2 polyprotein NS2B/NS3 cleavage site linker), and FlaviA-GFP with the internal NS3 cleavage site linker, which is present in many members of the *Flavivirus* genus. *A*, *in vitro* cleavage kinetics of the flavivirus-activatable GFP reporter. Purified reporter proteins were mixed with purified DENV-2 NS2B–NS3 protease (*left panels*) or ZIKV NS2B–NS3 protease (*right panels*) at a molar ratio of 1:1 and incubated for given times. The reactions were quenched by thermal treatment in SDS loading buffer, and samples were analyzed by SDS-PAGE and staining of the gels with Coomassie Blue. tRep/control is an engineered cleaved variant of the FlaviA-GFP protein and was used as size marker of cleaved reporters. Representative cropped images from three independent experiments are shown. *B*, cleavage efficiency kinetics of the purified flavivirus-activatable GFP reporter proteins treated with purified DENV-2 NS2B–NS3 protease (*left panel*) and ZIKV NS2B–NS3 protease (*right panel*). *C*, time-resolved fluorescence signal-to-noise ratio of the purified flavivirus-activatable GFP reporter proteins treated with purified DENV-2 NS2B–NS3 protease (*left panel*) and ZIKV NS2B–NS3 protease (*right panel*). The data are expressed as means ± S.D. of three independent experiments. **, $p < 0.001$ compared with the other two reporter variants at 20 h post-treatment.

tion at a low multiplicity of infection (MOI) of 0.25, we monitored the cellular fluorescence as a function of time using live imaging. A qualitative assessment of the images suggested that the cell fluorescence started to increase significantly at 48 h post-infection (Fig. 2*A* and Fig. S2*A*). To quantify this increase, we constructed an image analysis pipeline using CellProfiler 2.0 to identify single cells based on their nuclei, recognize their cytoplasms (white outlines), classify them as live (*blue dots*) or dead cells (*red outlines* and *dots*) and quantify the total cell fluorescence (Fig. 2, *A* and *B*). Our results showed that the viral-

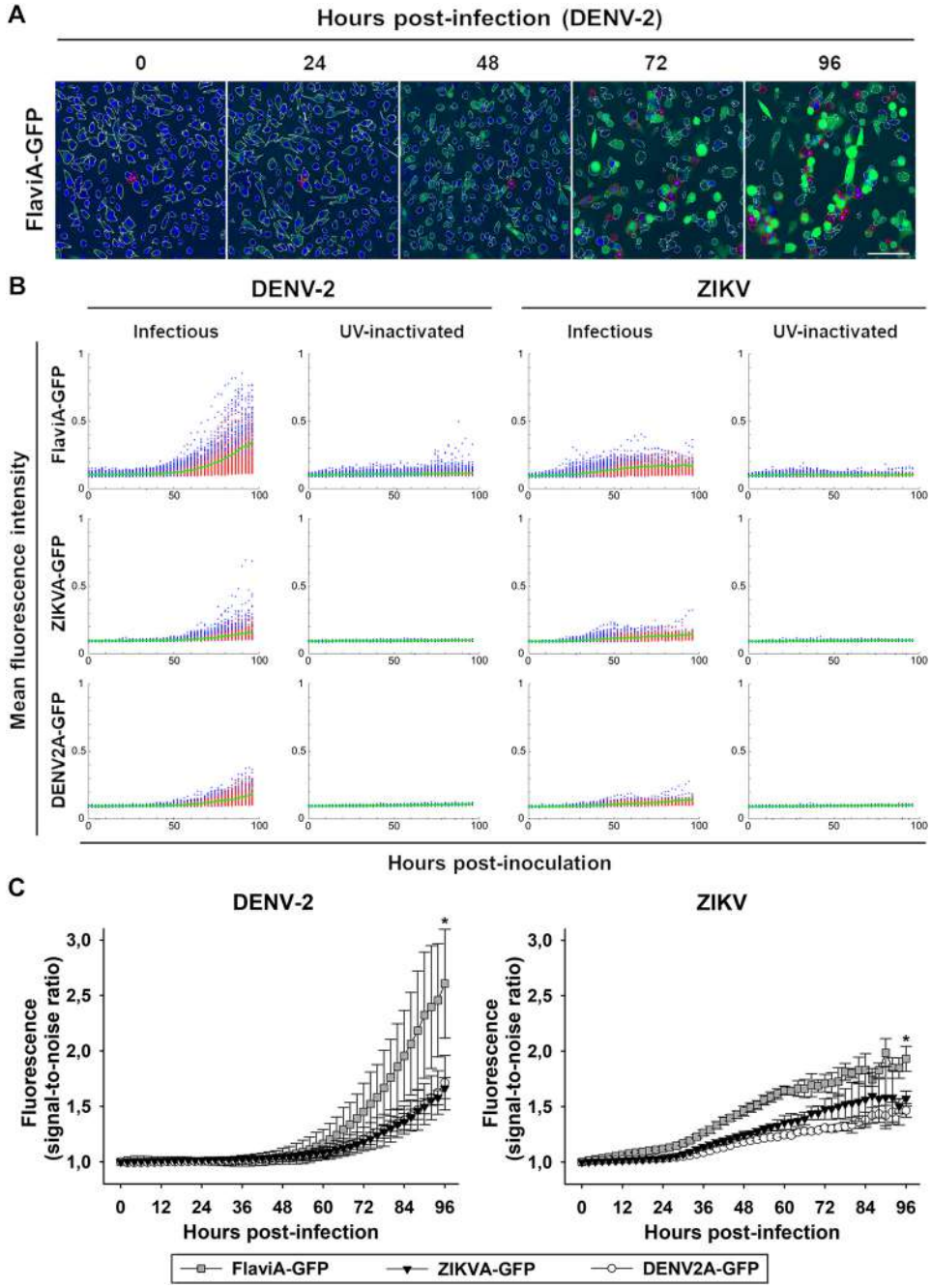

Figure 2. The FlaviA-GFP sensor reports the highest fluorescence increase in stably transduced mammalian cells upon DENV-2/ZIKV infection. We generated three BHK-21 stable cell lines expressing the flavivirus-activatable GFP reporters, each with one of the previously tested linker sequences. After cell sorting of subpopulations with homogeneous expression of each reporter, the cells were grown and infected with either infectious or UV-inactivated DENV-2 13538/ZIKV CIET-01 at a low MOI of 0.25, for the specified time periods. *A*, an automated image analysis protocol was constructed in CellProfiler 2.0 for the quantification of live (*white outline*), dead (*red outline*), and activated FlaviA-GFP fluorescent cells (*green*). A representative experiment is shown for the FlaviA-GFP stable cell line infected with DENV-2 (n = three independent experiments, magnification of 200×; *scale bar*, 100 μm). *B*, the flavivirus-activatable GFP reporter activation is represented by scatter plots showing the time-resolved fluorescence of the population of single live (*blue*) and dead (*red*) reporter cells after the exposure to infectious or UV-inactivated DENV-2 (*left panels*) or ZIKV (*right panels*). The population mean values for each condition are represented by the *green continuous lines*. Representative scatter plots are shown (n = three independent experiments). *C*, the cell population kinetics of the flavivirus-activatable GFP sensors fluorescence across multiple experiments confirmed that the flavivirus internal NS3 cleavage site linker (AAQRRGRIG) confers the highest signal-to-noise ratio to report the infection with both DENV-2 (*left panel*) and ZIKV (*right panel*) in stably transduced BHK-21 cells. The data are expressed as means ± S.D. of three independent experiments. *, $p < 0.05$ compared with both ZIKVA-GFP and DENV2A-GFP at 96 h postinfection.

induced cytotoxicity started ~50–60 h postinfection with DENV-2 and ~40–50 h post–ZIKV infection (Fig. 2*B*, *red dots*). However, the cellular fluorescence started to increase in living cells (Fig. 2*B*, *blue dots*) approximately at 48 h postinfection, and we could quantify living cells with increased fluorescence until the end of this time course (96 h). The population mean values for each condition are represented by the *green continuous lines*. To compare the different variants of the reporter, we monitored the cell population kinetics of the flavivirus-activatable GFP sensor's fluorescence across multiple

experiments and confirmed that the flavivirus internal NS3 cleavage site linker (AAQRRGRIG) confers the highest signal-to-noise ratio for reporting the infection of DENV-2 and ZIKV in stably transduced BHK-21 cells (Fig. 2*C*). These results confirm that our GFP-based fluorescence-activatable reporters of NS2B–NS3 protease activity can be used in living cells and that our variant harboring the flavivirus-conserved linker has the highest sensitivity to report viral infection for both DENV-2 and ZIKV at the single-cell level.

The fluorescence activation of the FlaviA-GFP reporter correlates with viral NS3 protease synthesis and activity in the cellular context

To validate the ability of the FlaviA-GFP construct to report the NS3 protease content in the cellular context, we first monitored the correlation of the reporter fluorescence with an anti-NS3 immunofluorescence staining. BHK-21 stable cells expressing the FlaviA-GFP reporter were infected with DENV-2 13538, and the NS3 protease was revealed by an immunofluorescence assay with an anti-DENV NS3 protein antibody 72 h postinoculation. High magnification images were obtained to study the cellular patterns of both fluorescent signals. The images showed a significant amount of colocalized fluorescence, suggesting a correlation between cellular NS3 amounts and the fluorescent form of the FlaviA-GFP reporter (Fig. 3*A*). To confirm this correlation, we obtained low magnification images and quantified the total cellular intensity for both fluorescent signals in many single cells using CellProfiler 2.0. This quantification confirmed an important correlation (Fig. 3*B*), suggesting that the fluorescence of the FlaviA-GFP reporter arises because of the viral-induced synthesis of NS3 protease in the cells. To confirm this hypothesis, we monitored for 72 h the cleavage kinetics of the FlaviA-GFP reporter in BHK-21 stable cells upon DENV-2 infection in parallel to the viral NS3 protease expression by Western blotting. Only the cells incubated with infectious DENV-2 showed a band of uncleaved NS3 protease. This signal was dim at 24 h but became more evident at 48 and 72 h, whereas a band corresponding to the cleaved NS3 protease became visible at 48 h postinfection, because of the autoproteolytic activity of NS3. On the other hand, the band of uncleaved FlaviA-GFP reporter was visible in lysates of cells incubated with UV-inactivated DENV-2, at all the times tested (Fig. 3*C*). In the presence of the infectious DENV-2 a slight band of cleaved FlaviA-GFP reporter appeared by 48 h, correlating with the onset of autoproteolytic activity of the viral NS3. This band showed a strong increase at 72 h postinfection similar to the increase of cleaved NS3 protease (Fig. 3*C*). This correlation was expected because both the FlaviA-GFP reporter and the viral NS3 protease contain the same flavivirus internal NS3 cleavage site (AAQRRGRIG). The cleavage of the NS3 protease itself therefore represents an excellent internal control for the NS3 protease activity in this experiment. Together, these results demonstrate that the fluorescence increase of the FlaviA-GFP reporter correlates with its proteolytic cleavage in the cellular context, and this cleavage depends on the presence of active viral NS3 protease.

The FlaviA-mNeptune, a far-red version of the flavivirus sensor, reports the best signal-to-noise ratio in a DENV-2/ZIKV fluorescent plaque assay

To ascertain the ability of the FlaviA-GFP version of the sensor to report the cell population-based kinetics of infection, we designed an experimental protocol for a Dulbecco's plaque assay in 96-well plates. Briefly, confluent cell monolayers of BHK-21 cells stably expressing the FlaviA-GFP reporter were infected with decimal dilutions of a DENV-2 or ZIKV viral seed and incubated with a medium containing carboxymethylcellulose for 120 h. The plaque-containing wells were completely imaged at 40× magnification, and the whole-well images of cell monolayers were generated with the stitching function of the Gen5 3.0 software (BioTek). However, as shown in Fig. 4*B*, the raw images of the FlaviA-GFP stable cell monolayers presented high backgrounds at low magnification in the green fluorescence channel, probably because of the autofluorescence of the phenol red and the fetal bovine serum of the culture medium. An alternative medium without phenol red (Gibco, catalog no. 11935-046) was tested but showed an increase in cytotoxicity (data not shown). These images could be enhanced by increasing the contrast but thereby lost a significant fraction of the cellular signal from the fluorescent viral plaques, as shown by the size comparison of the reporter plaques in the enhanced image to the plaques stained with an anti-NS3 antibody 120 h postinfection (Fig. 4*B*). Therefore, we envisaged a far-red version of our flavivirus reporter (FlaviA-mNeptune, Fig. 4*A*) based on our previously published CA-mNeptune sensor (28). We generated a new stable cell line with the far-red FlaviA-mNeptune reporter to compare the signal-to-noise ratio between the red fluorescent plaques and the green fluorescent plaques generated in FlaviA-GFP stable cells.

A time-based comparison of the plaque formation kinetics for both DENV-2 and ZIKV indicated that the FlaviA-mNeptune version of the reporter has a higher signal-to-noise ratio, revealing earlier evidence of red fluorescent plaques 48–72 h postinfection compared with the plaques produced by the fluorescence increase of the FlaviA-GFP reporter, which required 96–120 h to become evident (Fig. 4*C*). To confirm the higher potential of the FlaviA-mNeptune reporter to reveal fluorescent viral plaques, we compared the size of the plaques for both types of reporters with the respective size of the same plaques stained with both an anti-NS3 antibody and crystal violet staining. We also identified the plaque outlines for both reporters using an image analysis protocol constructed in CellProfiler 2.0 based on cell-by-cell neighbor counts and image thresholding (Fig. 5*A*). The protocol identified much larger plaques for FlaviA-mNeptune–infected cells compared with those of infected FlaviA-GFP cells. In addition, the size of the plaques generated in the FlaviA-mNeptune–infected cells was very similar to the size of the plaques revealed by the NS3 labeling and the crystal violet staining (Fig. 4*D*). Together, these results demonstrate that the mNeptune version of the flavivirus sensor reports the best signal-to-noise ratio in a Dulbecco's plaque assay, indicating that this reporter is a good marker of viral replication to study cell population-based kinetics of infection by this standard virological technique.

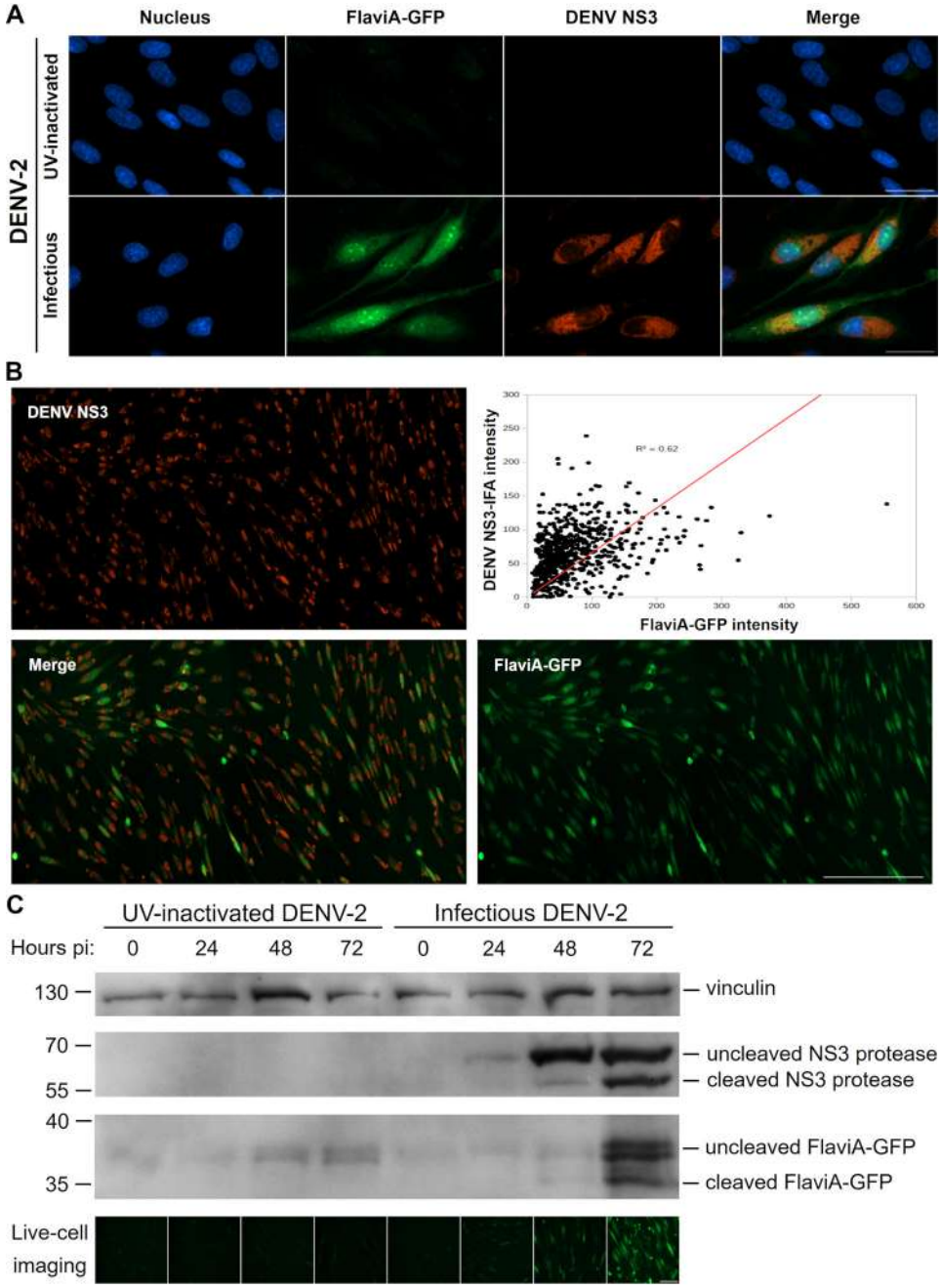

Figure 3. The FlaviA-GFP reporter becomes cleaved and fluorescent in stably transduced BHK-21 cells upon DENV-2 infection, which correlates with the viral NS3 protease synthesis and autoproteolysis. Stable BHK-21 cells expressing the FlaviA-GFP reporter were infected with either infectious or UV-inactivated DENV-2 13538 at a low MOI of 0.25, for the specified time periods postinoculation. *A*, comparison of DENV-2 infection detection by the FlaviA-GFP reporter (*green*) and immunostaining with an anti-DENV NS3 protease antibody (*orange*) in stably transduced BHK-21 cells at 72 h postinfection with DENV-2. Images from a representative experiment are shown (n = three independent experiments, magnification of 600×; *scale bar*, 30 μm). *B*, correlation of the total cell fluorescence intensity given by the FlaviA-GFP reporter (*green*) and an immunofluorescence assay (*IFA*) with an anti-DENV NS3 protease antibody (*orange*) in stably transduced BHK-21 cells at 72 h postinfection with DENV-2. A representative experiment is shown (n = three independent experiments, magnification of 200×; *scale bar*, 300 μm). *C*, cleavage and fluorescence kinetics of the FlaviA-GFP reporter in stable BHK-21 cells upon DENV-2 infection and subsequent viral NS3 protease production and activity. A representative Western blotting kinetics with its corresponding live-cell images set is shown (n = three independent experiments, magnification of 200×; *scale bar*, 100 μm).

A multireporter platform to study viral plaques formation at a single-cell resolution reveals differences in cell-population kinetics of infection and cell death induction by several flaviviruses

To further investigate the potential application of our FlaviA-mNeptune reporter system to study the cell population-based kinetics of viral infection and plaque formation, we designed an experimental protocol combining three types of reporters. The FlaviA-mNeptune reporter was used as a surrogate marker of viral replication, Hoechst 33342 was used to stain chromatin condensation as an early marker of an ongoing apoptosis, and SYTOX green was used to label nuclei of cells with permeabilized membranes as a late marker of cell death (Fig. 5*A*). We constructed an image analysis protocol in Cell-

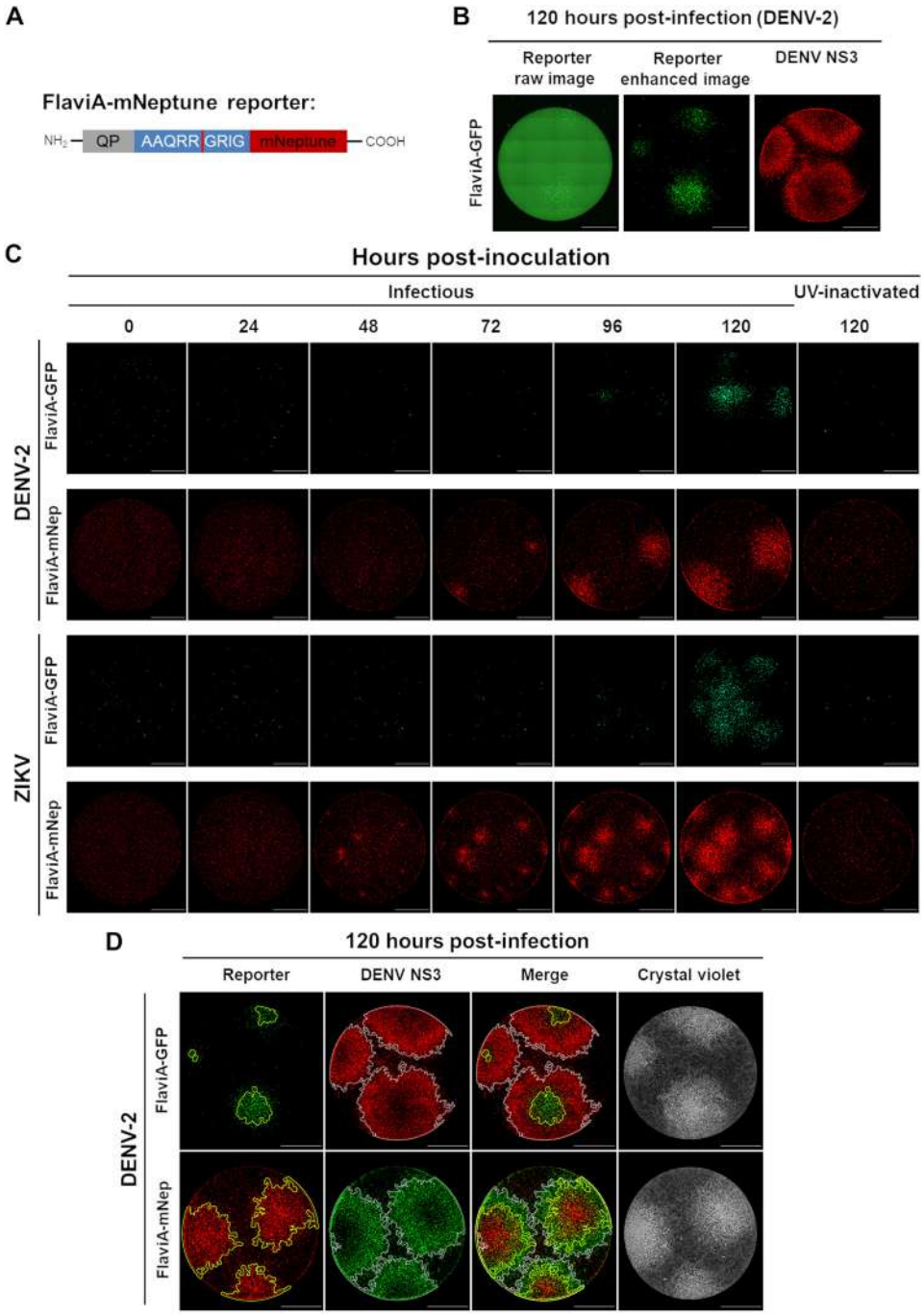

Figure 4. The FlaviA-mNeptune is a far-red version of the flavivirus reporter that enables earlier detection of the cell infection kinetics in a DENV-2/ZIKV plaque assay. We generated two BHK-21 stable cell lines expressing either a green or a far-red version of the flavivirus reporter. Both versions were compared by plaque assay upon infection with DENV-2 13538 and ZIKV CIET-01 at the specified time periods. *A*, the FlaviA-mNeptune reporter is a quenched version of the fluorescent protein mNeptune which contains a quenching peptide (*QP*) at the N terminus joint by a linker consisting of the internal NS3 cleavage site (AAQRRGRIG), which is conserved among many members of the *Flavivirus* genus. When the flavivirus protease cleaves the linker, the quenching peptide is removed, and the mNeptune adopts its fluorescent structural conformation. *B*, BHK-21 cells stably transduced with the FlaviA-GFP reporter and infected with DENV-2 required a contrast enhancement procedure to reveal viral plaques at 120 h postinfection but with a poor correlation when compared with the same plaques labeled with an anti-DENV NS3 protease antibody. *C*, the plaque assay kinetics showed that BHK-21 cells stably transduced with the FlaviA-mNeptune reporter accumulate enough intensity to reveal fluorescent plaques by 48 and 72 h postinfection with ZIKV and DENV-2, respectively, much earlier than their counterparts transduced with the FlaviA-GFP reporter. *D*, the performance of both GFP and mNeptune reporters was further evaluated by comparing the size of their resulting fluorescent plaques to the signal reported by an anti-DENV NS3 protease antibody and crystal violet staining, confirming that the FlaviA-mNeptune reporter has a better correlation to both the infection front (DENV NS3 immunostaining) and the cytopathic effect (crystal violet staining), compared with the FlaviA-GFP reporter. A representative experiment for each condition is shown (n = three independent experiments, magnification of 40×; *scale bar*, 1000 μm).

Profiler 2.0 to identify and characterize each individual plaque at a single-cell level. Briefly, the pipeline adds the images of the three channels into one (ImageMath) to identify all single cells with all possible combinations of the reporters (cell identification). These cells are characterized by the quantification of their neighbors within a specified distance (neighbor count)

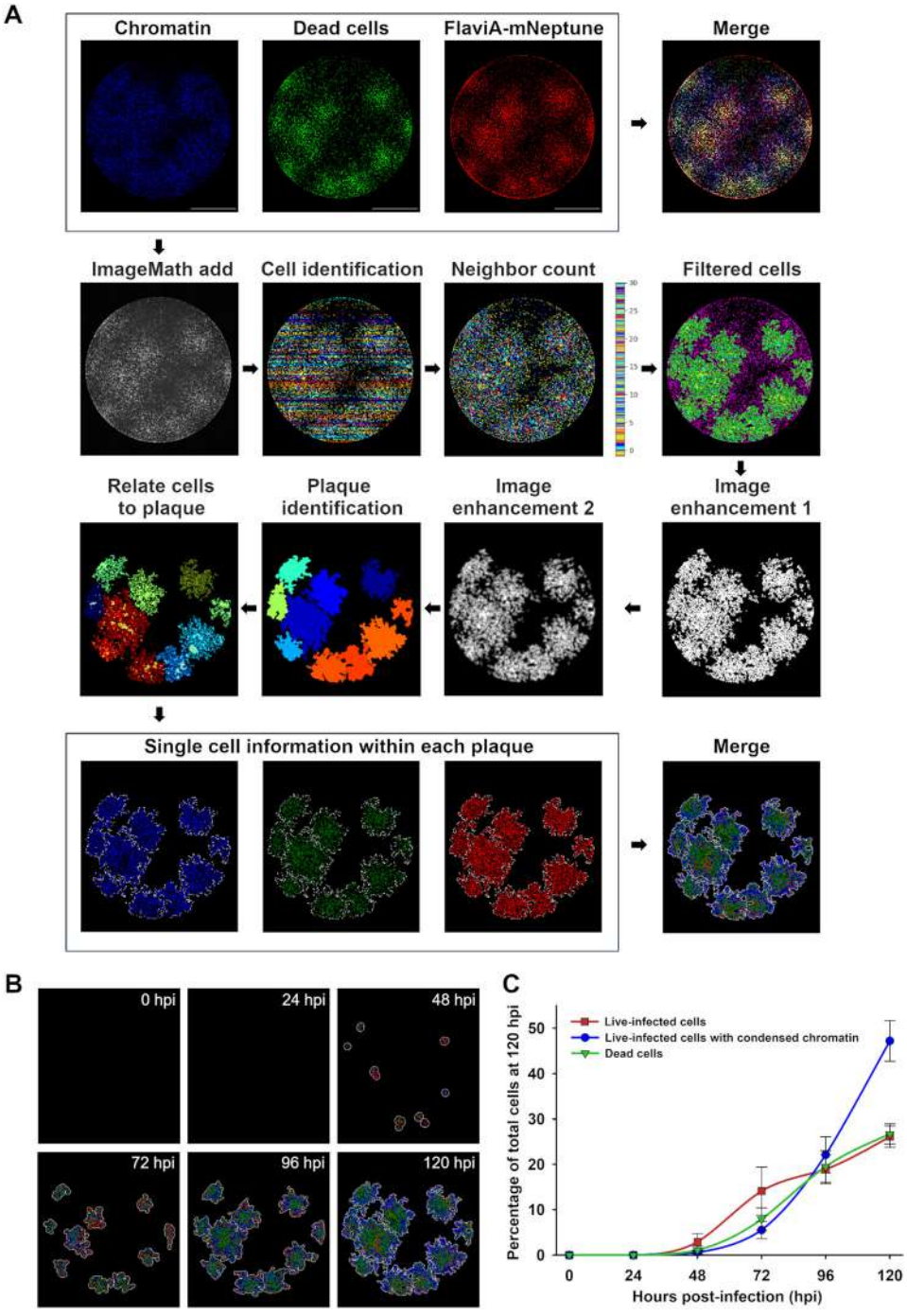

Figure 5. The FlaviA-mNeptune reporter enables analysis of the kinetics of ZIKV infection and induced cell death in single plaques and single cells. We constructed an image analysis protocol using the software CellProfiler 2.0 to characterize the kinetics of infection and cell death by the quantification of fluorescence features of cells imaged to assess DNA/chromatin condensation (Hoechst 33342), cell death (SYTOX green), and viral infection (FlaviA-mNeptune reporter). *A*, high resolution images were stitched into a single image of the well for all three fluorescent channels, which intensities were added into a single image to have a redundant single-cell identification. A neighbor count and threshold were performed to filter the cells belonging to plaques and achieve single plaque identification. The single cells previously identified were related to their respective parent plaques to quantify single-cell parameters within each plaque, including chromatin condensation (*blue*), cell death (*green*), and the intensity of the FlaviA-mNeptune reporter (*red*). *B*, the image analysis protocol was applied to analyze a representative kinetics of ZIKV plaque formation during 120 h postinfection (*hpi*), achieving the identification of individual plaques and the categorization of single cells within each plaque as live-infected (*red*), live-infected with chromatin condensation (*blue*), and dead (*green*). The 120-h postinfection image was reused from point A, because its generation was used in Fig. 5*A* to exemplify the image analysis pipeline applied to analyze the viral plaques at every postinfection time depicted in *B*. *C*, time-resolved kinetics of ZIKV infection described by parameters of percentage of live-infected cells (*red*), live-infected cells with chromatin condensation (*blue*), and dead cells (*green*) within the viral plaques. Images and data from a representative analyzed experiment are shown (n = three independent experiments, magnification of 40×; *scale bar*, 1000 μm). The data are expressed as means ± S.D. for the number of plaques identified at each time point depicted.

and filtered based on a minimal number of neighbors per cell (filtered cells) to identify the plaque-forming cells. Then a series of image enhancing steps enable us to perform the identification of plaques as new primary objects (plaque identification). Finally, with the identified plaques we were able to relate the single cells to their corresponding plaques and quantify thereby the number of live-infected cells (*red*), live-infected cells with chromatin condensation (*blue*), and dead cells (*green*) (Fig. 5*A*). Moreover, the time-based monitoring of these parameters for each fluorescent viral plaque enabled us to study the cell-population kinetics of infection for ZIKV plaque formation until 120 h (Fig. 5*B*). The quantification of these parameters indicated that the ratios of these three cell subpopulations over time are very similar among different plaques for this specific ZIKV strain, as depicted by the relatively low standard deviations observed (Fig. 5*C*). These results suggest that with the combination of a FlaviA-mNeptune reporter as a marker of infection with a reporter of chromatin condensation and a reporter for cell death, we can obtain a multireporter platform to characterize the infection kinetics induced by a specific viral strain.

To confirm the potential of this multireporter platform to reveal virus-specific differences in terms of viral replication, chromatin condensation, and cell death, we compared the fluorescent viral plaques generated upon the infection with different flaviviruses including DENV-2, ZIKV, and YFV. YFV represents an additional model to further validate the spectrum of application of our flavivirus reporter (Figs. S2*B* and S3) and to explore the heterogeneity in replication kinetics and cell death induction across multiple flaviviruses using our multireporter platform. The acquired images at 120 h post-infection with DENV-2, ZIKV, and YFV show qualitative differences (Fig. 6*A*) that were examined using the image analysis protocol presented above (Fig. 5*A*). The artificial images generated by the image analysis protocol highlighted those differences (single-cell plaque analysis; Fig. 6*A*). The identified plaques contained several subpopulations of infected cells: a central core of dead cells (*green*), surrounded by a ring of cells presenting chromatin condensation (*blue*), and another ring of live-infected cells (*red*). Nevertheless, the proportions of these cell subpopulations were very different for DENV-2, ZIKV, and YFV. Finally, the quantification of the percentage of cells corresponding to each subpopulation within each plaque confirmed the qualitative observations, indicating differential proportions of infection and induced cell death among the three viral species tested (Fig. 6*B*).

Next, we asked whether the presence of either type of reporters (FlaviA-GFP and FlaviA-mNeptune) and dyes (Hoechst 33342 and SYTOX green) could affect the viral replication by comparing the pfu determined with the standard crystal violet staining on WT cells with those generated on both reporter cell lines at 96 h postinfection with DENV-2, ZIKV, and YFV. A representative experiment for DENV-2 is shown in Fig. S4*A*, and the plaque count confirmed that there is no difference in viral replication among all three cell lines infected with all three viral species tested (Fig. S4*B*). This result validates that the behaviors observed for DENV-2, ZIKV, and YFV arise from intrinsic differences in viral replication kinetics and not from a differential effect of the reporters and dyes in viral replication. Together, these results demonstrate the applicability of our reporter to be used in combination with other molecular sensors to establish a multiparametric characterization of the infection produced by different flaviviruses.

Discussion

The present study reports the construction of fluorescent protein-based sensors of flavivirus NS2B–NS3 serine proteases activity that become fluorescent upon cleavage by recombinant DENV-2/ZIKV proteases *in vitro* (Fig. 1). Moreover, the variant of this sensor with the internal NS3 cleavage site linker (AAQRRGRIG) reported the highest fluorescence increase in stably transduced mammalian cells upon DENV-2/ZIKV infection, correlating with the viral induced NS3 protease activity in the cellular context (Figs. 2 and 3). A far-red version of this flavivirus sensor reported the best signal-to-noise ratio in a fluorescent Dulbecco's plaque assay, enabling the construction of a multireporter platform to study plaque formation with single-cell resolution (Figs. 4 and 5). Finally, the application of this platform revealed important differences in cell-population kinetics of infection and cell death induced by several flaviviruses (Fig. 6).

As a starting point, we developed this genetically encoded flavivirus reporter system by successfully engineering the linker of our previously published caspase-activatable reporters, CA-GFP and CA-mNeptune (26–28), to be recognized and cleaved by the flavivirus NS2B–NS3 proteases, giving rise to the FlaviA-GFP and FlaviA-mNeptune reporters, respectively. First, we focused on the validation of three proposed linkers *in vitro* as a proof of concept of the recognition and cleavage of our reporter upon treatment with flavivirus proteases, without the possible effect of other proteases that are present in the cellular context. Our results showed that all three linkers tested were cleaved as soon as 1 h post-treatment with both DENV-2 and ZIKV proteases (Fig. 1, *A* and *B*). This fast cleavage validated the amino acid sequences of our linkers as well as the application of "unlinked" versions of both recombinant DENV-2 and ZIKV proteases, in which the NS2B and NS3 regions were produced as independent polypeptides. This choice was based on our own demonstration that the "unlinked" version of DENV-2 protease rests predominantly in a "closed," active conformation, in contrast with the less active, relaxed conformation, adopted by the frequently used "linked" construct, in which NS2B and NS3 polypeptides are attached by a nine-amino acid linker (31).

Once the biochemical principle behind the preliminary variants of our reporter was confirmed *in vitro* with recombinant viral proteases, we decided to test its performance upon full flavivirus particle infection in mammalian cells. The highest fluorescence increase to report the infection with DENV-2 and ZIKV in stably transduced BHK-21 cells was obtained with the internal NS3 cleavage site linker (Fig. 2) present in many members of the *Flavivirus* genus (3, 5, 30). Moreover, a BLASTp search of the NCBI reference proteins database (32) using the query sequence AAQRRGRIG, revealed 100% coverage and 88.9–100% identity to >60 members of the *Flavivirus* genus. The alignment results included many medically important flaviviruses like WNV, YFV, SEV, DENV, JEV, ZIKV, and TBEV

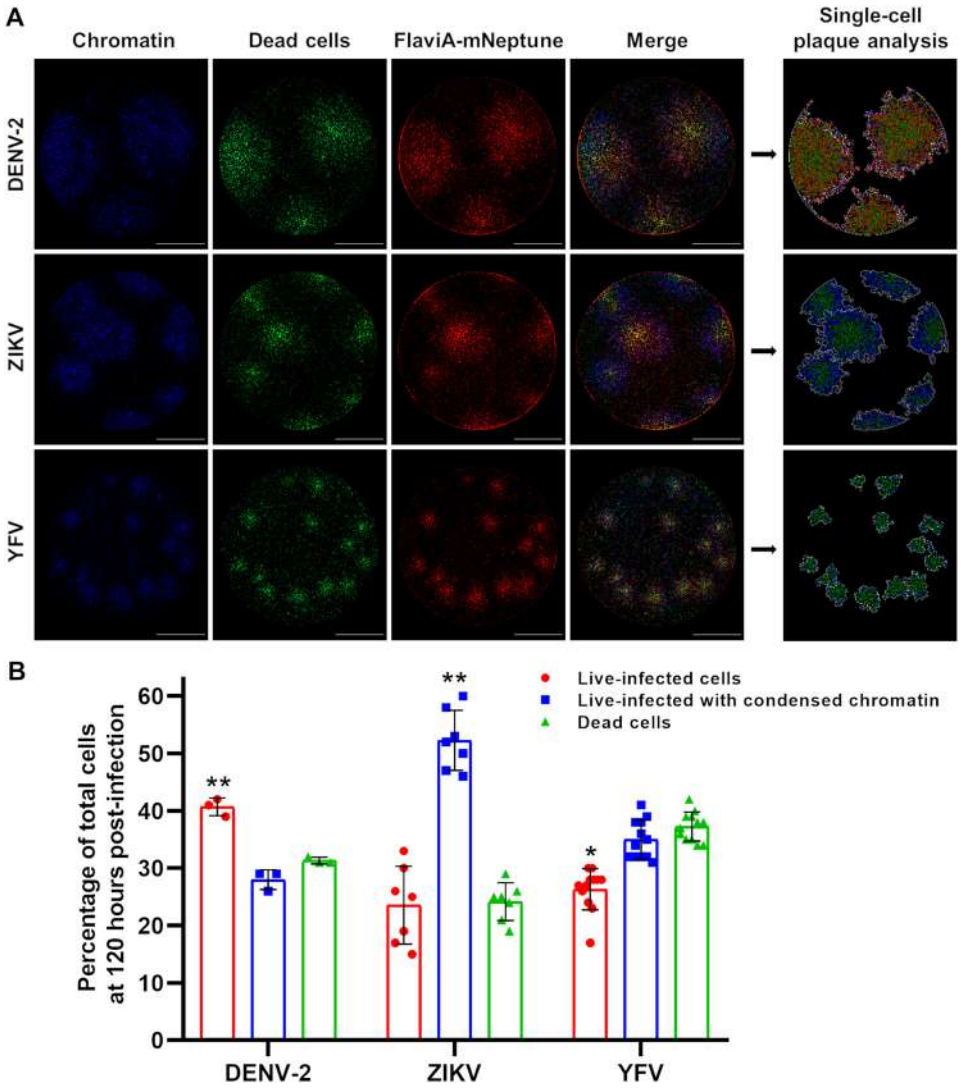

Figure 6. The FlaviA-mNeptune reporter enables the comparative characterization of the infection produced by flaviviruses in terms of viral replication and induced cell death at a single-cell level. We applied our image analysis protocol to characterize the DENV, ZIKV, and YFV infection and induced cell death by the quantification of fluorescence features of cells imaged to assess DNA/chromatin condensation (Hoechst 33342), cell death (SYTOX green), and viral infection (FlaviA-mNeptune reporter). *A*, the image analysis protocol was applied to achieve the identification of viral plaques produced by DENV, ZIKV, and YFV at 120 h postinfection and the categorization of single cells within each plaque as live-infected (*red*), live-infected with chromatin condensation (*blue*), and dead (*green*). *B*, DENV, ZIKV, and YFV infection described by parameters of percentage of live-infected cells (*red*), live-infected cells with chromatin condensation (*blue*), and dead cells (*green*) within the viral plaques at 120-h postinfection. The images and data from a representative analyzed experiment are shown (n = three independent experiments, magnification of 40×; *scale bar*, 1000 μm). The data are expressed as means ± S.D. for the number of plaques generated by each virus. *, $p < 0.05$; **, $p < 0.001$ compared with the other two cell populations conforming the plaques of the same viral species.

(Fig. S5), among others (1). This finding outlines the potential application of our reporter system to other flaviviruses and supports our hypothesis that the flavivirus internal NS3 cleavage site could represent a conserved viral target for the development of a single antiviral therapy against the members of the *Flavivirus* genus, as previously suggested for DENV (30). Nevertheless, further work using other flaviviruses is needed to establish the whole spectrum of utility and specificity of this reporter system.

Furthermore, our flavivirus reporter system proved to be a useful method for monitoring the kinetics of DENV-2 and ZIKV infection at a single-cell level by live-cell imaging (Fig. 2) and showed a positive correlation with standard virological approaches like detection of viral NS3 protease synthesis and activity by indirect immunofluorescence and Western blotting (Fig. 3). In this respect, flavivirus reporter replicons have been generated by engineering the viral genomes of reference strains (16–20). However, in recent years special effort has been invested in the development of cell-based molecular reporter systems for live-cell imaging of flavivirus infections (21–23), mainly for their application on the study of native viral strains and clinical isolates. Among the latter, our system shows some advantages in that it is a fluorescence-activatable reporter, which allows an easier interpretation of the results and simplifies the image analysis when compared with those systems based on the relocalization of the fluorescent signal across cellular compartments (21, 23). Moreover, the utility of our fluorescence activation approach arises from its low fluorescent background and the use of a single recombinant construct that codifies for a single fluorescent protein with intramolecular

quenching, in contrast with other, difficult to optimize strategies, like the FRET probes (26, 33) and the protease-triggered Cre-mediated reporter system, which rely on the cellular transfection of two different recombinant constructs (22) and could be sensitive to early changes in gene expression. Another great advantage over other systems is that our reporter has been validated with reference strains but also clinical isolates of different flavivirus species like DENV, ZIKV, and YFV, expanding its range of application to more than one flavivirus.

The fluorescence activation principle of our reporter also allowed us to envisage a cell-based fluorescent Dulbecco's plaque assay for flaviviruses (Fig. 4). The plaque assay is one of the "gold standard" virological techniques originally developed by d'Hérelle (34) for titration and isolation of single clones of bacteriophages and later adapted by Dulbecco (35) to animal viruses. Viral plaques arise after genome replication, transcription, translation, virus release from infected cells, and infection of surrounding cells (36). Thus, plaque development constitutes a hallmark of the infection carried out by a specific viral clone. To date, the kinetics of flavivirus plaque formation could only be monitored for transgenic fluorescent viruses made by modifying the genome of reference strains (16–20). However, we applied the far-red version of our flavivirus sensor to establish, for the first time, a mammalian reporter cell line where the plaque assay can be monitored over time with unlabeled native flavivirus strains. This way, we were able to study the kinetics of viral plaque development with the clinical isolate ZIKV CIET-01 (Fig. 4). Considering that viral plaques are clonal lesions of infected cells formed by the cytopathic effect of replicating viruses (36), we decided to incorporate molecular sensors for chromatin condensation (Hoechst 33342) and cell death (SYTOX green) to obtain multiparametric data from single viral plaques. This enabled us to construct a multireporter platform to study flavivirus plaque formation with single-cell resolution (Fig. 5) as a way to obtain a preliminary characterization of the infection produced by a particular flavivirus strain.

Following our approach, the quantification of the percentage of cells within each viral plaque corresponding to live-infected cells, live-infected cells with chromatin condensation, and dead cells indicated differential rates of infection and types of induced cell death for DENV-2, ZIKV, and YFV (Fig. 6). The infection with DENV-2 presents the highest proportion of live-infected cells, indicating that the infected cells take longer time to die upon infection and suggesting that this behavior drives to an increased viral production probably related to a faster infection kinetics leading to the formation of larger plaques (37). The amount of DENV-infected cells with chromatin condensation is very similar to that of dead cells, suggesting a fast type of cell demise once the cell death program is engaged, probably necrosis (38, 39). A similar scenario is shown by YFV that induces a fast type of cell death, probably necrosis, but earlier during the infection, which might limit viral spreading, leading to a lower proportion of live-infected cells and smaller viral plaques (40). On the other hand, ZIKV has a lower proportion of live-infected cells but a very high number of infected cells with chromatin condensation, suggesting that this viral strain induces a delayed type of cell death, probably apoptosis as previously reported (23, 41–43), preserving for a longer time the cell integrity to produce new viral particles and leading to larger plaques compared with YFV infection (44). However, this could be also related to differences in viral permissiveness of the BHK-21 cell line, because it is known that ZIKV virus tends to infect BHK-21 cells poorly compared with YFV, as demonstrated by envelope protein immunostaining (45, 46). Therefore, our multireporter platform serves only as a primary screening of the type of infection exposed by flavivirus strains. A more detailed exploration is needed using virological and cell biology methods to reach strong conclusions about the viral fitness and cell death mechanism induced by a specific viral strain. Nevertheless, our approach would be suitable for the screening of antiviral compounds by a plaque reduction assay, with the advantage of having a readout of the possible cytotoxicity induced by those compounds in a single experiment.

To our knowledge, this is the first fluorescence-activatable cell-based molecular reporter system for live-cell imaging of flavivirus infection suitable to be used in a plaque assay simultaneously with molecular sensors of other cellular or viral-induced processes. Moreover, taking into account the enormous need for preventative and therapeutic treatments for flavivirus infections like dengue and Zika (47), our multireporter platform enables the decoding of viral-specific fingerprints of Dulbecco-plaque formation with a potential future application for antiviral drug research and other studies on viral replication/cell death induction for both native flavivirus strains and clinical isolates.

Experimental procedures

Viruses

Clinical isolate DENV-2 13538 (DENV-2/CR/10066/2007) was provided by Instituto Costarricense de Investigación y Enseñanza en Nutrición y Salud, Cartago, Costa Rica (48). DENV-2 viruses were produced in C6/36 cells from *Aedes albopictus* (ATCC, Manassas, VA) by inoculating a cellular monolayer at a MOI of 0.01 and incubating for 3 days with RPMI 1640 medium (Gibco) supplemented with 2% fetal bovine serum (FBS; Gibco) at 33 °C in an atmosphere of 5% CO_2. Then culture supernatant was collected and centrifuged at 3000 × *g* for 10 min. Before storage at −80 °C, 23% newborn calf serum (Gibco) was added (49).

Clinical isolate ZIKV CIET-01 (ZIKV/CR/CIET-01/2016) was kindly provided by Claudio Soto-Garita from Universidad de Costa Rica. Vaccine strain YFV 17D (YFV/US/17D/1937) was isolated from the commercial vaccine YF-VAX® (Sanofi Pasteur, Lyon, France). ZIKV and YFV viruses were produced in Vero cells (ATCC) by inoculating cellular monolayers at a MOI of 0.1 and incubating for 5 days with minimum essential medium (MEM, Gibco) supplemented with 2% FBS at 37 °C in an atmosphere of 5% CO_2. Culture supernatants were collected, centrifuged at 3000 × *g* for 10 min, and stored at −80 °C.

Viruses were titrated by plaque assay in BHK-21 cells (ATCC) as previously described (50). Briefly, 10-fold serial dilutions of viruses were added to BHK-21 confluent monolayers. After 2 h of adsorption, the cells were incubated at 37 °C in an atmosphere of 5% CO_2 for 5 days with MEM supplemented

with 2% FBS and 1% carboxymethylcellulose (Sigma). Plaque numbers were counted after staining with crystal violet. Virus inactivation was carried out by five cycles of UV light (254 nm) exposure at an energy of 400,000 μJ/cm^2 in the CL-100 UV Cross-linker (UVP, Upland, CA).

Reporter development and molecular cloning

FlaviA-GFP, ZIKVA-GFP, and DENV2A-GFP reporters were developed by site-directed mutagenesis of the linker in the previously described CA-GFP reporter (26–28) to a sequence coding for the flavivirus NS3 internal cleavage site (AAQR-RGRIG), the ZIKV polyprotein NS2B/NS3 cleavage site (KTGKRSGAL), and the DENV-2 polyprotein NS2B/NS3 cleavage site (VKKQRAGVL), respectively, using the QuikChange approach (Agilent, Santa Clara, CA). The tRep/control, a truncated variant of the reporter protein, was generated by inserting a stop codon downstream the cleavage site in the linker of the FlaviA-GFP reporter. Then the genes of the flavivirus-activatable GFP reporters in the plasmid pET21b (Novagen, Madison, WI) were independently amplified by PCR and ligated into the SpeI and XhoI restriction sites of the pLenti-puro vector (a gift from Ie-Ming Shih, Addgene plasmid 39481) (51) to generate the constructs pLenti-ZIKVA-GFP-puro, pLenti-DENV2A-GFP-puro, and pLenti-FlaviA-GFP-puro. Likewise and based on the previously described CA-mNeptune reporter (28), we designed and commercially synthetized (Atum, Newark, CA) the FlaviA-mNeptune reporter gene by changing the linker sequence to codify for AAQRRGRIG. Finally, the FlaviA-mNeptune gene in the plasmid pD2109-CMV (Atum) was PCR-amplified and ligated into the XbaI and SalI restriction sites of the pLenti-CMV-GFP-Puro vector (a gift from Eric Campeau, Addgene plasmid 17448) (52) to produce the plasmid pLenti-CMV-FlaviA-mNeptune-puro. All constructs were confirmed by sequencing (Genewiz, South Plainfield, NJ).

Protein expression and purification

FlaviA-GFP, ZIKVA-GFP, DENV2A-GFP, and tRep/control expression constructs in pET21b vectors were transformed into *Escherichia coli* strain BL21(DE3). Flasks containing 2 liters of 2X YT media were inoculated with 8 ml of an overnight culture and grown at 37 °C to an A_{600} of 0.6. The cultures were then induced using 1 mM isopropyl β-D-1-thiogalactopyranoside (Sigma) and incubated at 20 °C for 5 h to allow protein expression. The cells were harvested by centrifugation and disrupted by microfluidization. Clarified lysates were prepared by centrifugation at 15,000 × *g* for 45 min. The reporter proteins were then purified using Co^{2+}-affinity LC with a 5-ml HiTrap Chelating HP column (GE Healthcare). The column was washed with a buffer composed of 50 mM imidazole, 300 mM NaCl, and 50 mM NaH_2PO_4, pH 8.0, and the proteins were eluted using a similar buffer with 300 mM imidazole and stored at 4 °C. Proteins purity was assessed in SDS-PAGE gels stained with Coomassie Blue.

DENV-2 protease was expressed as an "unlinked" construct by the cotransformation of BL21(DE3) cells with a pACYDuet plasmid encoding for residues 48–100 of the NS2B cofactor and a pETDuet plasmid comprising amino acids 1–187 of the NS3 protease (a gift from Thomas Keller) (53). ZIKV protease was expressed as an "unlinked" construct by the transformation of BL21(DE3) cells with pET15b vector encoding for amino acids 48–100 of the NS2B cofactor and 1–178 of the NS3 protease (54). The cells harboring either DENV-2 protease or ZIKV protease were grown in 2× YT medium with antibiotics at 37 °C to an A_{600} of 0.6. Protein expression was induced with 1 mM isopropyl β-D-1-thiogalactopyranoside and proceeded for 3 h at 25 °C. The proteases were purified using Ni^{2+}-affinity LC with a 5-ml HiTrap chelating HP column and eluted using a step gradient with 300 mM imidazole. The eluted proteases were further purified using anion exchange with a HiTrap Q HP column (GE Healthcare) with a linear gradient from 10 to 500 mM NaCl and stored at −80 °C. Protein purity was assessed in SDS-PAGE gels stained with Coomassie Blue.

Reporter cleavage and fluorescence assay in vitro

Samples containing 10 μM of either FlaviA-GFP, ZIKVA-GFP, or DENV2A-GFP reporters with and without 10 μM of DENV-2 or ZIKV proteases were prepared with digestion buffer (50 mM Tris buffer, pH 8.5, 0,1% CHAPS, 20% glycerol) in a final volume of 120 μl and added to a costar 96-well black plate. The fluorescence was measured every hour (excitation, 475 nm; emission, 512 nm) for 20 h at 27 °C. Another set of samples was incubated at 27 °C in 30-μl aliquots, to which SDS loading buffer was added at time points of 0, 1, 5, 10, 15, and 20 h. These samples were then run on SDS-PAGE and stained with Coomassie Blue to determine the cleavage kinetics of the flavivirus-activatable GFP reporters by DENV-2 and ZIKV proteases. Gel images were acquired with a ChemiDoc™ XRS+ System (Bio-Rad) and analyzed with the ImageJ software (National Institutes of Health, Bethesda, MD) (55) to determine the cleavage efficiency. The fluorescence signal-to-noise ratio was calculated by dividing the signal of the reporter treated with viral protease by the noise gave by the untreated reporter at every time point.

Lentiviral vectors assembly

HEK293T cells (ATCC) were cultured in Dulbecco's modified Eagle's medium (DMEM, Gibco) supplemented with 10% FBS, 1× GlutaMAX (Gibco), 1 mM sodium pyruvate (Gibco), and 1× antibiotic–antimycotic solution (Gibco). Lentiviral particles were generated in 60% confluent HEK293T cell monolayers by triple transfection with polyetilenimide (Polysciences, Warrington, PA) of either pLenti-FlaviA-GFP-puro, pLenti-ZIKVA-GFP-puro, pLenti-DENV2A-GFP-puro, or pLenti-CMV-FlaviA-mNeptune-puro constructs and both packaging plasmids pMD2.G and psPAX2 (a gift from Didier Trono, Addgene plasmids 12259 and 12260). At 72 h post-transfection, virus-containing medium was collected, filtered through a 0.45-μm membrane, supplemented with 5 μg/ml of Polybrene (Sigma), and stored at −80 °C. Finally, 10-fold serial dilutions of each lentiviral seed were added to HEK293T cells, and the biological titers in transducing units/ml were determined by flow cytometry at 48 h post-transduction using a BD Accuri™ C6 flow cytometer (BD Biosciences, Franklin Lakes, NJ), as previously described (56).

Reporter cell lines production and selection

BHK-21 cell monolayers at 80% confluency were stably transduced with lentiviral particles carrying a genetic construct codifying for either FlaviA-GFP, ZIKVA-GFP, DENV2A-GFP, or FlaviA-mNeptune reporters. For cell transduction, lentiviral vector particles were added to the cells at a MOI of 1 and centrifuged for 2 h at 300 × *g* at 25 °C. At 72 h post-transduction, the cells were selected with 8 μg/ml of puromycin (Sigma) in MEM 10% FBS during 2 days, and then cell populations with homogeneous levels of expression of the constructs were isolated by FACS with a BD FACSJazz™ cell sorter (BD Biosciences) based on the fluorescent basal signal of the reporter proteins. The selected stable cell lines were grown and maintained in MEM supplemented with 10% FBS and 0.5 μg/ml puromycin.

Infection kinetics in reporter cell lines by live-cell imaging

BHK-21 cells stably expressing the FlaviA-GFP, the ZIKVA-GFP or the DENV2A-GFP reporters were seeded on μClear black 96-well plates (Greiner Bio-One, Kremsmünster, Austria) at a density of 15,000 cells/well with MEM supplemented with 2% FBS. After 24 h of incubation at 37 °C with 5% CO_2, reporter cells were infected with either infectious or UV-inactivated DENV-2 13538 or ZIKV CIET-01 at a MOI of 0.25 and allowed to adsorb for 2 h at 37 °C. After labeling with 1 μg/ml Hoechst 33342 (Invitrogen) for 10 min, the cells were washed with 1× PBS and incubated for 96 h with FluoroBrite™ DMEM (Gibco) supplemented with 2% FBS and containing 2.5 μg/ml of propidium iodide (Invitrogen) at 37 °C in an atmosphere of 5% CO_2. Images were acquired every 2 h with a Cytation 3 cell imaging multimode reader (BioTek, Winooski, VT). The fluorescence signal-to-noise ratio was calculated by dividing the signal of the reporter cells treated with infectious virus by the noise gave by the reporter cells treated with UV-inactivated virus at every time point.

Kinetic plaque assay on reporter cell lines by live-cell imaging

BHK-21 cells stably expressing the FlaviA-mNeptune reporter were seeded on μClear black 96-well plates at a density of 25,000 cells/well with MEM supplemented with 10% FBS. After 24 h of incubation at 37 °C with 5% CO_2, reporter cells were infected with 10-fold serial dilutions of either infectious or UV-inactivated DENV-2 13538, ZIKV CIET-01, or YFV 17D. After 2 h of adsorption, the cells were labeled with 1 μg/ml Hoechst 33342 for 10 min, washed once with 1× PBS and incubated for 120 h at 37 °C with 5% CO_2 with MEM AutoMod™ (Sigma) supplemented with 2% FBS, 1% carboxymethylcellulose, and 500 nM SYTOX green (Invitrogen). Images of the whole well were acquired every 24 h with a Cytation 3 cell imaging multimode reader. Finally, at 120 h postinoculation, viral plaques were confirmed by crystal violet staining.

Indirect immunofluorescence

At 96 and 120 h postinfection with either infectious or UV-inactivated DENV-2 13538, the medium was removed, and cells were fixed for 1 h with 1% paraformaldehyde (Sigma). Later, the cells were permeabilized with 70% ethanol for 15 min and 0,001% Triton X-100 (Sigma) for 10 min at rate temperature. Then cells were incubated with a 1:800 dilution of rabbit polyclonal anti-DENV NS3 antibody (GeneTex, Irvine, CA, GTX124252) for 1 h at 37 °C, washed twice with 1× PBS, and incubated with a 1:400 dilution of goat polyclonal anti-rabbit IgG Alexa Fluor® 594 – conjugated antibody (Invitrogen, A11037) for 30 min at 37 °C. After three washes with 1× PBS, FluoroBrite™ DMEM was added, and images of the whole well were acquired with a Cytation 3 cell imaging multimode reader.

Western blotting

BHK-21 cells stably expressing the FlaviA-GFP reporter were seeded on 12-well plates (Greiner Bio-One) at a density of 350,000 cells/well with MEM supplemented with 2% FBS. After 24 h of incubation at 37 °C with 5% CO_2, reporter cells were infected with either infectious or UV-inactivated DENV-2 13538 at a MOI of 0.25 and allowed to adsorb for 2 h at 37 °C. Every 24 h during 96 h of incubation, images were acquired with the Cytation 3 cell imaging multimode reader, and the cells were lysed with 2% SDS solution and stored at −20 °C. Later, samples were run on a SDS-PAGE gel, transferred to a PVDF membrane (Millipore), and blotted in a single step with a mixture of 1:100 dilution of rabbit polyclonal anti-GFP antibody (Invitrogen, A-11122), 1:1000 dilution of rabbit polyclonal anti-DENV NS3 antibody, and 1:500 dilution of rabbit monoclonal anti-vinculin antibody (Invitrogen, 700062). Finally, the membrane was treated with a 1:500 dilution of goat polyclonal anti-rabbit IgG HRP-conjugated antibody (Invitrogen, G-21234) and visualized using the Super Signal West Pico Plus chemiluminescent substrate (Thermo Fisher Scientific). The images were acquired with a ChemiDoc™ XRS+ system.

Image analysis and statistics

Image analysis was performed with the software CellProfiler 2.0 (http://www.cellprofiler.org; Broad Institute, Cambridge, MA).[3] The data are expressed as means ± S.D. of three independent experiments. Statistical significance of the differences between mean values was determined by using one-way analysis of variance followed by a Tukey's post hoc test with the software SigmaPlot 14 (Systat Software Inc., San Jose, CA). The level of significance is denoted in each figure.

Author contributions—J. L. A.-A. and J. A. H. conceptualization; J. L. A.-A. data curation; J. L. A.-A. and R. M.-R. formal analysis; J. L. A.-A., D. J. M., and M. E. H. investigation; J. L. A.-A. and R. M.-R. writing-original draft; J. L. A.-A., J. A. H., and R. M.-R. writing-review and editing; J. L. A.-A., J. A. H. and R. M.-R. resources; J. A. H. and R. M.-R. supervision; J. A. H. and R. M.-R. funding acquisition; J. A. H. and R. M.-R. project administration; J. L. A.-A. and R. M.-R. methodology.

Acknowledgments—We thank Francisco Vega-Aguilar for technical assistance with viral strains. We thank Joseph P. Kennedy, Jr., and Derrick P. Feuerstein for support and suggestions during the experimentation. We also thank Ralf Bartenschlager (Heidelberg University) for his scientific advice and critical review of the manuscript. This work is dedicated with regard to Alina I. Arias-Barrantes and Alexander Mora-Solano.

References

1. Gould, E. A., and Solomon, T. (2008) Pathogenic flaviviruses. *Lancet* **371,** 500–509 CrossRef Medline
2. Lindenbach, B., Murray, C. L., Thiel, H.-J., and Rice, C. M. (2013) Flaviviridae. In *Fields Virology*, pp. 712–746, Lippincott Williams & Wilkins, Philadelphia, Pennsylvania
3. Teo, K. F., and Wright, P. J. (1997) Internal proteolysis of the NS3 protein specified by dengue virus 2. *J. Gen. Virol.* **78,** 337–341 CrossRef Medline
4. Lindenbach, B. D., and Rice, C. M. (2003) Molecular biology of flaviviruses. *Adv. Virus Res.* **59,** 23–61 CrossRef Medline
5. Bera, A. K., Kuhn, R. J., and Smith, J. L. (2007) Functional characterization of *cis* and *trans* activity of the flavivirus NS2B–NS3 protease. *J. Biol. Chem.* **282,** 12883–12892 CrossRef Medline
6. Ishikawa, T., Yamanaka, A., and Konishi, E. (2014) A review of successful flavivirus vaccines and the problems with those flaviviruses for which vaccines are not yet available. *Vaccine* **32,** 1326–1337 CrossRef Medline
7. Scott, L. J. (2016) Tetravalent dengue vaccine: a review in the prevention of dengue disease. *Drugs* **76,** 1301–1312 CrossRef Medline
8. Normile, D. (2017) Safety concerns derail dengue vaccination program. *Science* **358,** 1514–1515 CrossRef Medline
9. Chan, K. W., Watanabe, S., Kavishna, R., Alonso, S., and Vasudevan, S. G. (2015) Animal models for studying dengue pathogenesis and therapy. *Antiviral Res.* **123,** 5–14 CrossRef Medline
10. Reynolds, E. S., Hart, C. E., Hermance, M. E., Brining, D. L., and Thangamani, S. (2017) An overview of animal models for arthropod-borne viruses. *Comp. Med.* **67,** 232–241 Medline
11. Diamond, M. S., Edgil, D., Roberts, T. G., Lu, B., and Harris, E. (2000) Infection of human cells by dengue virus is modulated by different cell types and viral strains. *J. Virol.* **74,** 7814–7823 CrossRef Medline
12. Balsitis, S. J., Coloma, J., Castro, G., Alava, A., Flores, D., McKerrow, J. H., Beatty, P. R., and Harris, E. (2009) Tropism of replicating dengue virus in mice and humans defined by viral nonstructural protein 3-specific immunohistochemistry. *Am. J. Trop. Med. Hyg.* **80,** 416–424 CrossRef Medline
13. Arias-Arias, J. L., Vega-Aguilar, F., Corrales-Aguilar, E., Hun, L., Loría, G. D., and Mora-Rodríguez, R. (2018) Dengue virus infection of primary human smooth muscle cells. *Am. J. Trop. Med. Hyg.* **99,** 1451–1457 CrossRef Medline
14. Acosta, E. G., and Bartenschlager, R. (2016) The quest for host targets to combat dengue virus infections. *Curr. Opin. Virol.* **20,** 47–54 CrossRef Medline
15. de Wispelaere, M., Lian, W., Potisopon, S., Li, P. C., Jang, J., Ficarro, S. B., Clark, M. J., Zhu, X., Kaplan, J. B., Pitts, J. D., Wales, T. E., Wang, J., Engen, J. R., Marto, J. A., Gray, N. S., *et al.* (2018) Inhibition of flaviviruses by targeting a conserved pocket on the viral envelope protein. *Cell Chem. Biol.* **25,** 1006–1016.e8 CrossRef Medline
16. Li, S. H., Li, X. F., Zhao, H., Deng, Y. Q., Yu, X. D., Zhu, S. Y., Jiang, T., Ye, Q., Qin, E. D., and Qin, C. F. (2013) Development and characterization of the replicon system of Japanese encephalitis live vaccine virus SA14-14-2. *Virol. J.* **10,** 64 CrossRef Medline
17. Schmid, B., Rinas, M., Ruggieri, A., Acosta, E. G., Bartenschlager, M., Reuter, A., Fischl, W., Harder, N., Bergeest, J. P., Flossdorf, M., Rohr, K., Höfer, T., and Bartenschlager, R. (2015) Live cell analysis and mathematical modeling identify determinants of attenuation of dengue virus 2′-*O*-methylation mutant. *PLoS Pathog.* **11,** e1005345 CrossRef Medline
18. Xie, X., Zou, J., Shan, C., Yang, Y., Kum, D. B., Dallmeier, K., Neyts, J., and Shi, P. Y. (2016) Zika virus replicons for drug discovery. *EBioMedicine* **12,** 156–160 CrossRef Medline
19. Tamura, T., Fukuhara, T., Uchida, T., Ono, C., Mori, H., Sato, A., Fauzyah, Y., Okamoto, T., Kurosu, T., Setoh, Y. X., Imamura, M., Tautz, N., Sakoda, Y., Khromykh, A. A., Chayama, K., *et al.* (2018) Characterization of recombinant *Flaviviridae* viruses possessing a small reporter tag. *J. Virol.* **92,** e01582-17 Medline
20. Kümmerer, B. M. (2018) Establishment and application of flavivirus replicons. *Adv. Exp. Med. Biol.* **1062,** 165–173 CrossRef Medline
21. Medin, C. L., Valois, S., Patkar, C. G., and Rothman, A. L. (2015) A plasmid-based reporter system for live cell imaging of dengue virus infected cells. *J. Virol. Methods* **211,** 55–62 CrossRef Medline
22. Hsieh, M.-S., Chen, M.-Y., Hsieh, C.-H., Pan, C.-H., Yu, G.-Y., and Chen, H.-W. (2017) Detection and quantification of dengue virus using a novel biosensor system based on dengue NS3 protease activity. *PLoS One* **12,** e0188170 CrossRef Medline
23. McFadden, M. J., Mitchell-Dick, A., Vazquez, C., Roder, A. E., Labagnara, K. F., McMahon, J. J., Silver, D. L., and Horner, S. M. (2018) A fluorescent cell-based system for imaging Zika virus infection in real-time. *Viruses* **10,** E95 Medline
24. Winkler, G., Maxwell, S. E., Ruemmler, C., and Stollar, V. (1989) Newly synthesized dengue-2 virus nonstructural protein NS1 is a soluble protein but becomes partially hydrophobic and membrane-associated after dimerization. *Virology* **171,** 302–305 CrossRef Medline
25. Chung, K. M., Thompson, B. S., Fremont, D. H., and Diamond, M. S. (2007) Antibody recognition of cell surface-associated NS1 triggers Fc-receptor-mediated phagocytosis and clearance of West Nile virus-infected cells. *J. Virol.* **81,** 9551–9555 CrossRef Medline
26. Nicholls, S. B., Chu, J., Abbruzzese, G., Tremblay, K. D., and Hardy, J. A. (2011) Mechanism of a genetically encoded dark-to-bright reporter for caspase activity. *J. Biol. Chem.* **286,** 24977–24986 CrossRef Medline
27. Nicholls, S. B., and Hardy, J. A. (2013) Structural basis of fluorescence quenching in caspase activatable-GFP. *Protein Sci.* **22,** 247–257 CrossRef Medline
28. Wu, P., Nicholls, S. B., and Hardy, J. A. (2013) A tunable, modular approach to fluorescent protease-activated reporters. *Biophys. J.* **104,** 1605–1614 CrossRef Medline
29. Shiryaev, S. A., Kozlov, I. A., Ratnikov, B. I., Smith, J. W., Lebl, M., and Strongin, A. Y. (2007) Cleavage preference distinguishes the two-component NS2B–NS3 serine proteinases of dengue and West Nile viruses. *Biochem. J.* **401,** 743–752 CrossRef Medline
30. Constant, D. A., Mateo, R., Nagamine, C. M., and Kirkegaard, K. (2018) Targeting intramolecular proteinase NS2B/3 cleavages for trans-dominant inhibition of dengue virus. *Proc. Natl. Acad. Sci. U.S.A.* **115,** 10136–10141 CrossRef Medline
31. Hill, M. E., Yildiz, M., and Hardy, J. A. (2019) Cysteine disulfide traps reveal distinct conformational ensembles in dengue virus NS2B–NS3 protease. *Biochemistry* **58,** 776–787 CrossRef Medline
32. Altschul, S. F., Gish, W., Miller, W., Myers, E. W., and Lipman, D. J. (1990) Basic local alignment search tool. *J. Mol. Biol.* **215,** 403–410 CrossRef Medline
33. Leavesley, S. J., and Rich, T. C. (2016) Overcoming limitations of FRET measurements. *Cytometry A.* **89,** 325–327 CrossRef Medline
34. d'Hérelle, F. (1926) The bacteriophage and its behavior. *Nature* **118,** 183–185 CrossRef
35. Dulbecco, R. (1952) Production of plaques in monolayer tissue cultures by single particles of an animal virus. *Proc. Natl. Acad. Sci. U.S.A.* **38,** 747–752 CrossRef Medline
36. Yakimovich, A., Andriasyan, V., Witte, R., Wang, I. H., Prasad, V., Suomalainen, M., and Greber, U. F. (2015) Plaque2.0: a high-throughput analysis framework to score virus-cell transmission and clonal cell expansion. *PLoS One* **10,** e0138760 CrossRef Medline
37. Goh, K. C., Tang, C. K., Norton, D. C., Gan, E. S., Tan, H. C., Sun, B., Syenina, A., Yousuf, A., Ong, X. M., Kamaraj, U. S., Cheung, Y. B., Gubler, D. J., Davidson, A., St. John, A. L., Sessions, O. M., *et al.* (2016) Molecular determinants of plaque size as an indicator of dengue virus attenuation. *Sci. Rep.* **6,** 26100 CrossRef Medline
38. Ghosh Roy, S., Sadigh, B., Datan, E., Lockshin, R. A., and Zakeri, Z. (2014) Regulation of cell survival and death during Flavivirus infections. *World J. Biol. Chem.* **5,** 93–105 Medline
39. Galluzzi, L., Vitale, I., Aaronson, S. A., Abrams, J. M., Adam, D., Agostinis, P., Alnemri, E. S., Altucci, L., Amelio, I., Andrews, D. W., Andrews, D. W., Annicchiarico-Petruzzelli, M., Antonov, A. V., Arama, E., Baehrecke, E. H., Barlev, N. A., *et al.* (2018) Molecular mechanisms of cell death: Recommendations of the Nomenclature Committee on Cell Death 2018. *Cell Death Differ.* **25,** 486–541 CrossRef Medline
40. Liprandi, F. (1981) Isolation of plaque variants differing in virulence from the 17D strain of yellow fever virus. *J. Gen. Virol.* **56,** 363–370 CrossRef Medline

41. Liu, J., Li, Q., Li, X., Qiu, Z., Li, A., Liang, W., Chen, H., Cai, X., Chen, X., Duan, X., Li, J., Wu, W., Xu, M., Mao, Y., Chen, H., *et al.* (2018) Zika virus envelope protein induces G_2/M cell cycle arrest and apoptosis via an intrinsic cell death signaling pathway in neuroendocrine PC12 cells. *Int. J. Biol. Sci.* **14,** 1099–1108 CrossRef Medline
42. Limonta, D., Jovel, J., Kumar, A., Airo, A. M., Hou, S., Saito, L., Branton, W., Ka-Shu Wong, G., Mason, A., Power, C., and Hobman, T. C. (2018) Human fetal astrocytes infected with Zika virus exhibit delayed apoptosis and resistance to interferon: Implications for persistence. *Viruses* **10,** E646 Medline
43. Anfasa, F., Goeijenbier, M., Widagdo, W., Siegers, J. Y., Mumtaz, N., Okba, N., van Riel, D., Rockx, B., Koopmans, M. P. G., Meijers, J. C. M., and Martina, B. E. E. (2019) Zika virus infection induces elevation of tissue factor production and apoptosis on human umbilical vein endothelial cells. *Front. Microbiol.* **10,** 817 CrossRef Medline
44. Kato, F., Tajima, S., Nakayama, E., Kawai, Y., Taniguchi, S., Shibasaki, K., Taira, M., Maeki, T., Lim, C. K., Takasaki, T., and Saijo, M. (2017) Characterization of large and small-plaque variants in the Zika virus clinical isolate ZIKV/Hu/S36/Chiba/2016. *Sci. Rep.* **7,** 16160 CrossRef Medline
45. Chan, J. F., Yip, C. C., Tsang, J. O., Tee, K. M., Cai, J. P., Chik, K. K., Zhu, Z., Chan, C. C., Choi, G. K., Sridhar, S., Zhang, A. J., Lu, G., Chiu, K., Lo, A. C., Tsao, S. W., *et al.* (2016) Differential cell line susceptibility to the emerging Zika virus: implications for disease pathogenesis, non-vector-borne human transmission and animal reservoirs. *Emerg. Microbes Infect.* **5,** e93 Medline
46. Petrova, E., Gracias, S., Beauclair, G., Tangy, F., and Jouvenet, N. (2019) Uncovering flavivirus host dependency factors through a genome-wide gain-of-function screen. *Viruses* **11,** E68 Medline
47. Zakaria, M. K., Carletti, T., and Marcello, A. (2018) Cellular targets for the treatment of flavivirus infections. *Front. Cell Infect. Microbiol.* **8,** 398 CrossRef Medline
48. Soto-Garita, C., Somogyi, T., Vicente-Santos, A., and Corrales-Aguilar, E. (2016) Molecular characterization of two major dengue outbreaks in Costa Rica. *Am. J. Trop. Med. Hyg.* **95,** 201–205 CrossRef Medline
49. Medina, F., Medina, J. F., Colon, C., Vergne, E., Santiago, G. A., and Munoz-Jordan, J. L. (2012) Dengue virus: isolation, propagation, quantification, and storage. *Curr. Protoc. Microbiol.* chapter 15, unit 15D.2 CrossRef Medline
50. Morens, D. M., Halstead, S. B., Repik, P. M., Putvatana, R., and Raybourne, N. (1985) Simplified plaque reduction neutralization assay for dengue viruses by semimicro methods in BHK-21 cells: comparison of the BHK suspension test with standard plaque reduction neutralization. *J. Clin. Microbiol.* **22,** 250–254 CrossRef Medline
51. Guan, B., Wang, T. L., and Shih, I. M. (2011) ARID1A, a factor that promotes formation of SWI/SNF-mediated chromatin remodeling, is a tumor suppressor in gynecologic cancers. *Cancer Res.* **71,** 6718–6727 CrossRef Medline
52. Campeau, E., Ruhl, V. E., Rodier, F., Smith, C. L., Rahmberg, B. L., Fuss, J. O., Campisi, J., Yaswen, P., Cooper, P. K., and Kaufman, P. D. (2009) A versatile viral system for expression and depletion of proteins in mammalian cells. *PLoS One* **4,** e6529 CrossRef Medline
53. Kim, Y. M., Gayen, S., Kang, C.., Joy, J., Huang, Q., Chen, A. S., Wee, J. L., Ang, M. J., Lim, H. A., Hung, A. W., Li, R., Noble, C. G., Lee, L. T., Yip, A., Wang, Q. Y., *et al.* (2013) NMR analysis of a novel enzymatically active unlinked dengue NS2B–NS3 protease complex. *J. Biol. Chem.* **288,** 12891–12900 CrossRef Medline
54. Hill, M. E., Kumar, A., Wells, J. A., Hobman, T. C., Julien, O., and Hardy, J. A. (2018) The unique cofactor region of Zika virus NS2B–NS3 protease facilitates cleavage of key host proteins. *ACS Chem. Biol.* **13,** 2398–2405 CrossRef Medline
55. Schneider, C. A., Rasband, W. S., and Eliceiri, K. W. (2012) NIH Image to ImageJ: 25 years of image analysis. *Nat. Methods* **9,** 671–675 CrossRef Medline
56. Tiscornia, G., Singer, O., and Verma, I. M. (2006) Production and purification of lentiviral vectors. *Nat. Protoc.* **1,** 241–245 CrossRef Medline

A fluorescence-activatable reporter of flavivirus NS2B–NS3 protease activity enables live imaging of infection in single cells and viral plaques

Jorge L. Arias-Arias, Derek J. MacPherson, Maureen E. Hill, Jeanne A. Hardy and Rodrigo Mora-Rodríguez

J. Biol. Chem. 2020, 295:2212-2226.
doi: 10.1074/jbc.RA119.011319 originally published online January 9, 2020

A fluorescence activatable reporter of flavivirus NS2B-NS3 protease activity enables live imaging of infection in single cells and viral plaques

Jorge L. Arias-Arias[1], Derek J. MacPherson[2], Maureen E. Hill[2], Jeanne A. Hardy[2], and Rodrigo Mora-Rodríguez[1*]

From [1]Centro de Investigación en Enfermedades Tropicales (CIET), Facultad de Microbiología, Universidad de Costa Rica, San José 11501-2060, Costa Rica; [2]Department of Chemistry, 104 LGRT, 710 N. Pleasant St., University of Massachusetts Amherst, MA 01003, USA

Supporting information file containing:

- Table S1. Reporter variants tested *in vitro* for cleavage and fluorescence activation upon treatment with recombinant DENV-2 NS2B-NS3 protease.

- Figure S1. Cleavage kinetics of fluorescence-activated GFP reporter variants by DENV-2/ZIKV NS2B-NS3 proteases *in vitro*.

- Figure S2. The FlaviA-GFP reporter becomes fluorescent in stably-transduced BHK-21 cells upon DENV-2, ZIKV, and YFV infection.

- Figure S3. The FlaviA-GFP reporter becomes cleaved in stably-transduced BHK-21 cells upon YFV infection.

- Figure S4. Stable expression of the FlaviA-GFP and FlaviA-mNeptune reporters in combination with dyes of chromatin and cell death has no effect on flaviviruses replication in mammalian cells.

- Figure S5. Multiple sequence alignment of the internal NS3 cleavage site from ten medically important flaviviruses.

Table S1. Reporter variants tested *in vitro* for cleavage and fluorescence activation upon treatment with recombinant DENV-2 NS2B-NS3 protease.

Reporter variant	Linker sequence													State after treatment with recombinant DENV-2 NS2B-NS3 protease
	P6	P5	P4	P3	P2	P1	P1'	P2'	P3'	P4'	P5'	P6'	P7'	
DENVA-GFPv1	*GFP*[*]			G	R	R	D	F	Q	G	P	C	*QP*[+]	Uncleaved, Non-fluorescent
DENVA-GFPv2	*GFP*			G	R	R	G	F	Q	G	P	C	*QP*	Uncleaved, Non-fluorescent
DENVA-GFPv3	*GFP*	D	E	G	R	R	G	G	P	C	*QP*			Uncleaved, Non-fluorescent
DENVA-GFPv4	*GFP*	D	K	K	R	R	G	G	S	G	*QP*			Cleaved, Non-fluorescent
FlaviA-GFP	*GFP*	A	A	Q	R	R	G	R	I	G	*QP*			Cleaved, Fluorescent
ZIKVA-GFP	*GFP*	K	T	G	K	R	S	G	A	L	*QP*			Cleaved, Fluorescent
DENV2A-GFP	*GFP*	V	K	K	Q	R	A	G	V	L	*QP*			Cleaved, Fluorescent

[*]*Position within the green fluorescent protein sequence.*
[+]*Position within the quenching peptide sequence.*

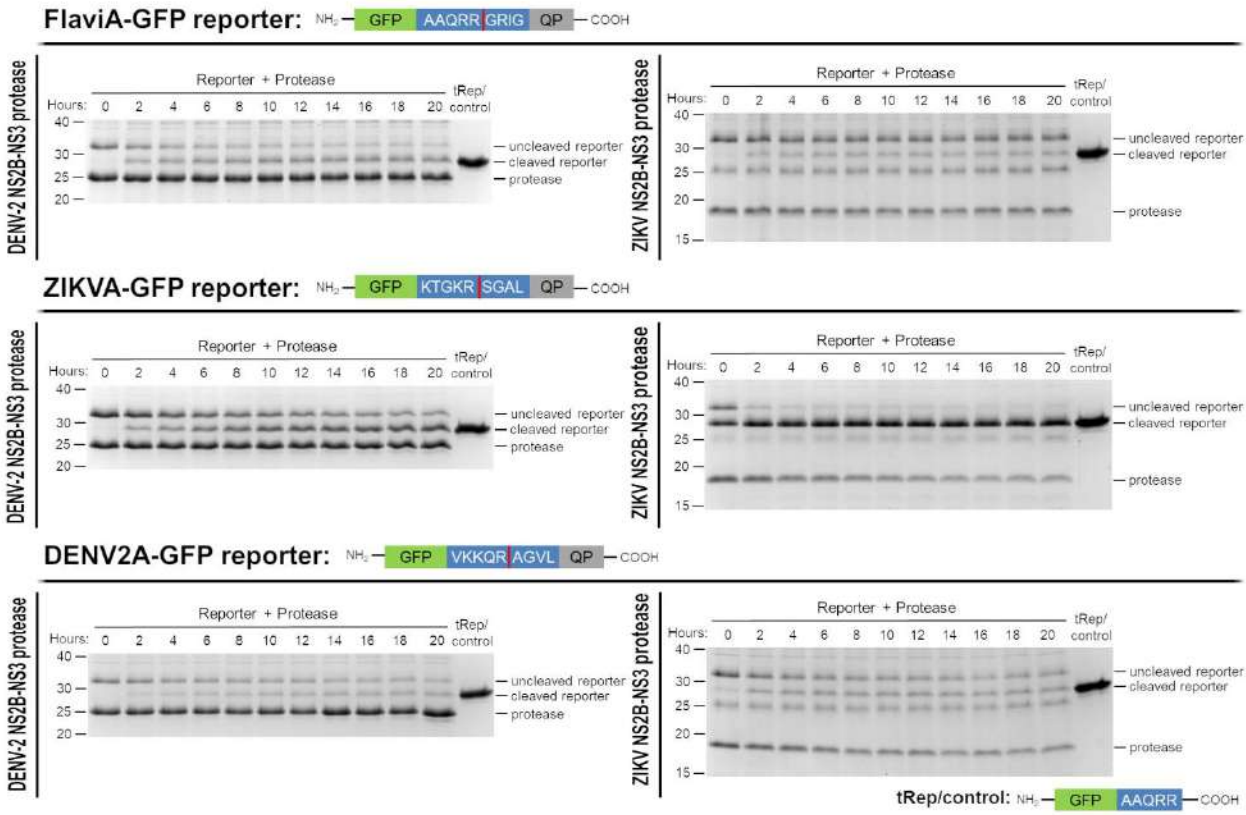

Figure S1. Cleavage kinetics of flavivirus-activatable GFP reporter variants by DENV-2/ZIKV NS2B-NS3 proteases *in vitro*. Three variants of the flavivirus-activatable GFP reporter were developed by changing the linker sequence: ZIKVA-GFP (ZIKV polyprotein NS2B/NS3 cleavage site linker), DENV2A-GFP (DENV-2 polyprotein NS2B/NS3 cleavage site linker), and FlaviA-GFP with the internal NS3 cleavage site linker which is present in many members of the *Flavivirus* genus. For the *in vitro* cleavage kinetics, purified reporter proteins were mixed with purified DENV-2 NS2B-NS3 protease (left panel) or ZIKV NS2B-NS3 protease (right panel) at a molar ratio of 1:1 and incubated for given times. Reactions were quenched by thermal treatment in SDS loading buffer and samples were analyzed by SDS-PAGE and staining of the gels with Coomassie blue. tRep/control is an engineered cleaved version of the FlaviA-GFP protein and was used as size marker of cleaved reporters.

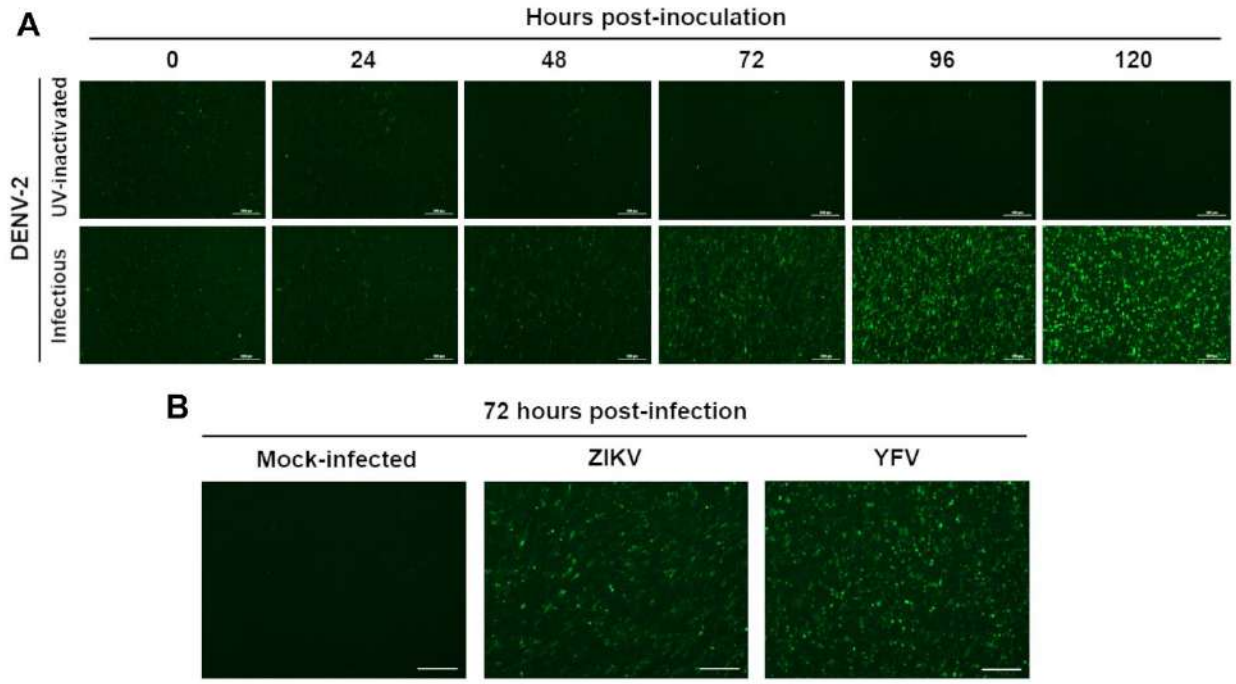

Figure S2. The FlaviA-GFP reporter becomes fluorescent in stably-transduced BHK-21 cells upon DENV-2, ZIKV, and YFV infection. Stable BHK-21 cells expressing the FlaviA-GFP reporter were inoculated with DENV-2 13538, ZIKV CIET-01, and YFV 17D at a low MOI of 0.1, for the specified time periods. **(A)** Fluorescence kinetics of the FlaviA-GFP reporter in stable BHK-21 cells after inoculation with infectious and UV-inactivated DENV-2. **(B)** Fluorescence of the FlaviA-GFP reporter in stable BHK-21 cells after 72 hour post-infection with ZIKV and YFV. Magnification of 40X, scale bar = 100 µm.

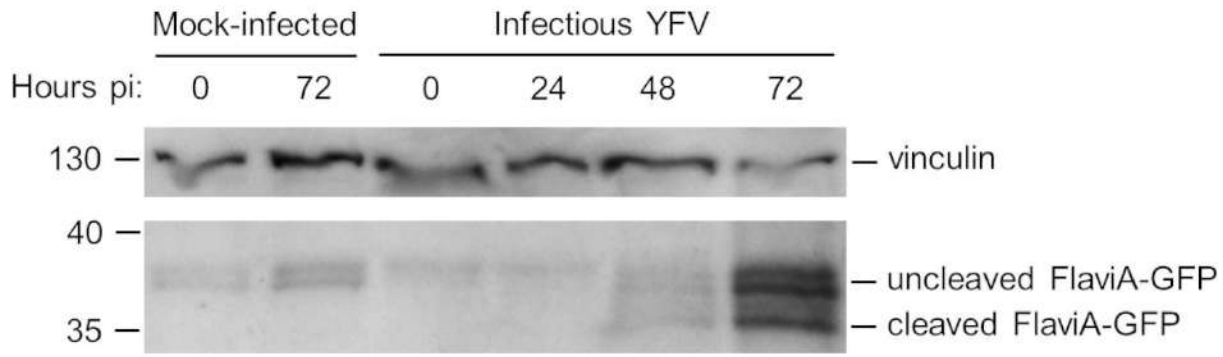

Figure S3. The FlaviA-GFP reporter becomes cleaved in stably-transduced BHK-21 cells upon YFV infection. The cleavage kinetics of the FlaviA-GFP reporter in stable BHK-21 cells upon mock or YFV 17D infection at a low MOI of 0.1 was made by western blot for the depicted time periods post-inoculation (pi) and following the protocol described in the experimental procedures.

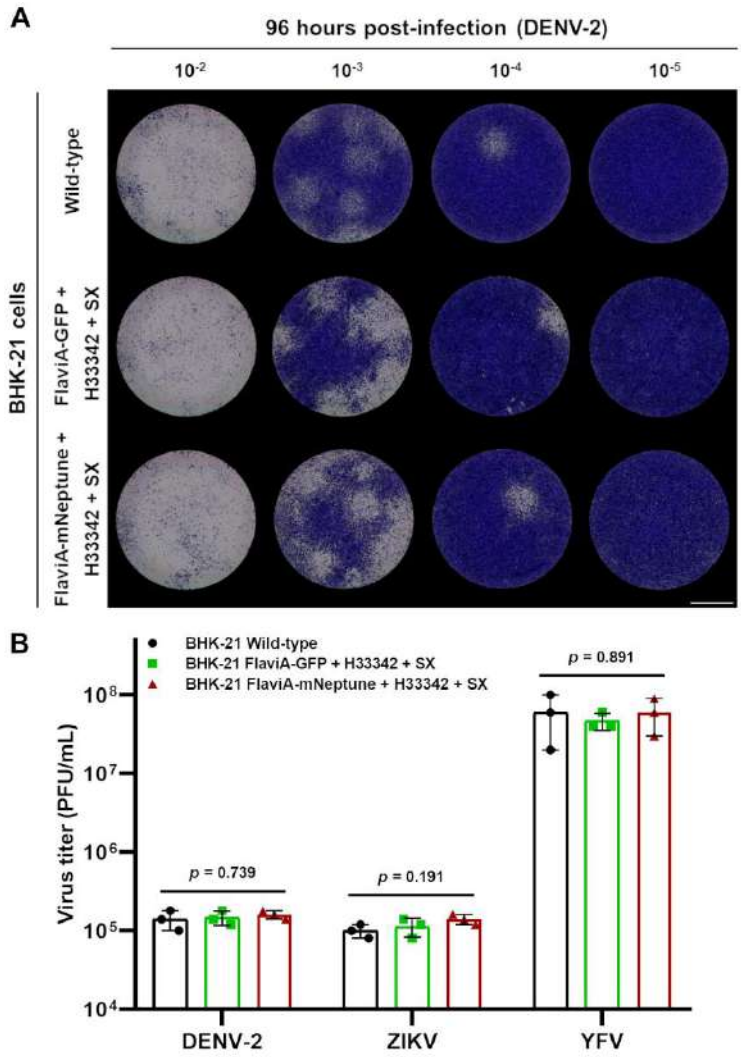

Figure S4. Stable expression of the FlaviA-GFP and FlaviA-mNeptune reporters in combination with dyes of chromatin and cell death has no effect on flaviviruses replication in mammalian cells. Wild-type and stable BHK-21 cells expressing either the FlaviA-GFP or the FlaviA-mNeptune reporter together with dyes of chromatin and cell death were used to perform a plaque assay with viral seeds of DENV-2 13538, ZIKV CIET-01, and YFV 17D. **(A)** Comparison of DENV-2 plaque assay in wild-type and stable BHK-21 cells expressing either the FlaviA-GFP or the FlaviA-mNeptune reporter in combination with Hoechst 33342 (H33342) and SYTOX green (SX) at 96 hours post-infection. Images from a representative experiment are shown (n = three independent experiments, magnification of 40X, scale bar = 1000 µm). **(B)** Virus titers for DENV-2, ZIKV, and YFV in wild-type and stable BHK-21 cells expressing either the FlaviA-GFP or the FlaviA-mNeptune reporter together with Hoechst 33342 (H33342) and SYTOX green (SX) at 96 hours post-infection. Data are expressed as mean ± SD of three independent experiments.

Figure S5. Multiple sequence alignment of the internal NS3 cleavage site from ten medically important flaviviruses. Protein sequences of the internal NS3 cleavage site from DENV-1 to 4, ZIKV, YFV, WNV, SLEV, JEV, and TBEV were obtained from the NCBI reference proteins data base (accession numbers NP_059433.1, NP_056776.2, YP_001621843.1, NP_073286.1, YP_009428568.1, NP_041726.1, YP_001527877.1, YP_001008348.1, NP_059434.1, and NP_043135.1, respectively), aligned by Clustal Omega (https://www.ebi.ac.uk/Tools/msa/clustalo/), and visualized with WebLogo (https://weblogo.berkeley.edu/logo.cgi).

viruses

MDPI

Article

A Fluorescent Real-Time Plaque Assay Enables Single-Cell Analysis of Virus-Induced Cytopathic Effect by Live-Cell Imaging

Jorge L. Arias-Arias [1,2,*], Eugenia Corrales-Aguilar [1] and Rodrigo A. Mora-Rodríguez [1]

[1] Centro de Investigación en Enfermedades Tropicales (CIET), Facultad de Microbiología, Universidad de Costa Rica, San José 11501-2060, Costa Rica; eugenia.corrales@ucr.ac.cr (E.C.-A.); rodrigo.morarodriguez@ucr.ac.cr (R.A.M.-R.)
[2] Dulbecco Lab Studio, Residencial Lisboa 2G, Alajuela 20102, Costa Rica
* Correspondence: jorgeluis.arias@ucr.ac.cr

Abstract: Conventional plaque assays rely on the use of overlays to restrict viral infection allowing the formation of distinct foci that grow in time as the replication cycle continues leading to countable plaques that are visualized with standard techniques such as crystal violet, neutral red, or immunolabeling. This classical approach takes several days until large enough plaques can be visualized and counted with some variation due to subjectivity in plaque recognition. Since plaques are clonal lesions produced by virus-induced cytopathic effect, we applied DNA fluorescent dyes with differential cell permeability to visualize them by live-cell imaging. We could observe different stages of that cytopathic effect corresponding to an early wave of cells with chromatin-condensation followed by a wave of dead cells with membrane permeabilization within plaques generated by different animal viruses. This approach enables an automated plaque identification using image analysis to increase single plaque resolution compared to crystal violet counterstaining and allows its application to plaque tracking and plaque reduction assays to test compounds for both antiviral and cytotoxic activities. This fluorescent real-time plaque assay sums to those next-generation technologies by combining this robust classical method with modern fluorescence microscopy and image analysis approaches for future applications in virology.

Keywords: vesicular stomatitis; herpes simplex; yellow fever; animal viruses; plaque assay; real-time; live-cell imaging; automated image analysis; DNA fluorescent dyes; antiviral screening

Citation: Arias-Arias, J.L.; Corrales-Aguilar, E.; Mora-Rodríguez, R.A. A Fluorescent Real-Time Plaque Assay Enables Single-Cell Analysis of Virus-Induced Cytopathic Effect by Live-Cell Imaging. *Viruses* **2021**, *13*, 1193. https://doi.org/10.3390/v13071193

Academic Editor: Allan Brasier

Received: 31 May 2021
Accepted: 17 June 2021
Published: 22 June 2021

1. Introduction

To date, plaque assay continues to be considered the "gold standard" virological technique for quantifying viral titers of lytic virions [1]. This method was originally described by d'Hérelle for the titration and isolation of bacteriophages [2] and later was modified and adapted by Dulbecco to animal viruses such as Western Equine Encephalitis virus and poliovirus [3,4]. The great advantage of plaque assay in viral titers determination lies in its capacity to quantify the current number of infectious viral particles within a sample [5].

The typical plaque assay relies on the use of solid or semisolid overlays (i.e., agarose or carboxymethyl cellulose, respectively) to restrict viral infection and spreading to the surrounding cells of the monolayer. This allows the formation of distinct foci of cell death that grow in time as the replication-lysis-infection cycle continues, finally arising as discrete and countable plaques that are visualized after fixation and counterstained with colorimetric dyes such as neutral red or crystal violet [5,6]. However, this classical approach takes several days until large enough plaques can be visualized and present wide variations in plaque recognition and counting among different analysts [1].

Alternatively, immunofluorescent staining of viral plaques have been used to increase the sensitivity and reduce the duration of plaque assays, since fluorescence labeling of

early viral proteins enables faster identification of small plaques that are not visible by colorimetric counterstainings [1,7,8]. Nevertheless, this approach still requires cell fixation and a time-consuming immunolabeling procedure with virus-specific antibodies to reveal the plaques, making it expensive and not entirely amenable for high-throughput screenings.

Plaque growth implies viral replication, transcription, translation, release, and infection of surrounding cells [9]. Thus, the kinetic study of viral plaques formation in time at a cellular level could give valuable information about the infection established by a specific viral clone and can be used for the prediction of viral spreading behavior in vivo [9,10]. Such analysis requires live-cell imaging approaches for the kinetic visualization and monitoring of viral plaques on living cell monolayers, which presently can only be accomplished using transgenic fluorescent viruses constructed by extensive molecular work to modify the genome of reference strains [11–13].

Based on the fact that plaques are clonal lesions produced by virus-induced cytopathic effect, we applied DNA fluorescent dyes to label chromatin condensation and cell death as a way to visualize viral plaques by live-cell imaging. This approach allowed us to develop a fluorescent real-time plaque assay for the automated identification and tracking of individual viral plaques using a customized image analysis pipeline to monitor plaque formation kinetics at a single-cell level, using unlabeled wild-type viral strains. Such a procedure also enabled the automated characterization with a single-cell resolution of the cytopathic effect produced by both RNA and DNA animal viruses in terms of chromatin condensation and membrane permeabilization.

Furthermore, we describe the implementation of this novel approach for a real-time plaque reduction assay able to simultaneously screen both antiviral and cytotoxic effects in a single live cell imaging experiment. This approach will potentially enable a more efficient high-throughput screening of antiviral compounds and the evaluation of single-cell dynamics of infection within individual plaques to identify different clones within viral isolates.

2. Materials and Methods

2.1. Viruses

VSV-NJ Hazelhurst and HSV-1 F viruses were purchased from American Type Culture Collection (ATCC). Fluorescent HSV-1 F-ΔgE-GFP virus was kindly provided by David C. Johnson (Oregon Health and Science University) [11]. Vaccine strain YFV 17D was isolated in Vero cells from *Cercopithecus aethiops* (ATCC) using the commercial vaccine YF-VAX® (Sanofi Pasteur) as inoculum. All viral stocks were produced in Vero cells by inoculating cellular monolayers at a multiplicity of infection (MOI) of 0.01–0.1 and incubating for 2–5 days with Minimum Essential Medium (MEM, Gibco) supplemented with 2% fetal bovine serum (FBS, Gibco) at 37 °C in an atmosphere of 5% CO_2. Culture supernatants were collected, centrifuged at 3000× *g* for 10 min, aliquoted, and stored at −80 °C. Culture supernatant from uninfected Vero cells was also collected, stored, and used for mock infections. All viruses were titrated by plaque assay in Vero cells. Briefly, 10-fold serial dilutions of viruses were added to confluent monolayers of Vero cells. After 2 h of adsorption, cells were incubated at 37 °C in 5% CO_2 for 5 days with MEM AutoMod™ (Sigma) supplemented with 2% FBS and 1% carboxymethylcellulose (Sigma). Plaque numbers were counted after staining with crystal violet. Virus inactivation was carried out by five cycles of UV light (254 nm) exposure at an energy of 400,000 J/cm^2 in a CL-100 UV Cross-linker (UVP).

2.2. Live-Cell Imaging-Based Fluorescent Real-Time Plaque Assay

Vero cells were seeded on µClear black 96-well plates (Greiner Bio-One) at a density of 25,000 cells/well with MEM supplemented with 10% FBS. Wells from the periphery of the plate were not used to seed cells and were filled instead with 1X PBS in order to avoid desiccation in the wells with cells during long-term incubations. After 24 h of incubation at 37 °C with 5% CO_2, cells were infected with 10-fold serial dilutions of either infectious

or UV-inactivated VSV-NJ, HSV-1 F, HSV-1 F-ΔgE-GFP, or YFV 17D viruses. After 2 h of adsorption, cells were labeled with 1 µg/mL Hoechst 33342 (Invitrogen) for 10 min, washed once with 1X PBS supplemented with 1% FBS and incubated for 72–120 h at 37 °C −5% CO_2 with MEM AutoMod™ supplemented with 2% FBS, 1% carboxymethylcellulose, and 2.5 µg/mL of propidium iodide (Invitrogen) or 500 nM of SYTOX Green (Invitrogen). Washing and media addition steps were done fast and carefully in order to avoid desiccation that could kill and label with the death markers the cells on the periphery of the wells. The incubation was carried out using the above-mentioned conditions into the chamber of a Lionheart™ FX automated microscope (BioTek). Images of the whole well were acquired every 3–24 h. After the final read, viral plaques were confirmed by crystal violet staining. Automated plaque counts and single-cell analysis of viral plaques were performed by image analysis with the software CellProfiler 4.0 (http://www.cellprofiler.org; Broad Institute), using our previously reported pipelines for plaque identification (PlaqueIdentification.cpproj) and plaque tracking (PlaqueTracking.cpproj) [14], as well as a new customized pipeline for the quantification of chromatin-condensed and dead cells within individual plaques (PlaqueTrackingSX&Hoechst.cpproj, Supplementary Material). A detailed visual representation of this procedure is described in Figure S1.

2.3. Live-Cell Imaging-Based Fluorescent Real-Time Plaque Reduction Assay

Vero cells were seeded on a µClear black 96-well plate at a density of 25,000 cells/well with MEM supplemented with 10% FBS. After 24 h of incubation at 37 °C with 5% CO_2, cells were infected with 10-fold serial dilutions of HSV-1 F. After 2 h of adsorption, cells were labeled with 1 µg/mL Hoechst 33342 for 10 min, washed once with 1X PBS supplemented with 1% FBS and incubated for 96 h at 37 °C-5% CO_2 with MEM AutoMod™ supplemented with 2% FBS, 1% carboxymethylcellulose, 2.5 µg/mL of propidium iodide, and different rising concentrations of acyclovir (Sigma, 0–3000 ng/mL). Images of the whole well were acquired at 96 h post-infection with a Lionheart™ FX automated microscope and viral plaques were confirmed by crystal violet staining. Automated viral plaques and dead cells counts were performed by image analysis with the software CellProfiler 4.0, using a customized pipeline called "Plaques&CytotoxicityAnalysis.cpproj" (Supplementary Material). The 50% inhibitory concentration (IC_{50}), defined as the concentrations of antiviral required to reduce virus titers by 50%, as well as the 50% cytotoxic concentration (CC_{50}), defined as the concentration of antiviral that reduces cell viability by 50%, were calculated using non-linear regression with the software GraphPad Prism 8.0. (GraphPad Software).

2.4. Statistics

Data are expressed as mean ± standard deviation (SD) of three independent experiments. Statistical significance of the differences between mean values was determined by using either an unpaired Student's t-test or a one-way ANOVA followed by a Tukey's post hoc test with the software GraphPad Prism 8.0. The level of significance is denoted in figure legends.

3. Results

3.1. The Differential Cell Permeability of DNA Fluorescent Dyes Enables the Visualization of Different Stages of the Cytopathic Effect at a Single-Cell Level within Individual Viral Plaques

DNA fluorescent dyes have differential cell permeability properties. Hoechst 33342 (referred hereafter as Hoechst) is typically used in fluorescence microscopy and flow cytometry to stain cell nuclei and chromatin condensation, an early marker of cell death since it is able to cross cell membranes of both living and dying cells [15,16]. In addition, cell-impermeant dyes such as SYTOX Green and propidium iodide (PI), are used to stain the nuclei of dead cells with terminal membrane permeabilization, which correlates with the final stages of a viral cytopathic effect [10,17]. To investigate whether we can translate those properties to observe a differential spatial distribution of the different stages of

the virus-induced cytopathic effect, we implemented the staining of a bidimensional cell monolayer of infected viral cells with a late marker of cell death (SYTOX Green or PI) and an earlier marker for chromatin condensation (Hoechst).

First, we assessed Vesicular Stomatitis Virus (VSV) plaque formation in Vero cells as a proof of principle with an RNA virus considered to have a lytic cytopathic effect [18]. Indeed, Hoechst labeled two larger plaques than those revealed by SYTOX Green. Interestingly, the staining with Hoechst was much weaker in the internal region of the plaque indicating a loss of chromatin staining in the zone stained by SYTOX Green. A merge of those two images shows that SYTOX Green-stained cells form an internal core of late cell death, suggesting that chromatin condensation occurs earlier than membrane permeabilization and this can be reflected as a differential spatial distribution (Figure 1A). A similar distribution was observed for VSV-infected PI stained cells together with Hoechst (Figure 1B). This differential distribution cannot be observed by crystal violet staining that includes both stages into a single cell-free counterstained area (Figure 1).

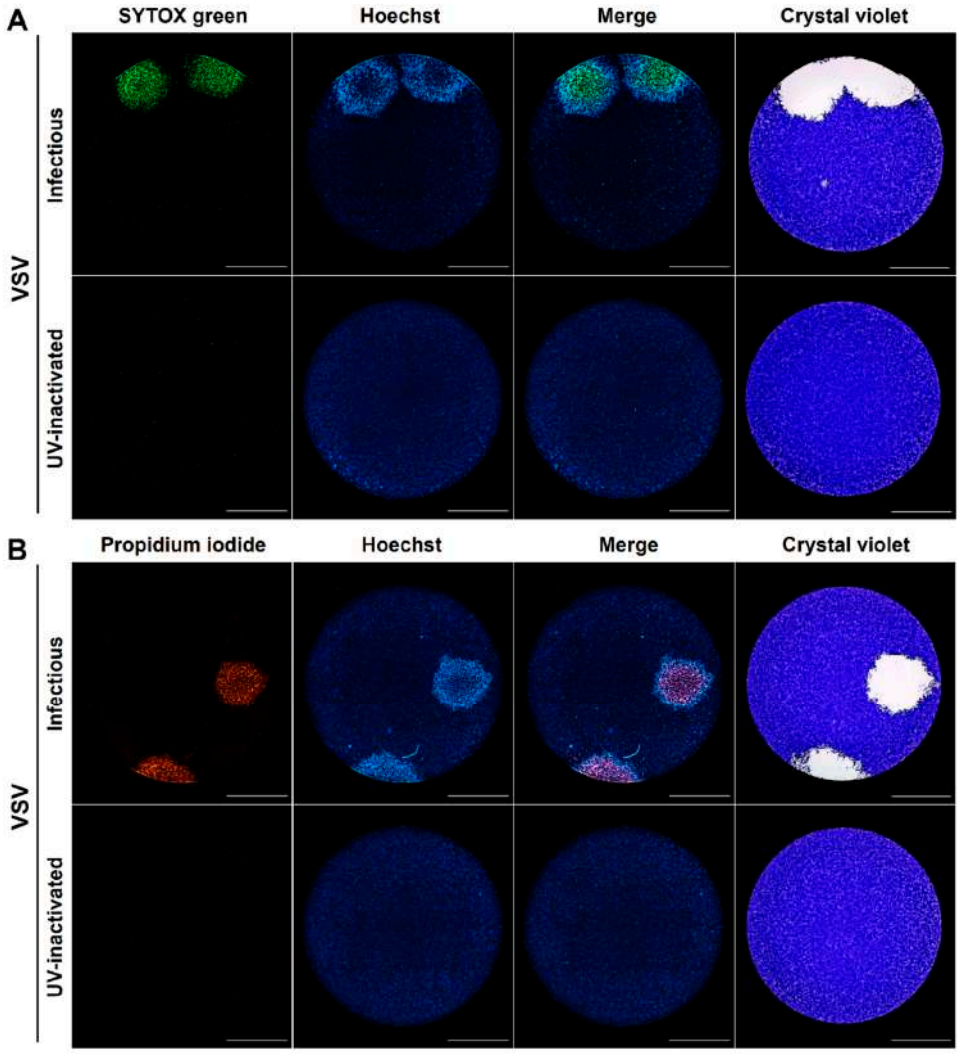

Figure 1. DNA fluorescent dyes with differential cell permeability enable the visualization by live-cell imaging of different stages of virus-induced cytopathic effect at a single-cell and single-plaque level. Vero cells were inoculated with either infectious or UV-inactivated VSV seeds, cell nuclei were stained with Hoechst, and cells were subjected to plaque assay for 72 h with a medium containing the cell death staining SYTOX Green (**A**) or propidium iodide (**B**). After live-cell imaging, acquisition viral plaques were confirmed by the standard crystal violet staining. A representative experiment is shown in each panel (n = three independent experiments), total magnification of 40X, scale bar = 2000 µm.

Second, we assessed the plaque formation of two viruses considered to have a non-cytolytic cytopathic effect, Yellow Fever Virus (YFV) and Herpes Simplex Virus (HSV) [9,19,20]. A similar spatial distribution was observed inside the plaques for both viruses with an inner core of membrane permeabilization (SYTOX Green) and an outer ring of chromatin condensation, which cannot be observed with crystal violet (Figure 2A). In addition, we assessed the effect of the current concentrations of those DNA fluorescent dyes on viral replication to rule out any interference in this assay. We revealed and counted the plaques using the standard crystal violet staining for the calculation of viral titers and observed no difference in viral replication in the presence or absence of these DNA dyes in Vero cells (Figure 2B). These results suggest that the staining with DNA fluorescent dyes with differential membrane permeability enables the visualization of different stages of the cytopathic effect at a single-cell level within individual viral plaques and indicates that DNA staining does not interfere with viral replication of both RNA and DNA animal viruses.

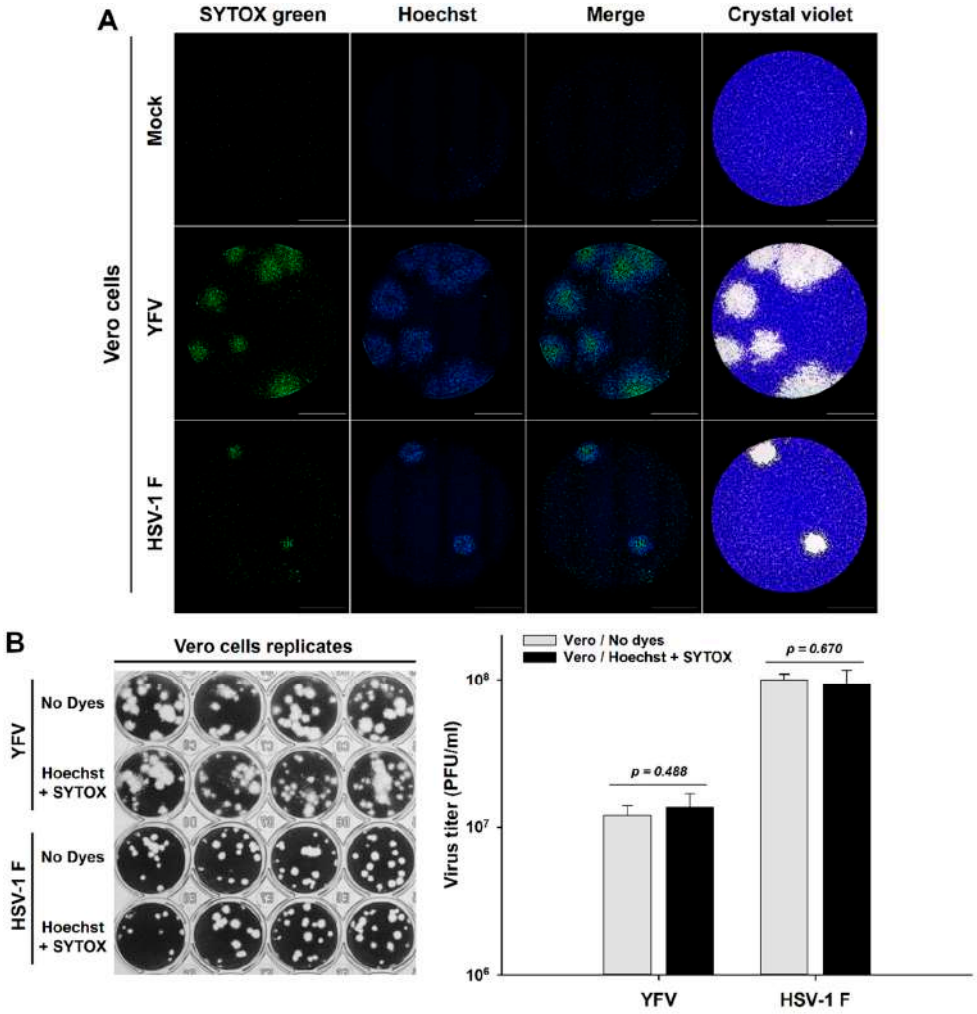

Figure 2. Labeling of virus-induced cytopathic effect with DNA fluorescent dyes has no effect on the replication of RNA and DNA animal viruses. (**A**) Vero cells were inoculated with either YFV or HSV-1 F seeds, cell nuclei were Hoechst stained, and cells were subjected to plaque assay during 120 h with a medium containing the cell death staining SYTOX Green. After live-cell imaging acquisition, viral plaques were confirmed by the standard crystal violet staining. (**B**) Vero cells were inoculated with either YFV or HSV-1 F seeds and subjected to plaque assay for 120 h both in the presence or absence of the DNA fluorescent dyes Hoechst and SYTOX Green. Plaques were revealed and counted using the standard crystal violet staining for the calculation of viral titers. A representative experiment is shown in each panel (n = three independent experiments), total magnification of 40X, scale bar = 2000 μm.

3.2. Time-Lapse Microscopy of Viral Plaques Labeled with DNA Fluorescent Dyes Enables the Real-Time Kinetic Identification of an Early Chromatin Condensation Wave Followed by a Membrane Permeabilization Wave with Single-Cell Resolution

In order to ascertain whether the differential spatial distribution observed in the viral plaques stained with DNA fluorescent dyes correspond to time-resolved stages of the viral-induced cytopathic effect, we implemented a real-time plaque assay for the kinetic monitoring of viral plaques formation by live-cell imaging. VSV-infected Vero cells were monitored for 72 h after staining with Hoechst and in medium with either SYTOX Green or PI. Indeed, the first plaque-forming cells detected had an increased Hoechst staining and this behavior spread across the neighbor cells in the first wave of chromatin condensation that was followed by a second wave of plasma membrane permeabilization after a determined delay (Figure 3A, Video S1 and Video S2). Similar behavior was observed for YFV and HSV-1 F infection in Vero cells (Figure 3B).

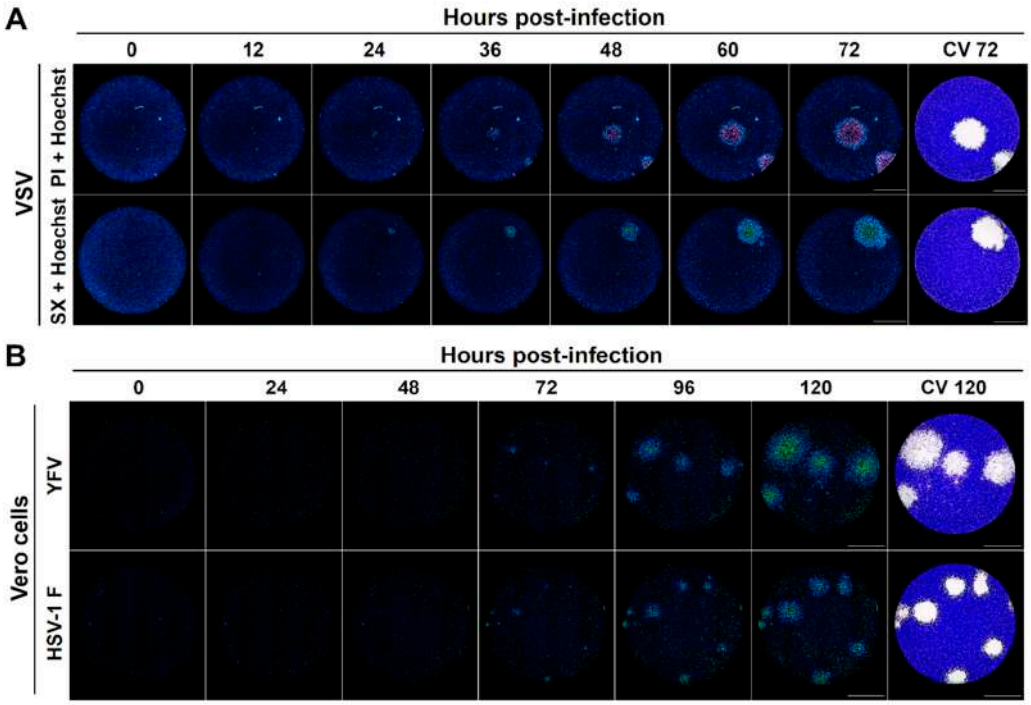

Figure 3. Labeling of individual viral plaques with DNA fluorescent dyes allows the development of a real-time plaque assay for the kinetic analysis of virus-induced cytopathic effect by live-cell imaging. (**A**) Vero cells were inoculated with infectious VSV seed, cell nuclei were stained with Hoechst, and cells were subjected to a kinetic plaque assay for 72 h with a medium containing one of the cell death dyes propidium iodide (PI) or SYTOX Green (SX). Live-cell imaging acquisition was performed every 12 h and after the final read viral plaques were confirmed by the standard crystal violet staining. (**B**) Vero cells were inoculated with either infectious YFV or HSV-1 F seeds, cell nuclei were Hoechst stained, and cells were subjected to a kinetic plaque assay for 120 h with a medium containing the cell death staining SYTOX Green. Live-cell imaging acquisition was performed every 24 h, and at the end of the experiment, viral plaques were confirmed by the standard crystal violet staining. A representative experiment is shown in each panel (n = three independent experiments), total magnification of 40X, scale bar = 2000 μm.

To confirm these findings, we analyzed the viral plaques produced by a transgenic fluorescent HSV-1 (HSV-1 F-ΔgE-GFP) using live-cell imaging. This modified virus contains a GFP insert that confers green fluorescence to the infected cells [11]. Infected and Hoechst-stained Vero cells were subjected to plaque assay during 120 h with medium containing PI and then were analyzed by live-cell imaging for red (PI), blue (Hoechst), and green (GFP) fluorescence. Again, a differential spatial distribution was observed with small PI plaques

that seem to be surrounded by larger Hoechst plaques and those by even larger GFP plaques. Both GFP and Hoechst images showed a decrease in fluorescence of their internal cores suggesting that a first wave of viable cells with viral replication (GFP) is followed by a wave of cells undergoing chromatin condensation (Hoechst) and finally by a wave of dead cells with membrane permeabilization (PI) (Figure 4). Those differences cannot be observed by classical crystal violet staining, confirming that the use of DNA fluorescent dyes with differential membrane permeability enables the time-resolved visualization of different stages of the virus-induced cytopathic effect at a single-cell level within individual viral plaques.

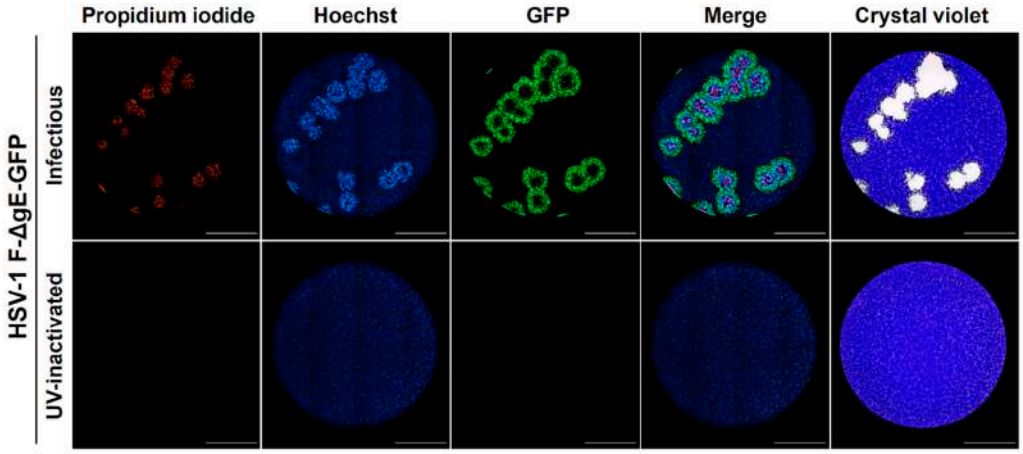

Figure 4. Comparison of DNA fluorescent dyes with a transgenic fluorescent virus for the identification of individual viral plaques by live-cell imaging. Vero cells were inoculated with either infectious or UV-inactivated HSV-1 F-ΔgE-GFP fluorescent virus, cell nuclei were Hoechst stained, and cells were subjected to plaque assay for 120 h with a medium containing the cell death dye propidium iodide. Viral plaques were confirmed by the standard crystal violet staining. Both fluorescent approaches allowed the identification of all plaques present in the samples analyzed. A representative experiment is shown (n = three independent experiments), total magnification of 40X, scale bar = 2000 μm.

3.3. The Real-Time Plaque Assay with DNA Stains of Differential Membrane Permeability Enables Automated Identification of Single Viral Plaques with Higher Resolution When Compared to the Standard Crystal Violet Staining

To evaluate the capability of a real-time plaque assay based on the staining of the different stages of viral cytopathic effect for individual plaque recognition and counting, we compared its performance to the standard crystal violet staining. We assessed two cases of viral plaques generated by YFV (case 1) and HSV-1 F (case 2) in Vero cells by those two different approaches upon interpretation by three different analysts (Figure 5A). For both cases, the plaque counts and calculated virus titers were significantly lower for the standard crystal violet staining compared to the plaques counted upon staining with Hoechst and SYTOX Green, due to an underestimation of the number of plaques in areas with plaque overlapping (Figure 5C). A closer view reveals that DNA staining increases the resolution in those areas, as it also allows the visualization of the development of individual plaques in time, enabling the identification of the initial focus of infection before overlapping (Figure 5B).

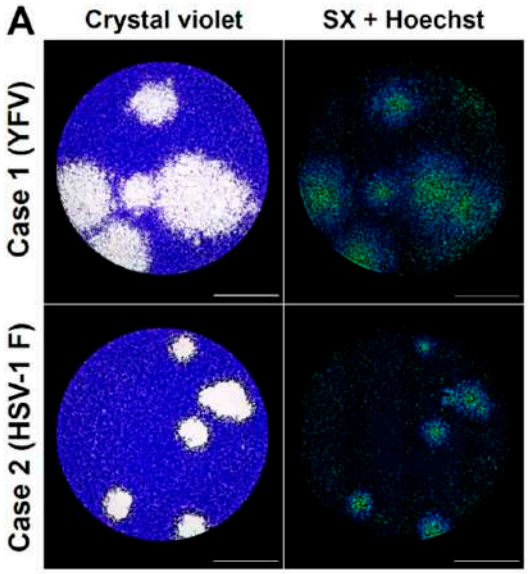

C

Method:		Crystal violet		SX + Hoechst		
Case	Analyst	PFU count	Virus titer (PFU/ml)	PFU count	Virus titer (PFU/ml)	*t* test *p* value
1	A	5	1.0×10^7	6	1.2×10^7	0.0047
	B	5	1.0×10^7	7	1.4×10^7	
	C	6	1.2×10^7	7	1.4×10^7	
2	A	5	1.0×10^8	7	1.4×10^8	0.0075
	B	5	1.0×10^8	7	1.4×10^8	
	C	6	1.2×10^8	7	1.4×10^8	

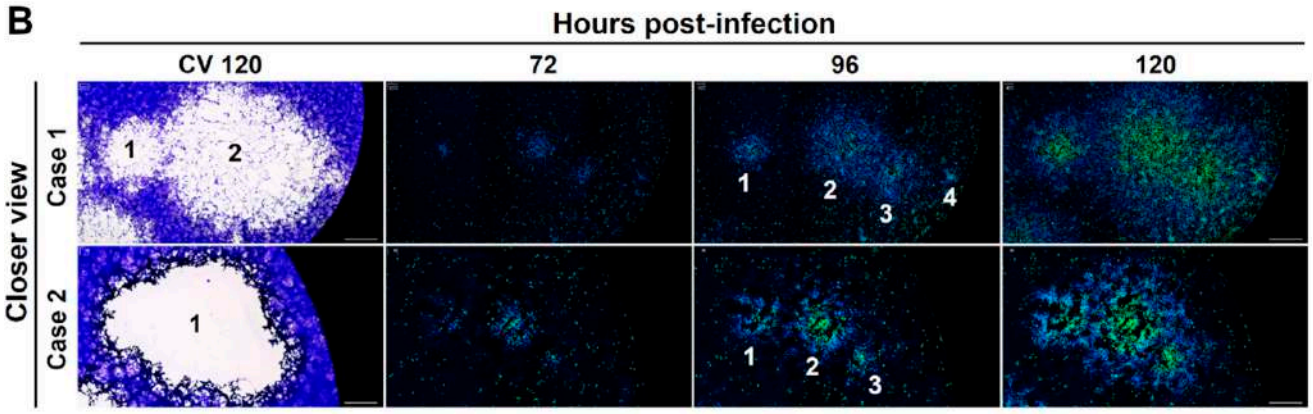

Figure 5. The fluorescent real-time plaque assay constitutes a better approach for the identification of single viral plaques when compared to the standard crystal violet staining. Two example cases of viral plaques generated by YFV (case 1) and HSV-1 F (case 2) in Vero cells were studied by both crystal violet staining and our real-time plaque assay with DNA fluorescent dyes (**A**). The kinetic analysis of viral plaques formation with our real-time plaque assay was a better approach for the calculation of the exact PFU count in those areas with plaque overlapping (**B**), as exposed by the differences in the PFU counts and final virus titers determined by three independent analysts using both the crystal violet staining and our real-time approach (**C**). Total magnification of 40X, scale bar = 2000 μm.

In order to automate the identification of viral plaques and their tracking over time, we analyzed images with our previously published image analysis pipelines developed in CellProfiler (PlaqueIdentification.cpproj and PlaqueTracking.cpproj) [14] obtaining a good time-resolved identification of individual plaques (Figure 6A). In addition, this approach allowed us to calculate the total number of cells composing the individual viral plaques over time (Figure 6B).

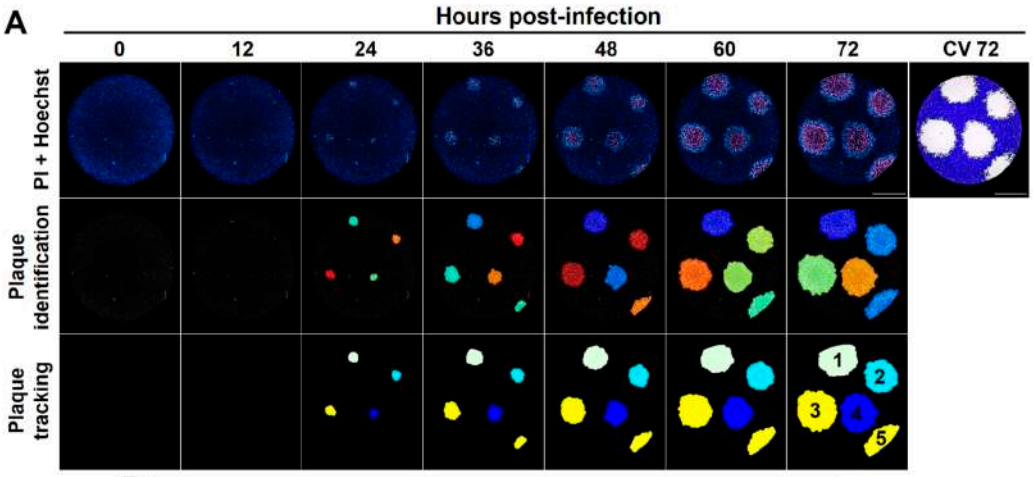

B

Cell count for each plaque at every post-infection time

Plaque	*0h*	*12h*	*24h*	*36h*	*48h*	*60h*	*72h*
1	0	0	292	780	2628	3607	6274
2	0	0	277	930	1191	5051	8572
3	0	0	264	976	1772	2299	5918
4	0	0	164	428	1870	3725	5931
5	0	0	0	660	2212	3439	3716

Figure 6. The fluorescent real-time plaque assay enables the automated analysis of the kinetics of viral plaques formation at a single-plaque and single-cell level. The kinetics of VSV plaques formation in Vero cells using our real-time plaque assay was analyzed with two different image analysis pipelines for plaque identification and plaque tracking (**A**), allowing the calculation of the cell counts for each identified viral plaque at every time point studied (**B**). A representative experiment is shown (n = three independent experiments), total magnification of 40X, scale bar = 2000 μm.

Furthermore, we developed a new image analysis pipeline (PlaqueTrackingSX& Hoechst.cpproj) to extract individual plaque information such as the total number of cells with chromatin condensation and plasma membrane permeabilization (death cells) for three animal viruses (VSV, YFV, and HSV-1 F, Figure 7A). With this approach, we noticed that the percentage of those cell subpopulations changes among different virus types (Figure 7B). These findings suggest that the ratio of single cells with a different stage of the viral cytopathic effect within a plaque could be used to differentiate plaque types in viral isolates from mixed infections or to identify mutant clones of the same virus strain. These results indicate that the labeling of viral plaques with DNA fluorescent dyes of differential cell permeability enables a high-resolution real-time plaque assay with the potential to be automated by the use of image analysis software to identify and characterize individual viral plaques.

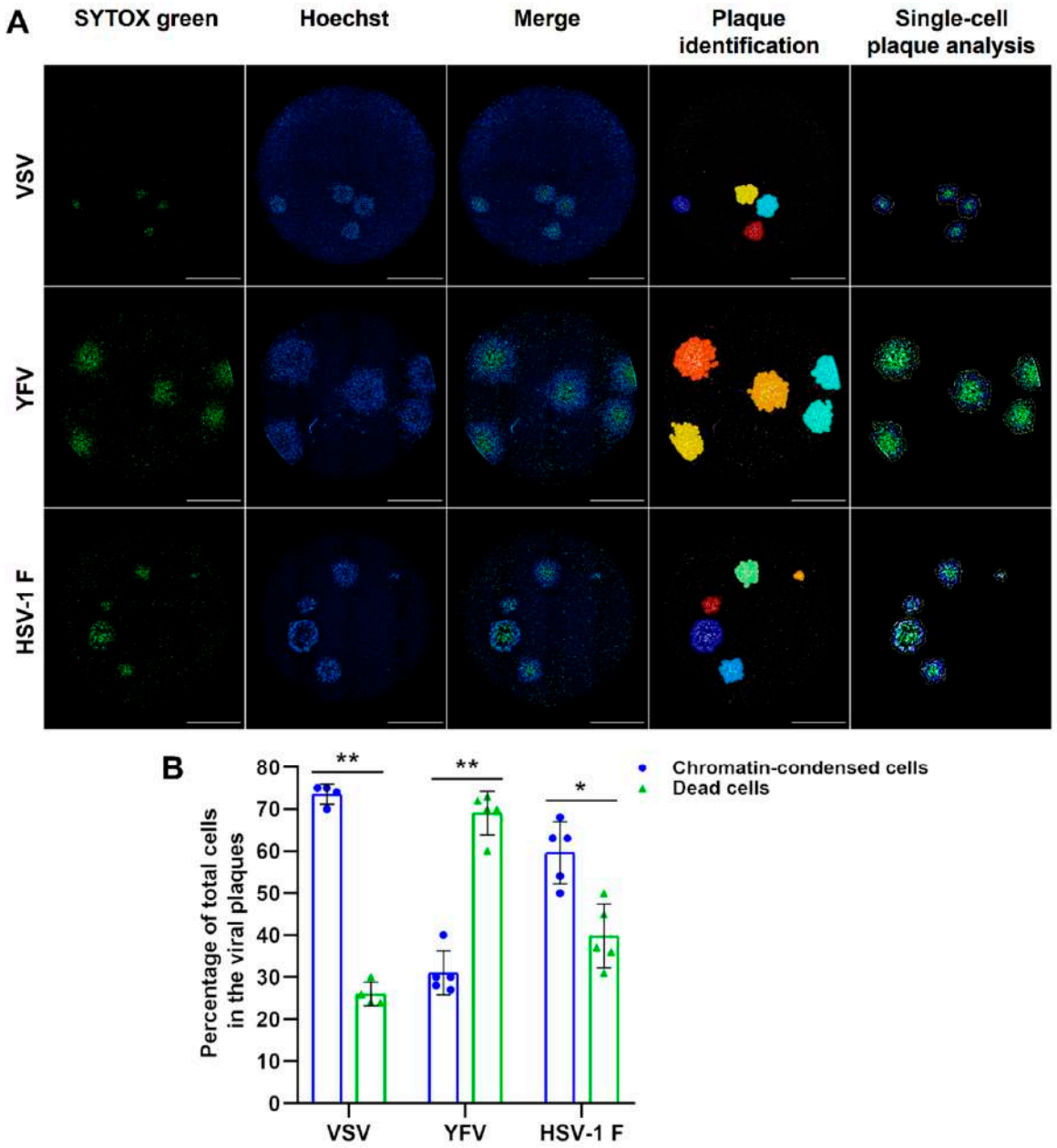

Figure 7. The fluorescent real-time plaque assay enables the automated comparative characterization of the cytopathic effect produced by different animal viruses in terms of chromatin condensation and induced cell death at a single-cell level. We applied an image analysis protocol to characterize the VSV, YFV, and HSV-1 F cytopathic effect by the quantification of fluorescence features of cells imaged to assess chromatin condensation (Hoechst) and cell death (SYTOX Green). (**A**) The image analysis protocol was applied to achieve the identification and single-cell analysis of the plaques produced by VSV at 36 h post-infection (hpi) and by YFV and HSV-1 F at 120 hpi, allowing the quantification and categorization of single cells within each plaque as chromatin-condensed (blue) and dead (green). (**B**) VSV, YFV, and HSV-1 F infection described by parameters of the percentage of chromatin-condensed and dead cells within individual viral plaques (blue dots and green triangles, respectively). Images and data from a representative analyzed experiment are shown (n = three independent experiments, magnification of 40X, scale bar = 2000 μm). Data are expressed as mean ± SD of the cell percentages calculated from the total number of plaques generated by each virus. * $p < 0.001$, ** $p < 0.00001$.

3.4. The Combination of the Real-Time Plaque Assay with Automated Image Analysis Enables a High-Resolution Real-Time Plaque Reduction Assay for the Simultaneous Screening of Drugs in Terms of Antiviral and Cytotoxic Effect

Using classical virological methods for antiviral screening, a researcher must test in a first experiment the cytotoxicity of compounds to identify sublethal concentrations before attempting to test the antiviral activity in a subsequent experiment. To confirm the potential application of our real-time plaque assay to the screening of antiviral compounds, we aimed to develop a real-time plaque reduction assay that is able to simultaneously differentiate an antiviral effect from a cytotoxic effect. First, we inoculated Vero cells with infectious HSV-1 F virus, cell nuclei were stained with Hoechst and the cells were subjected to plaque assay for 96 h in the presence of medium containing PI and rising acyclovir concentrations ranging from 0 to 3000 ng/mL. Live-cell images were obtained at 96 h and the viral plaques were confirmed at the end of the experiment with crystal violet staining. Then, we aimed to develop a new advanced image analysis pipeline for the automated counting of viral plaques to test antiviral activities and the simultaneous measurement of dead cells present in uninfected zones outside viral plaques as a measure of the cytotoxicity induced by tested compounds.

Using such an image analysis pipeline (Plaques&CytotoxicityAnalysis.cpproj), we effectively quantified the number of HSV-1 F plaques to test the antiviral activity and the number of dead cells outside those plaques to simultaneously assess for cytotoxicity induced by acyclovir treatment (Figure 8A). This allowed us to demonstrate that the antiviral compound acyclovir indeed reduced the viral titer by several logarithms (Figure 8B) and that the concentration of 3000 ng/mL was cytotoxic, displaying a significant increase of dead cells compared to lower concentrations tested (Figure 8C). With these results, it was possible to calculate the 50% inhibitory concentration (IC_{50}), 50% cytotoxic concentration (CC_{50}), and selectivity index (SI: CC_{50}/IC_{50}) for in vitro acyclovir treatment of HSV-1 F infection in Vero cells (Figure 8D). These results demonstrate the potential application of these approaches for the automated and high-resolution image analysis of a real-time plaque reduction assay for the simultaneous screening of drugs in terms of antiviral and cytotoxic effects by live-cell imaging.

Taken together, our results indicate that the use of DNA fluorescent dyes with differential permeability enables the visualization and automated quantification of different stages of the cytopathic effect at a single-cell level. These stages correspond to an early chromatin condensation wave followed by a wave of dead cells with membrane permeabilization that can be observed by time-lapse microscopy with single-cell resolution within individual viral plaques. Moreover, this approach enables the implementation of fluorescent real-time plaque assays for the identification of single viral plaques with higher resolution when compared to the standard crystal violet staining and, if enhanced with advanced image analysis, it is possible to perform an automated real-time plaque reduction assay for the simultaneous screening of drugs in terms of both antiviral and cytotoxic effects by live-cell imaging.

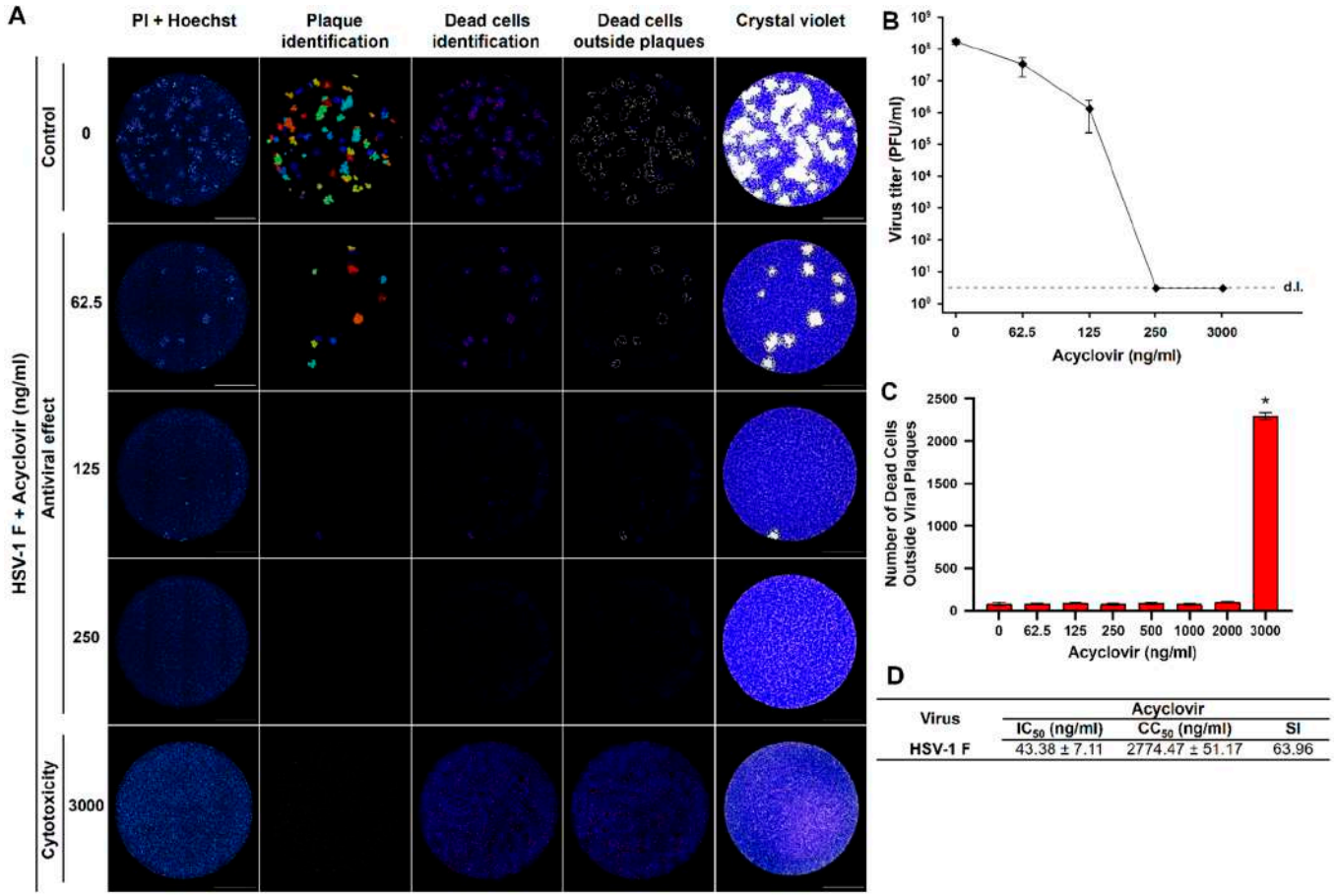

Figure 8. The fluorescent real-time plaque assay enables the application of a plaque reduction assay for the simultaneous screening of drugs in terms of antiviral and cytotoxic effects by live-cell imaging. (**A**) Vero cells were inoculated with infectious HSV-1 F virus, cell nuclei were Hoechst stained, and cells were subjected to plaque assay for 96 h with a medium containing the cell death staining propidium iodide (PI) and rising concentrations of acyclovir in the range 0–3000 ng/mL. After live-cell imaging acquisition, viral plaques were confirmed by the standard crystal violet staining. An image analysis pipeline was applied for the simultaneous counting and identification of viral plaques and the total number of dead cells. The plaque identification images were used to mask the dead cells identification images in order to obtain the number of dead cells outside the viral plaques, as a measure of the cytotoxicity generated by each concentration of the antiviral in non-infected cells. A representative experiment is shown (n = three independent experiments), total magnification of 40X, scale bar = 2000 μm. (**B**) The antiviral effect is exposed by the reduction in HSV-1 F titers produced by rising concentrations of acyclovir. d.l. = assay detection limit. (**C**) The cytotoxic effect of acyclovir is denoted by the statistically significant increment in the number of dead cells at the highest concentration tested (3000 ng/mL). * $p < 0.001$ compared to all other antiviral doses tested. (**D**) Calculated 50% inhibitory concentration (IC_{50}), 50% cytotoxic concentration (CC_{50}) and selectivity index (SI: CC_{50}/IC_{50}) for in vitro acyclovir treatment of HSV-1 F infection in Vero cells. Data are expressed as mean ± SD of three independent experiments.

4. Discussion

The present study reports the application of DNA fluorescent dyes with differential cell permeability for the development of a real-time plaque assay suitable for the automated single-cell analysis of the cytopathic effect induced by both RNA and DNA animal viruses within individual plaques. Such an approach represents a technological advance in the way that a plaque assay is conceived and expands the spectrum of utilities of this elegant virological technique that classically has been used mainly to determine infectious virus titers and for the isolation of individual viral clones [4,5,21].

However, plaques bear important information about the infection elicited by a particular virus at the cellular level. Since plaques are clonal lesions of infected cells formed by

cell-to-cell or cell-free transmission of replicating viruses leading to a subsequent cytopathic effect [9,22,23], one can conceive plaques as models to study viral infection with an intrinsic type of timeline. Thereby, the first infected cells constitute the core of the plaques and newer neighboring and radial infections occur as the virus spreads to the periphery establishing a frontal wave of viral replication and infection. Moreover, the cell monolayer surrounding viral plaques is formed by non-infected healthy cells within the same well, constituting the perfect internal control of cell viability for the tested experimental conditions. Nevertheless, the classical counterstaining-based endpoint plaque assay using crystal violet does not leave cells for further analysis and even if plaques are revealed by immunofluorescence, such an approach still requires fixation hindering the investigation of the onset and kinetics of viral infection.

Therefore, we envisaged that DNA fluorescent dyes with differential cell membrane permeability could be used not only to label viral plaques but also to obtain important information about the virus-induced cytopathic effect at the cellular level, simultaneously enabling the analysis of infection kinetics in real-time by the live-cell imaging of the individual plaques. Using this rationale, we developed a fluorescent real-time plaque assay whereby we could observe a differential spatial distribution in the virus-induced cytopathic effect within viral plaques of VZV, YFV, and HSV-1 F, characterized by an early chromatin condensation wave arising first in the origin of the plaque and followed by a membrane permeabilization wave. This leads to a clear partition of the plaque with a core of terminally dead cells surrounded by a ring of cells with chromatin condensation in the periphery (Figures 1–4, Video S1 and Video S2).

A deeper single-cell analysis of those time-resolved cellular subpopulations within viral plaques allowed us to identify interesting differences among virus types (Figure 7). We assessed the plaque formation by a virus considered to have a lytic cytopathic effect, VSV, and two other viruses considered to have a non-cytolytic cytopathic effect, YFV and HSV-1 F. Using our approach, we quantified the percentage of cells within each viral plaque corresponding to chromatin-condensed cells (Hoechst-intense cells) and dead cells with membrane permeabilization (PI or SYTOX Green positive cells). The observed variations indicate differential rates of infection and virus interaction with the cell death programs. The plaques produced by the infection with VSV have the highest proportion of chromatin condensed cells, suggesting that this VSV strain elicits a slow type of cell death in Vero cells, probably apoptosis as previously reported [24]. This finding suggests that VSV induces an early type of apoptosis reflected by a faster wave of chromatin condensation compared to the subsequent membrane permeabilization wave. Although this virus is typically considered highly cytolytic [18], Gadaleta and collaborators reported that VSV actually induces apoptosis at early stages in the viral cycle that does not depend on virus replication [24]. On the other hand, YFV-17D induces plaques with the highest proportion of dead cells suggesting a fast type of cell demise once the cell death program is engaged, probably necrosis [25]. Conversely, the cells with membrane permeabilization of the inner core of the YFV plaques keep also the Hoechst staining. This suggests that despite membrane permeabilization, the chromatin integrity is maintained, and, therefore, no empty space is visible within the Hoechst images of YFV plaques. Although YFV is typically considered as non-cytolytic [20], it was previously shown that different clones of YFV could induce small plaques or large plaques [21], probably reflecting different kinetics of cell death phases or a variable interaction with cell death mechanisms [26]. Indeed, it has been previously reported that YFV infection induces both pro-apoptotic [27] and anti-apoptotic [28] responses in vitro. Additionally, HSV-1 F has an intermediate behavior with a more similar proportion of chromatin-condensed and membrane-permeabilized cells, suggesting that HSV-1 F induced cell death has a relatively long phase of chromatin-related alterations before plasma membrane permeabilization, which is consistent with a budding virus able to delay late apoptosis and necroptosis [29]. Together, these results indicate that an intrinsic type of timeline of cell death-associated events is represented in the spatial distribution of chromatin-condensed and membrane-permeabilized cells within

each individual viral plaque. These differences can potentially be used to distinguish viral clones or viral strains in mixed infections with potential applications to high-content screening assays of antiviral compounds affecting the rates of those cell death-associated events related to infection. Indeed, additional molecular sensors can be added to the cells in order to increase the content of information and the mechanistic insights that could be obtained about virus-induced alterations in a time-resolved manner. We have previously implemented such an approach with a reporter of flavivirus protease activity [10], but other interesting molecular sensors could be added to investigate the viral activities over different cellular processes like apoptosis [30] or autophagy [31], among others.

Yakimovich and collaborators [9] pointed out the utility of multi-parametric and automated kinetic analysis of viral plaques, however, they used transgenic viruses expressing fluorescent proteins to perform time-lapse microscopy, which up to date, is the method of choice to perform a kinetic viral plaque assay [12]. We reported an alternative approach based on the development of genetically modified reporter cell lines expressing a molecular sensor of viral infection [10]. Nevertheless, these methodologies are still virus-specific and extensive molecular biology work is required in order to develop and validate such modified viruses and cell lines. In contrast, the approach described in the present work is based on the use of low-cost DNA fluorescent dyes with differential cell membrane permeability, which not only allows the kinetic monitoring of plaque formation with unlabeled wild-type viral strains but also enables the characterization of the cytopathic effect produced by both RNA and DNA animal viruses in terms of chromatin condensation and induced cell death with single-cell resolution. In theory, this methodology could be applied to any plaque-forming virus as it involves the induction of cytopathic effect that could be labeled with the mentioned DNA fluorescent dyes.

The traditional plaque assay is multi-day, labor-intensive, and can be subjective due to visual inspection and manual plaque counting by different analysts. The time-resolved monitoring of viral plaques and the associated image analysis pipelines available here represent a technological advance compared to the classic crystal violet counterstaining. The approach presented here will pave the way towards an optimal identification and characterization of viral plaques with higher resolution, objectiveness, and information content. The image analysis pipelines (step-by-step protocols of image analysis) were developed in CellProfiler, an open-source software designed to share so that they could be available for all the interested scientific community (see Supplementary Material). We have developed a specific pipeline optimized to analyze the data of a real-time plaque reduction assay able to simultaneously screen for antiviral activities in plaques labeled with DNA dyes of differential membrane permeability and the cytotoxic effect of any chemical compound to be tested (Figure 8). Using this approach we were able to calculate an IC_{50} of 0.04 µg/mL of acyclovir for the inhibition of HSV-1 replication in vitro. These results are similar to those obtained with conventional plaque-reduction assays, as it has been previously reported that the IC_{50} of acyclovir against HSV-1 isolates ranges from 0.02 to 13.50 µg/mL [32–35]. This all-in-one assay will help to dissect confounding results of compounds with apparent antiviral activities that, in fact, lead to cellular alterations in viability or cell death subroutines that also impair viral replication by non-specific mechanisms.

Current advances in time-resolved microscopy and live-cell imaging are changing the methodological paradigm in many fields of biological sciences, including virology, which is reflected by the increasing number of procedures based on the kinetic visualization of the phenomenon being studied. Our fluorescent real-time plaque assay sums to those next-generation technologies by the combination of this robust classical method with the modern fluorescence microscopy and image analysis approaches. We envisaged that customized adaptations of this technology would be applied in future studies aimed to understand and decipher the mechanisms behind virus-host cell interactions, a pivotal knowledge for the development of vaccines and antiviral drugs to treat viral infections.

Supplementary Materials: The following are available online at https://www.mdpi.com/article/10.3390/v13071193/s1, Figure S1: Methodological workflow of the fluorescent real-time plaque assay, Video S1: Kinetics of VSV-NJ plaques formation in living Vero cells (0–72 h) using Hoechst 33342 and propidium iodide, Video S2: Kinetics of VSV-NJ plaques formation in living Vero cells (0–72 h) using Hoechst 33342 and SYTOX Green, CellProfiler image analysis pipelines: PlaqueIdentification.cpproj, PlaqueTracking.cpproj, PlaqueTrackingSX&Hoechst.cpproj, and Plaques&CytotoxicityAnalysis.cpproj.

Author Contributions: Conceptualization, J.L.A.-A.; methodology, J.L.A.-A. and R.A.M.-R.; investigation, J.L.A.-A.; data curation, J.L.A.-A.; validation, J.L.A.-A.; visualization, J.L.A.-A.; formal analysis, J.L.A.-A. and R.A.M.-R.; resources, J.L.A.-A., E.C.-A., and R.A.M.-R.; writing—original draft preparation, J.L.A.-A. and R.A.M.-R.; writing—review and editing, J.L.A.-A. and R.A.M.-R.; supervision, R.A.M.-R.; funding acquisition, R.A.M.-R.; project administration, R.A.M.-R. All authors have read and agreed to the published version of the manuscript.

Funding: International Centre for Genetic Engineering and Biotechnology Grant CRP/CRI18-02.

Data Availability Statement: Data is contained within the article.

Acknowledgments: The authors thank Francisco Vega-Aguilar (Universidad de Costa Rica) for technical assistance with viral stocks preparation.

Conflicts of Interest: The authors declare no conflict of interest. The funders had no role in the design of the study; in the collection, analyses, or interpretation of data; in the writing of the manuscript, or in the decision to publish the results.

References

1. Wen, Z.; Citron, M.; Bett, A.J.; Espeseth, A.S.; Vora, K.A.; Zhang, L.; DiStefano, D.J. Development and application of a higher throughput RSV plaque assay by immunofluorescent imaging. *J. Virol. Methods* **2019**, *263*, 88–95. [CrossRef]
2. d'Hérelle, F. The bacteriophage and its behavior. *Nature* **1926**, *118*, 183–185. [CrossRef]
3. Dulbecco, R. Production of plaques in monolayer tissue cultures by single particles of an animal virus. *Proc. Natl. Acad. Sci. USA* **1952**, *38*, 747–752. [CrossRef] [PubMed]
4. Dulbecco, R.; Vogt, M. Plaque formation and isolation of pure lines with poliomyelitis viruses. *J. Exp. Med.* **1954**, *99*, 167–182. [CrossRef] [PubMed]
5. Baer, A.; Kehn-Hall, K. Viral concentration determination through plaque assays: Using traditional and novel overlay systems. *J. Vis. Exp.* **2014**, 1–10. [CrossRef]
6. Mendoza, E.J.; Manguiat, K.; Wood, H.; Drebot, M. Two detailed plaque assay protocols for the quantification of infectious SARS-CoV-2. *Curr. Protoc. Microbiol.* **2020**, *57*, cpmc105. [CrossRef] [PubMed]
7. Masci, A.L.; Menesale, E.B.; Chen, W.C.; Co, C.; Lu, X.; Bergelson, S. Integration of fluorescence detection and image-based automated counting increases speed, sensitivity, and robustness of plaque assays. *Mol. Ther. Methods Clin. Dev.* **2019**, *14*, 270–274. [CrossRef] [PubMed]
8. Amarilla, A.A.; Modhiran, N.; Setoh, Y.X.; Peng, N.Y.G.; Sng, J.D.J.; Liang, B.; McMillan, C.L.D.; Freney, M.E.; Cheung, S.T.M.; Chappell, K.J.; et al. An optimized high-throughput immuno-plaque assay for SARS-CoV-2. *Front. Microbiol.* **2021**, *12*, 1–17. [CrossRef]
9. Yakimovich, A.; Andriasyan, V.; Witte, R.; Wang, I.H.; Prasad, V.; Suomalainen, M.; Greber, U.F. Plaque2.0-a high-throughput analysis framework to score virus-cell transmission and clonal cell expansion. *PLoS ONE* **2015**, *10*, e0138760. [CrossRef] [PubMed]
10. Arias-Arias, J.L.; MacPherson, D.J.; Hill, M.E.; Hardy, J.A.; Mora-Rodríguez, R. A fluorescence-activatable reporter of flavivirus NS2B–NS3 protease activity enables live imaging of infection in single cells and viral plaques. *J. Biol. Chem.* **2020**, *295*, 2212–2226. [CrossRef]
11. Farnsworth, A.; Goldsmith, K.; Johnson, D.C. Herpes Simplex virus glycoproteins gD and gE/gI serve essential but redundant functions during acquisition of the virion envelope in the cytoplasm. *J. Virol.* **2003**, *77*, 8481–8494. [CrossRef]
12. Van Remmerden, Y.; Xu, F.; Van Eldik, M.; Heldens, J.G.M.; Huisman, W.; Widjojoatmodjo, M.N. An improved respiratory syncytial virus neutralization assay based on the detection of green fluorescent protein expression and automated plaque counting. *Virol. J.* **2012**, *9*, 1–7. [CrossRef]
13. Tamura, T.; Fukuhara, T.; Uchida, T.; Ono, C.; Mori, H.; Sato, A.; Fauzyah, Y.; Okamoto, T.; Kurosu, T.; Setoh, Y.X.; et al. Characterization of recombinant Flaviviridae viruses possessing a small reporter tag. *J. Virol.* **2017**, *92*, e01582-17. [CrossRef]
14. Arias-Arias, J.L.; Mora-Rodríguez, R. Generation and Implementation of Reporter BHK-21 Cells for Live Imaging of Flavivirus Infection. *Bio-Protocol* **2021**, *11*, e3942. [CrossRef]
15. Xiang, Y.; Cox, H.; Lebedeva, I.; Coleman, J.; Shen, D.; Pande, P.; Schultz, J.; Patton, W.F. A cell-permeant dye for cell cycle analysis by flow and laser-scanning microplate cytometry. *Nat. Methods* **2009**, *6*, an2–an3. [CrossRef]
16. Hubbard, K.S.; Gut, I.M.; Scheeler, S.M.; Lyman, M.E.; McNutt, P.M. Compatibility of SYTO 13 and Hoechst 33342 for longitudinal imaging of neuron viability and cell death. *BMC Res. Notes* **2012**, *5*, 1. [CrossRef] [PubMed]

17. Wlodkowic, D.; Faley, S.; Darzynkiewicz, Z.; Cooper, J.M. Real-time cytotoxicity assays. *Methods Mol. Biol.* **2011**, *731*, 285–291. [CrossRef] [PubMed]
18. Bishnoi, S.; Tiwari, R.; Gupta, S.; Byrareddy, S.N.; Nayak, D. Oncotargeting by Vesicular Stomatitis Virus (VSV): Advances in cancer therapy. *Viruses* **2018**, *10*, 90. [CrossRef]
19. Yoon, M.; Spear, P.G. Disruption of adherens junctions liberates Nectin-1 to serve as receptor for herpes simplex virus and pseudorabies virus entry. *J. Virol.* **2002**, *76*, 7203–7208. [CrossRef] [PubMed]
20. Ghosh Roy, S.; Sadigh, B.; Datan, E.; Lockshin, R.A.; Zakeri, Z. Regulation of cell survival and death during Flavivirus infections. *World J. Biol. Chem.* **2014**, *5*, 93–105. [CrossRef] [PubMed]
21. Liprandi, F. Isolation of plaque variants differing in virulence from the 17D strain of yellow fever virus. *J. Gen. Virol.* **1981**, *56*, 363–370. [CrossRef]
22. Burckhardt, C.J.; Greber, U.F. Virus movements on the plasma membrane support infection and transmission between cells. *PLoS Pathog.* **2009**, *5*, e1000621. [CrossRef]
23. Mothes, W.; Sherer, N.M.; Jin, J.; Zhong, P. Virus cell-to-cell transmission. *J. Virol.* **2010**, *84*, 8360–8368. [CrossRef]
24. Gadaleta, P.; Vacotto, M.; Coulombié, F. Vesicular stomatitis virus induces apoptosis at early stages in the viral cycle and does not depend on virus replication. *Virus Res.* **2002**, *86*, 87–92. [CrossRef]
25. Quaresma, J.A.S.; Barros, V.L.R.S.; Pagliari, C.; Fernandes, E.R.; Guedes, F.; Takakura, C.F.H.; Andrade, H.F.; Vasconcelos, P.F.C.; Duarte, M.I.S. Revisiting the liver in human yellow fever: Virus-induced apoptosis in hepatocytes associated with TGF-β, TNF-α and NK cells activity. *Virology* **2006**, *345*, 22–30. [CrossRef] [PubMed]
26. Pan, Y.; Cheng, A.; Wang, M.; Yin, Z.; Jia, R. The dual regulation of apoptosis by flavivirus. *Front. Microbiol.* **2021**, *12*, 574. [CrossRef] [PubMed]
27. Holanda, G.M.; Casseb, S.M.M.; Quaresma, J.A.S.; Vasconcelos, P.F.C.; Cruz, A.C.R. Yellow fever virus modulates cytokine mRNA expression and induces activation of caspase 3/7 in the human hepatocarcinoma cell line HepG2. *Arch. Virol.* **2019**, *164*, 1187–1192. [CrossRef] [PubMed]
28. Airo, A.M.; Urbanowski, M.D.; Lopez-Orozco, J.; You, J.H.; Skene-Arnold, T.D.; Holmes, C.; Yamshchikov, V.; Malik-Soni, N.; Frappier, L.; Hobman, T.C. Expression of flavivirus capsids enhance the cellular environment for viral replication by activating Akt-signalling pathways. *Virology* **2018**, *516*, 147–157. [CrossRef] [PubMed]
29. Yu, X.; He, S. The interplay between human herpes simplex virus infection and the apoptosis and necroptosis cell death pathways. *Virol. J.* **2016**, *13*, 1–8. [CrossRef] [PubMed]
30. Zhang, Q.; Schepis, A.; Huang, H.; Yang, J.; Ma, W.; Torra, J.; Zhang, S.Q.; Yang, L.; Wu, H.; Nonell, S.; et al. Designing a green fluorogenic protease reporter by flipping a beta strand of GFP for imaging apoptosis in animals. *J. Am. Chem. Soc.* **2019**, *141*, 4526–4530. [CrossRef] [PubMed]
31. Tanida, I.; Ueno, T.; Uchiyama, Y. A super-ecliptic, phluorin-mkate2, tandem fluorescent protein-tagged human LC3 for the monitoring of mammalian autophagy. *PLoS ONE* **2014**, *9*, e110600. [CrossRef] [PubMed]
32. Schaeffer, H.J.; Beauchamp, L.; De Miranda, P.; Elion, G.B.; Bauer, D.J.; Collins, P. 9-(2-Hydroxyethoxymethyl)guanine activity against viruses of the herpes group. *Nature* **1978**, *272*, 583–585. [CrossRef] [PubMed]
33. Crumpacker, C.S.; Schnipper, L.E.; Zaia, J.A.; Levin, M.J. Growth inhibition by acycloguanosine of herpesviruses isolated from human infections. *Antimicrob. Agents Chemother.* **1979**, *15*, 642–645. [CrossRef] [PubMed]
34. Andrei, G.; Snoeck, R.; Desmyter, J.; Hospital, A. Comparative activity of various compounds against clinical strains of Herpes Simplex Virus. *Eur. J. Clin. Microbiol. Infect. Dis. Vol.* **1992**, *11*, 143–151. [CrossRef] [PubMed]
35. Weinberg, A.; Bate, B.J.; Masters, H.B.; Schneider, S.A.; Clark, J.C.; Wren, C.G.; Allaman, J.A.; Levin, M.J. In vitro activities of penciclovir and acyclovir against herpes simplex virus types 1 and 2. *Antimicrob. Agents Chemother.* **1992**, *36*, 2037–2038. [CrossRef] [PubMed]

Chapter 3

Fluorescence live-cell imaging protocols to study flavivirus infection kinetics in animal cells

Summary

Presently, the study of flavivirus infection kinetics by live-cell imaging is based on the application of either recombinant viral genomes/replicons or the use of cell-based molecular reporters of the viral NS2B-NS3 protease activity, such as the already discussed flavivirus-activatable GFP and mNeptune reporters that we developed here. During this research we also introduced and validated a new approach based on the fluorescent labeling of virus-induced CPE, as presented before in this dissertation. The present chapter includes a detailed protocol for the generation, selection and implementation of stable BHK-21 cells expressing our flavivirus genetically-encoded molecular reporters, suitable to monitor the viral infection kinetics by live-cell imaging. Special attention has been given on the description of the cell image analysis procedures applied to obtain the final results, in terms of number of infected cells/viral plaques and reporter's integrated fluorescence intensity. Besides, a detailed protocol for the kinetic monitoring of flavivirus infection by the fluorescent labeling of CPE is also described in detail at the end of this chapter. Such protocols can be combined in a multireporter platform for the implementation of cell-population kinetics of infection in single cells as well as in viral plaques using both reference and wild-type flaviviral strains.

Published article

Arias-Arias J.L., Mora-Rodríguez R., 2021. *Generation and implementation of reporter BHK-21 cells for live imaging of flavivirus infection*. Bio-protocol 11, e3942. https://doi.org/10.21769/BioProtoc.3942

Please cite this article as: Arias-Arias and Mora-Rodríguez, (2021). Generation and Implementation of Reporter BHK-21 Cells for Live Imaging of Flavivirus Infection,*Bio-protocol* 11 (5): e3942. DOI: 10.21769/BioProtoc.3942.

bio-protocol www.bio-protocol.org/e3942 Bio-protocol 11(05): e3942. DOI:10.21769/BioProtoc.3942

Generation and Implementation of Reporter BHK-21 Cells for Live Imaging of Flavivirus Infection

Jorge L. Arias-Arias and Rodrigo Mora-Rodríguez*

Centro de Investigación en Enfermedades Tropicales, Facultad de Microbiología, Universidad de Costa Rica, San José, 11501-2060, Costa Rica

*For correspondence: rodrigo.morarodriguez@ucr.ac.cr

[Abstract] The genus *Flavivirus* within the family Flaviviridae includes many viral species of medical importance, such as yellow fever virus (YFV), Zika virus (ZIKV), and dengue virus (DENV), among others. Presently, the identification of flavivirus-infected cells is based on either the immunolabeling of viral proteins, the application of recombinant reporter replicons and viral genomes, or the use of cell-based molecular reporters of the flaviviral protease NS2B-NS3 activity. Among the latter, our flavivirus-activatable GFP and mNeptune reporters contain a quenching peptide (QP) joined to the fluorescent protein by a linker consisting of a cleavage site for the flavivirus NS2B-NS3 proteases (AAQRRGRIG). When the viral protease cleaves the linker, the quenching peptide is removed, and the fluorescent protein adopts a conformation promoting fluorescence. Here we provide a detailed protocol for the generation, selection and implementation of stable BHK-21 cells expressing our flavivirus genetically-encoded molecular reporters, suitable to monitor the viral infection by live-cell imaging. We also describe the image analysis procedures and provide the required software pipelines. Our reporter cells allow the implementation of single-cell infection kinetics as well as plaque assays for both reference and native strains of flaviviruses by live-cell imaging.

Graphic abstract:

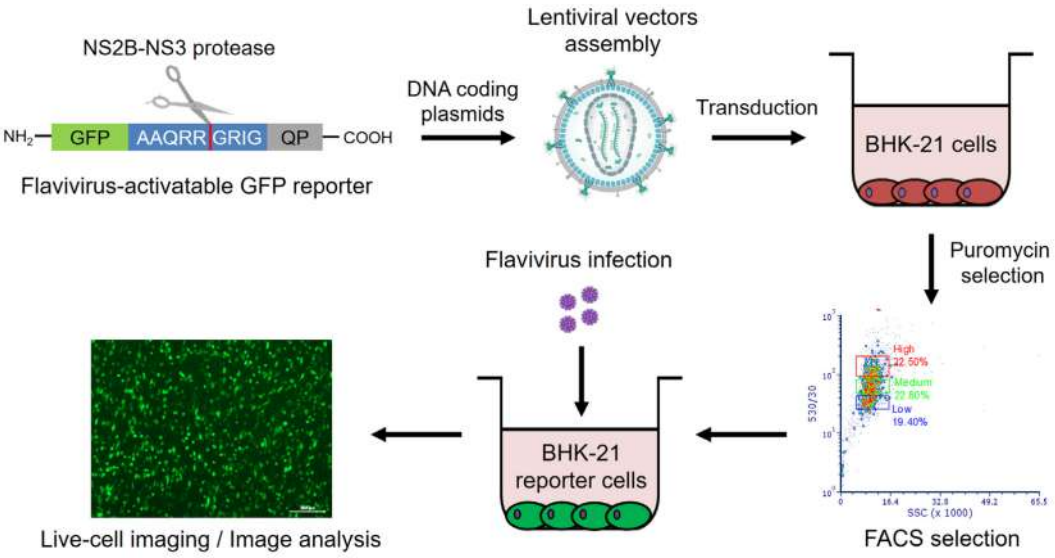

Workflow for the generation and implementation of reporter BHK-21 cells for live imaging of flavivirus infection.

Please cite this article as: Arias-Arias and Mora-Rodríguez, (2021). Generation and Implementation of Reporter BHK-21 Cells for Live Imaging of Flavivirus Infection,*Bio-protocol* 11 (5): e3942. DOI: 10.21769/BioProtoc.3942.

Keywords: Flavivirus, Fluorescence, NS2B-NS3, Protease, Live-cell imaging, Reporter cells, Plaque assay, Image analysis

[Background] Flaviviruses represent an emerging and re-emerging global threat that cause diseases both in animals and humans, including many medically relevant viruses like yellow fever virus (YFV), West Nile virus (WNV), Japanese encephalitis virus (JEV), dengue virus (DENV), and Zika virus (ZIKV), among others (Gould and Solomon, 2008). At present, the detection of flavivirus-infected cells is based on either the antibody labeling of viral proteins (Balsitis *et al.*, 2008), the use of recombinant reporter replicons and viral genomes (Li *et al.*, 2013; Schmid *et al.*, 2015; Xie *et al.*, 2016; Tamura *et al.*, 2017; Kümmerer, 2018), or the application of genetically-encoded molecular reporters of the flavivirus NS2B-NS3 proteolytic activity (Medin *et al.*, 2015; Hsieh *et al.*, 2017; McFadden *et al.*, 2018). Immunolabeling implies both fixation and permeabilization which hamper their implementation for studies in living cells. Reporter replicons and viral genomes are suitable for live-cell imaging assays, but they are restricted to particular molecular clones mainly derived from reference strains and thus, not applicable when working with clinical isolates or native viral strains. In this context, cell-based molecular reporters of the flaviviral proteases constitute a favorable alternative for the study of native flavivirus strains by live-cell imaging. Based on our recently published flavivirus-activatable GFP (FlaviA-GFP) and flavivirus-activatable mNeptune (FlaviA-mNeptune) reporters (Arias-Arias *et al.*, 2020), here we describe in detail a protocol for the generation, selection, and implementation of stably-transduced reporter BHK-21 cells for live imaging of flavivirus infection in single cells and viral plaques. Furthermore, we provide a rationale for a software-based image analysis approach to demonstrate the capabilities of this reporter cell line for single-cell and viral-plaque tracking. In addition, we include the optimized CellProfiler analysis pipelines for studies employing this or other cell-based reporters. Our approach represents the first fluorescence activatable cell-based reporter system for monitoring the kinetics of infection by both reference and native strains of flaviviruses like DENV, ZIKV, and YFV using live-cell imaging.

Materials and Reagents

1. Cell culture flasks, 75 cm^2 (Greiner Bio-One, CELLSTAR®, catalog number: 658175)
2. Cell culture dishes, 100/20 mm (Greiner Bio-One, CELLSTAR®, catalog number: 664160)
3. 2 ml reaction tubes (Greiner Bio-One, catalog number: 623201)
4. 3 ml sterile syringes (Ultident Scientific, catalog number: BD-309657)
5. Syringe filters 0.2 µm hydrophilic polyethersulfone, 32 mm diameter (Pall, Acrodisc®, catalog number: 4652)
6. 10 ml sterile syringes (Ultident Scientific, catalog number: BD-302995)
7. Syringe filters 0.45 µm hydrophilic cellulose acetate, 28 mm diameter (Sartorius, Minisart®, catalog number: 16555)

8. 15 ml conical tubes (Greiner Bio-One, CELLSTAR®, catalog number: 188271)
9. 0.5 ml reaction tubes (Greiner Bio-One, catalog number: 667201)
10. Hexadimethrine bromide (Merck, Sigma-Aldrich, catalog number: H9268)
11. 48-well cell culture plates (Greiner Bio-One, CELLSTAR®, catalog number: 677180)
12. 1.5 ml reaction tubes (Greiner Bio-One, catalog number: 616201)
13. 12-well cell culture plates (Greiner Bio-One, CELLSTAR®, catalog number: 665180)
14. 1.5 ml light protection reaction tubes (Greiner Bio-One, catalog number: 616283)
15. Cell culture flasks, 25 cm^2 (Greiner Bio-One, CELLSTAR®, catalog number: 690175)
16. 6-well cell culture plates (Greiner Bio-One, CELLSTAR®, catalog number: 657160)
17. 96-well black cell culture plates (Greiner Bio-One, µCLEAR®, catalog number: 655096)
18. 24-well cell culture plates (Greiner Bio-One, CELLSTAR®, catalog number: 662160)
19. HEK 293T cells (ATCC, catalog number: CRL-3216)
20. Plasmids:
    pLenti-FlaviA-GFP-puro (a gift from Jorge L. Arias-Arias, Addgene plasmid #140088)
    pLenti-CMV-FlaviA-mNeptune-puro (a gift from Jorge L. Arias-Arias, Addgene plasmid #140091)
    pMD2.G (a gift from Didier Trono, Addgene plasmid #12259)
    psPAX2 (a gift from Didier Trono, Addgene plasmid #12260)
21. LB agar plates with 100 µg/ml ampicillin (Merck, Sigma-Aldrich, catalog number: L5667)
22. LB broth (Miller) (Merck, Sigma-Aldrich, catalog number: L2542)
23. 100 mg/ml ampicillin solution (Merck, Sigma-Aldrich, catalog number: A5354)
24. NucleoSpin plasmid mini kit (Macherey-Nagel, catalog number: 740588.50)
25. DMEM, high glucose, GlutaMAX™, pyruvate (Thermo Fisher Scientific, Gibco, catalog number: 10569044)
26. Antibiotic-antimycotic 100× (Thermo Fisher Scientific, Gibco, catalog number: 15240062)
27. Fetal bovine serum (FBS) qualified, heat inactivated (Thermo Fisher Scientific, Gibco, catalog number: 10438-026)
28. Polyethylenimine (PEI), linear, MW 25000, transfection grade (Polysciences, PEI 25K™, catalog number: 23966-1)
29. UltraPure™ DNase/RNase-free distilled water (Thermo Fisher Scientific, Invitrogen, catalog number: 10977015)
30. Hydrochloric acid, 36.5-38.0%, BioReagent (Merck, Sigma-Aldrich, catalog number: H1758)
31. BHK-21 [C-13] (ATCC, catalog number: CCL-10)
32. MEM, GlutaMAX™ supplement (Thermo Fisher Scientific, Gibco, catalog number: 41090101).
33. Sodium pyruvate, 100 mM (Thermo Fisher Scientific, Gibco, catalog number: 11360070).
34. PBS, pH 7.4 (Thermo Fisher Scientific, Gibco, catalog number: 10010023).
35. TrypLE™ express enzyme (1×), no phenol red (Thermo Fisher Scientific, Gibco, catalog number: 12604013)
36. Puromycin dihydrochloride from *Streptomyces alboniger* (Merck, Sigma-Aldrich, catalog number: P8833)

Please cite this article as: Arias-Arias and Mora-Rodríguez, (2021). Generation and Implementation of Reporter BHK-21 Cells for Live Imaging of Flavivirus Infection,*Bio-protocol* 11 (5): e3942. DOI: 10.21769/BioProtoc.3942.

37. Clinical isolate DENV-2/CR/13538/2007 (Instituto Costarricense de Investigación y Enseñanza en Nutrición y Salud, Cartago, Costa Rica) (Soto-Garita *et al.*, 2016)
38. Vaccine strain YFV/US/17D/1937 (Sanofi Pasteur, YF-VAX®)
39. FluoroBrite™ DMEM (Thermo Fisher Scientific, Gibco, catalog number: A1896701)
40. GlutaMAX™ supplement (Thermo Fisher Scientific, Gibco, catalog number: 35050061)
41. Minimum essential medium eagle AutoMod™ (Merck, Sigma-Aldrich, catalog number: M0769)
42. Carboxymethylcellulose sodium salt (Merck, Sigma-Aldrich, catalog number: C4888)
43. Sodium bicarbonate (Merck, Sigma-Aldrich, catalog number: S5761)
44. Complete DMEM (see Recipes)
45. PEI solution (1 mg/ml) (see Recipes)
46. Polybrene solution (10 mg/ml) (see Recipes)
47. Complete MEM (see Recipes)
48. PBS 1% FBS (see Recipes)
49. Puromycin solution (10 mg/ml) (see Recipes)
50. FluoroBrite™ DMEM 2% FBS (see Recipes)
51. Plaque media 2% FBS (see Recipes)

Equipment

1. Biological safety cabinet (ESCO, Labculture® Class II, Type A2, catalog number: LA2-3A2-E)
2. CO_2 incubator (Thermo Scientific, model: Forma Series II, catalog number: 3110)
3. 4 °C refrigerator (Thermo Scientific, Value Lab, catalog number: 20LREETSA)
4. -20 °C freezer (Thermo Scientific, Value Lab, catalog number: 20LFEETSA)
5. -80 °C freezer (Sanyo, VIP series, catalog number: MDF-U32V)
6. Water bath (PolyScience, catalog number: WBE20A12E)
7. Centrifuge (Eppendorf, model: 5810)
8. Microcentrifuge (Eppendorf, model: 5418)
9. Pipettes (Thermo Scientific, Finnpipette™ F2 GLP Kit, catalog number: 4700880)
10. Pipet filler (Thermo Scientific, S1, catalog number: 9511)
11. Hemocytometer (Boeco, Neubauer improved, catalog number: BOE 13)
12. Shaking incubator (Shel Lab, catalog number: SSI3)
13. ThermoMixer® C block (Eppendorf, catalog number: 5382000015)
14. Vortex mixer (Thermo Scientific, MaxiMix™, catalog number: M16715Q)
15. Ultraviolet crosslinker (UVP, CL-100, catalog number: UVP95017401)
16. NanoDrop™ 2000 spectrophotometer (Thermo Scientific, catalog number: ND-2000)
17. Steam sterilizer (Yamato, catalog number: SQ510)
18. Water purification system (Merck, Milli-Q advantage A10)
19. Inverted microscope (Nikon, Eclipse, catalog number: TS100)
20. Flow cytometer (BD Biosciences, BD Accuri™ C6)

Please cite this article as: Arias-Arias and Mora-Rodríguez, (2021). Generation and Implementation of Reporter BHK-21 Cells for Live Imaging of Flavivirus Infection,*Bio-protocol* 11 (5): e3942. DOI: 10.21769/BioProtoc.3942.

21. Cell sorter (BD Biosciences, BD FACSJazz™)
22. Automated fluorescence microscope (Biotek, Lionheart FX) with:
    CO_2 gas controller (Biotek, catalog number: 1210012)
    Humidity chamber (Biotek, catalog number: 1450006)
    4× objective (Biotek, catalog number: 1220519)
    20× objective (Biotek, catalog number: 1220517)
    GFP filter cube (Biotek, catalog number: 1225101)
    465 nm LED cube (Biotek, catalog number: 1225001)
    Cy5 filter cube (Biotek, catalog number: 1225105)
    623 nm LED cube (Biotek, catalog number: 1225005)

Software

1. Gen5 Image+ (Biotek, https://www.biotek.com)
2. CellProfiler 4.0 (Broad Institute, https://cellprofiler.org/releases)

Procedure

A. Lentiviral vectors assembly and titration

Assembly

1. Prepare plasmid stocks following standard molecular biology procedures (https://www.jove.com/v/5062/plasmid-purification) and the protocol provided by the manufacturer of the NucleoSpin plasmid mini kit (Macherey-Nagel).
2. Manually seed 6,000,000 HEK 293T cells in 100/20 mm cell culture dishes with 8 ml of DMEM 10% FBS (Recipe 1) and incubate overnight at 37 °C and 5% CO_2 to reach 70-80% confluency. For a detailed procedure of seeding cells please refer to the bio-protocol paper by Freppel *et al*., 2018 (reference 3).
3. Using a pipette, replace the medium by removing and discarding all the DMEM 10% FBS in the dishes (~8 ml) and adding 4 ml of fresh DMEM 2% FBS (Recipe 1).
4. Prepare the transfection mix as follows:
   Suspension A: 45 µl PEI 1 mg/ml (Recipe 2) + 955 µl unsupplemented DMEM (without FBS and antibiotic-antimycotic).
   Suspension B: 6 µg pLenti-FlaviA-GFP-puro or pLenti-CMV-FlaviA-mNeptune-puro + 6 µg pMD2.G + 6 µg psPAX2 and bring to 1,000 µl with unsupplemented DMEM.
   Mix suspensions A with B and incubate for 15 min at room temperature.
5. Add the 2 ml transfection mix to the cells (dropwise) and incubate overnight at 37 °C and 5% CO_2.
6. Replace the medium with 6 ml of fresh DMEM 2% FBS and incubate for 48 h at 37 °C and 5% CO_2.

7. Harvest culture supernatants and filter them (0.45-µm pore size) to eliminate cells and debris. Use filters with low protein adherence, like cellulose acetate or polyethersulfone (PES). Do not use nitrocellulose filters as they could bind the lentiviral particles.
8. Prepare 500 µl aliquots and store at -80 °C.

Titration

1. As described above, seed 50,000 BHK-21 cells per well in a 48-well cell culture plate with 500 µl/well of MEM 2% FBS (Recipe 4) and incubate overnight at 37 °C and 5% CO_2. Prepare extra wells to be used as control cells.
2. Thaw in a water bath (37 °C) one of the lentiviral 500 µl stock aliquots and add polybrene (Recipe 3) at a final concentration of 5 µg/ml.
3. Prepare 10-fold serial dilutions (10^{-1}-10^{-6}) of the lentiviral stock in 1.5 ml reaction tubes. Start mixing 50 µl of the lentiviral particles in 450 µl of DMEM 2% FBS + 5 µg/ml polybrene (10^{-1}). Vortex the tube for 5 s and mix 50 µl of the 10^{-1} lentiviral dilution in 450 µl of DMEM 2% FBS + 5 µg/ml polybrene (10^{-2}). Repeat this procedure for the other dilutions (10^{-3}-10^{-6}) and incubate for 15 min at room temperature. Change the tip between dilutions to avoid cross-contamination. For a detailed and graphical explanation of 10-fold serial dilutions preparation please refer to the bio-protocol paper by Freppel *et al*., 2018 (reference 3).
4. Replace the medium of the cells with 150 µl/well of undiluted lentiviral stock and each serial dilution thereof. Add 150 µl/well of DMEM 2% FBS + 5 µg/ml polybrene to the control cells. To avoid cross contamination, make the inoculation of the samples in order, starting with the control, following with the serial dilutions (from higher to lower dilution), and ending with the undiluted lentiviral stock.
5. Centrifuge at 300 × *g* for 2 h at 25 °C for viral adsorption.
6. Replace the inoculum with 500 µl/well of DMEM 2% FBS and incubate for 48 h at 37 °C and 5% CO_2.
7. Discard the medium, wash the cells once with 100 µl/well of PBS, add 100 µl/well of TrypLE™ express (no phenol red), incubate for 5 min at 37 °C, and resuspend the cells with 400 µl/well of PBS 1% FBS (Recipe 5).
8. Based on the basal background of the reporter proteins and by comparison with the non-transduced control cells (Figure 1), determine by flow cytometry the percentage of GFP+ (488 nm laser - 530/30 nm filter) or mNeptune+ (640 nm laser -675/25 nm filter) cells present in the samples infected with different dilutions of the lentiviral seed. For a detailed procedure about flow cytometry of fluorescent proteins please refer to the protocol by Hawley *et al*., 2004 (reference 5).
9. Using the data of the higher dilution with detectable transduced cells, calculate the biological titer in transducing units per milliliter (TU/ml), applying the following formula:

$$TU/ml = (P \times N / 100 \times V) \times 1/DF$$

where P = % GFP+ or mNeptune+ cells, N = number of cells at transduction = 50,000, V = volume of inoculum per well = 0.15 ml, and DF = dilution factor = 1 (undiluted), 10^{-1} (diluted 1/10), 10^{-2} (diluted 1/100), and so on (Tiscornia *et al.*, 2006).

B. Reporter cell lines production and selection

Production

1. As described above, seed 100,000 BHK-21 cells per well in a 12-well cell culture plate with 1 ml/well of MEM 2% FBS and incubate overnight at 37 °C and 5% CO_2. Prepare an extra well for the control cells.
2. Thaw in a water bath (37 °C) one of the 500 µl stock aliquots of lentiviral particles carrying genetic constructs codifying for either the FlaviA-GFP or the FlaviA-mNeptune reporters and add polybrene at a final concentration of 5 µg/ml.
3. Based on the previously calculated biological titer in TU/ml, prepare 500 µl/well of lentiviral inoculum at a multiplicity of infection (MOI) of 1 (1 TU per cell). As 100,000 cells per well were plated in manteinance medium (MEM 2% FBS), 100,000 TU must be diluted in MEM 2% FBS + 5 µg/ml polybrene to a final volume of 500 µl. Incubate for 15 min at room temperature.
4. Replace the medium of the cells with the 500 µl/well of lentiviral inoculum. Add 500 µl/well of MEM 2% FBS + 5 µg/ml polybrene to the control cells.
5. Centrifuge at 300 × *g* for 2 h at 25 °C for viral adsorption.
6. Replace the inoculum with 1 ml/well of MEM 2% FBS and incubate for 48 h at 37 °C and 5% CO_2.
7. Based on the basal background of the reporter proteins, monitor the effectiveness of the transduction by fluorescence microscopy in the green/GFP (FlaviA-GFP) and far-red/Cy5 (FlaviA-mNeptune) channels.

Selection

1. For the antibiotic selection of transduced cells, replace the medium with 750 µl/well of MEM 10% FBS containing 8 µg/ml of puromycin (Recipe 6) and incubate overnight at 37 °C and 5% CO_2. Apply the same treatment to the control cells.
2. Replace the medium of both transduced and control cells with 1 ml/well of MEM 10% FBS containing 4 µg/ml of puromycin. Incubate at 37 °C and 5% CO_2 until 100% mortality of the control cells is evidenced by light microscopy (commonly 24-48 h).
3. Replace the medium of the selected cells with 1 ml/well of MEM 10% FBS + 0.5 µg/ml puromycin and incubate at 37 °C and 5% CO_2 until reaching confluency of 80-90%.
4. Passage the selected cells to 25 cm² culture flasks with 5 ml of MEM 10% FBS + 0.5 µg/ml puromycin and incubate at 37 °C and 5% CO_2 until reaching a confluency of 80-90% (https://www.jove.com/v/5052/passaging-cells).

Please cite this article as: Arias-Arias and Mora-Rodríguez, (2021). Generation and Implementation of Reporter BHK-21 Cells for Live Imaging of Flavivirus Infection,*Bio-protocol* 11 (5): e3942. DOI: 10.21769/BioProtoc.3942.

5. For the FACS selection, discard the medium, wash the cells once with 1 ml of PBS, add 500 µl of TrypLE™ express (no phenol red), incubate for 5 min at 37 °C, and resuspend the cells with 1 ml of PBS 1% FBS.
6. Count the cells with a hemocytometer (https://www.jove.com/v/5048/using-a-hemacytometer-to-count-cells) and prepare 2 ml of cell suspensions at 1,000,000 cells/ml in PBS 1% FBS.
7. Aspirate the cell suspensions into the cell sorter. For the FlaviA-GFP reporter isolate at least two cell subpopulations with different but homogeneous levels of the reporter's basal background using the FL1 detector (488 nm laser - 530/30 nm filter) (Figure 1). Apply the same procedure to the FlaviA-mNeptune reporter but using the FL4 detector (640 nm laser - 675/25 nm filter).

   Note: The basal background of the FlaviA-GFP and FlaviA-mNeptune reporters make them sensitive to the levels of cellular expression: If the expression is too high the background will mask the signal produced upon activation of the reporters. If the expression is too low there will not be enough reporter's signal over the background.

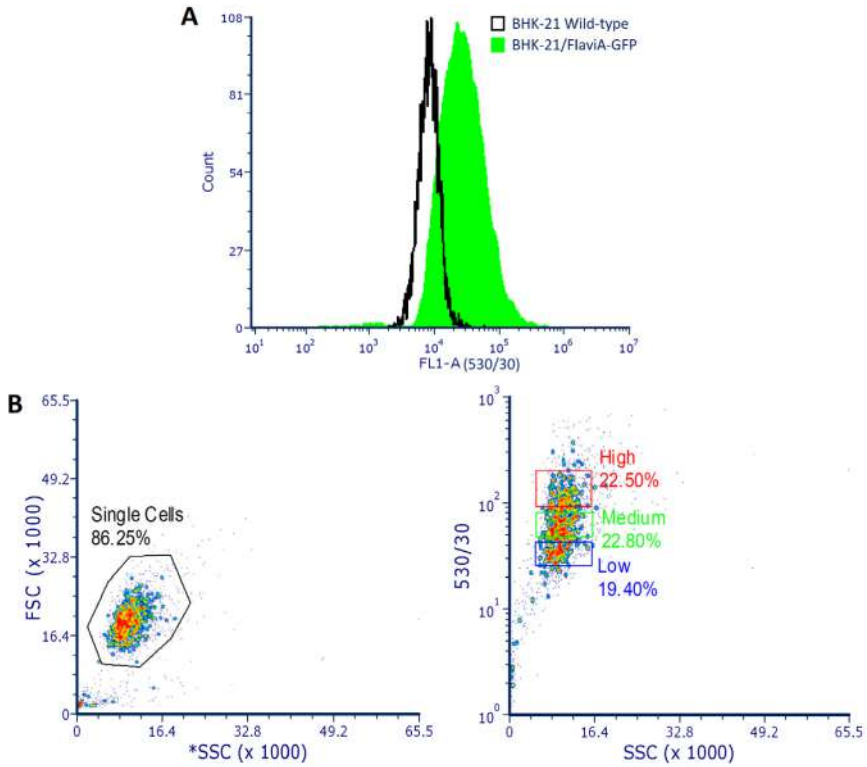

Figure 1. FACS analysis of BHK-21/FlaviA-GFP stable cells. A. Histogram showing the difference in the green fluorescence (FL1 detector- 530/30 nm filter) between wild-type and reporter BHK-21 cells due to the basal background of the FlaviA-GFP reporter proteins. B. Scatter plots showing the heterogeneity in the population of stable BHK-21 cells with different levels of expression of the FlaviA-GFP reporter. For the selection of the best reporter cells

Please cite this article as: Arias-Arias and Mora-Rodríguez, (2021). Generation and Implementation of Reporter BHK-21 Cells for Live Imaging of Flavivirus Infection,*Bio-protocol* 11 (5): e3942. DOI: 10.21769/BioProtoc.3942.

(highest signal-to-noise ratio), at least two cell subpopulations with different (low, medium or high) but homogeneous levels of the reporter's basal background must be isolated and tested by live-cell imaging upon flavivirus infection.

8. Seed the isolated cell suppopulations in different wells of a 48-well cell culture plate with 1 ml/well of MEM 10% FBS + 0.5 µg/ml puromycin and incubate at 37 °C and 5% CO_2 until reaching a confluency of 80-90%.
9. Passage the selected cells to a 6-well cell culture plate with 3 ml of MEM 10% FBS + 0.5 µg/ml puromycin and incubate at 37 °C and 5% CO_2 until reaching a confluency of 80-90%.
10. Test the different isolated cell suppopulations by a live-cell imaging flavivirus infection kinetics according to the protocol described in Procedure C.
    Note: The best reporter cells will be those with the highest signal-to-noise ratio upon flavivirus infection. The fluorescence signal-to-noise ratio is calculated by dividing the signal of the reporter cells treated with infectious virus by the noise given by the reporter cells treated with UV-inactivated virus at the same post-inoculation time.

C. Infection kinetics in reporter cells by live-cell imaging
1. Prepare and titer the flaviviral seed of your choice (*e.g.*, DENV, ZIKV, or YFV) according tostandard virological methodologies (Medina *et al.*, 2012; Freppel *et al.*, 2018). For viral inactivation, place 200 µl/well of the flaviviral seed in a 24-well cell culture plate, remove the lid and apply 5 cycles of UV light (254 nm) exposure at an energy of 400,000 µJ/cm^2 into an ultraviolet crosslinker. Between cycles, shake the plate for 5 s using your hands.
2. As described above, seed 15,000 BHK-21/FlaviA-GFP stable cells per well in a µClear black 96-well plate with 100 µl/well of MEM 2% FBS and incubate overnight at 37 °C and 5% CO_2.
3. Based on the calculated titer of the flaviviral seed in plaque forming units (PFU)/ml, prepare 50 µl/well of inoculum at a low MOI (between 0.1 and 0.25). As 15,000 cells per well were plated in maintenance medium, between 1,500 and 3,750 PFUs must be diluted in MEM 2% FBS to a final volume of 50 µl/well. Multiply for the total number of wells to be inoculated and prepare a single inoculum suspension. Likewise, prepare the UV-inactivated inoculum suspension.
4. Replace the medium of the cells with 50 µl/well of either the infectious or the UV-inactivated flaviviral inoculum and incubate for 2 h at 37 °C and 5% CO_2 for viral adsorption. Using your hands, shake the plate for 5 s every 15 min.
5. Replace the inoculum with 150 µl/well of FluoroBrite™ DMEM 2% FBS (Recipe 7) and incubate for the desired time of your kinetics (*e.g.*, 120 h) at 37 °C and 5% CO_2 into the automated fluorescence microscope. Add 200 µl/well of PBS to the surrounding wells to avoid desiccation.
6. Using your microscope's software (*e.g.*, Gen5 Image+), program the image acquisition with the 4× or the 20× objective in the green/GFP channel at the desired post-infection times (Figure 2A).
    Note: The acquisition parameters (excitation intensity, exposure time, and camera gain) of the

Please cite this article as: Arias-Arias and Mora-Rodríguez, (2021). Generation and Implementation of Reporter BHK-21 Cells for Live Imaging of Flavivirus Infection,*Bio-protocol* 11 (5): e3942. DOI: 10.21769/BioProtoc.3942.

images are variable according to the particular reporter cell subpopulation isolated by FACS. Always include an extra well of control cells for the adjustment of the acquisition parameters as the overexposure to the excitation light may harm the cells of the experimental conditions. Our recommendation is to set those parameters to a level where the background signal of the reporter proteins is just perceptible in the first images of the kinetics, in order to increase the dynamic range of the reporter's fluorescence upon activation by flaviviral proteases.

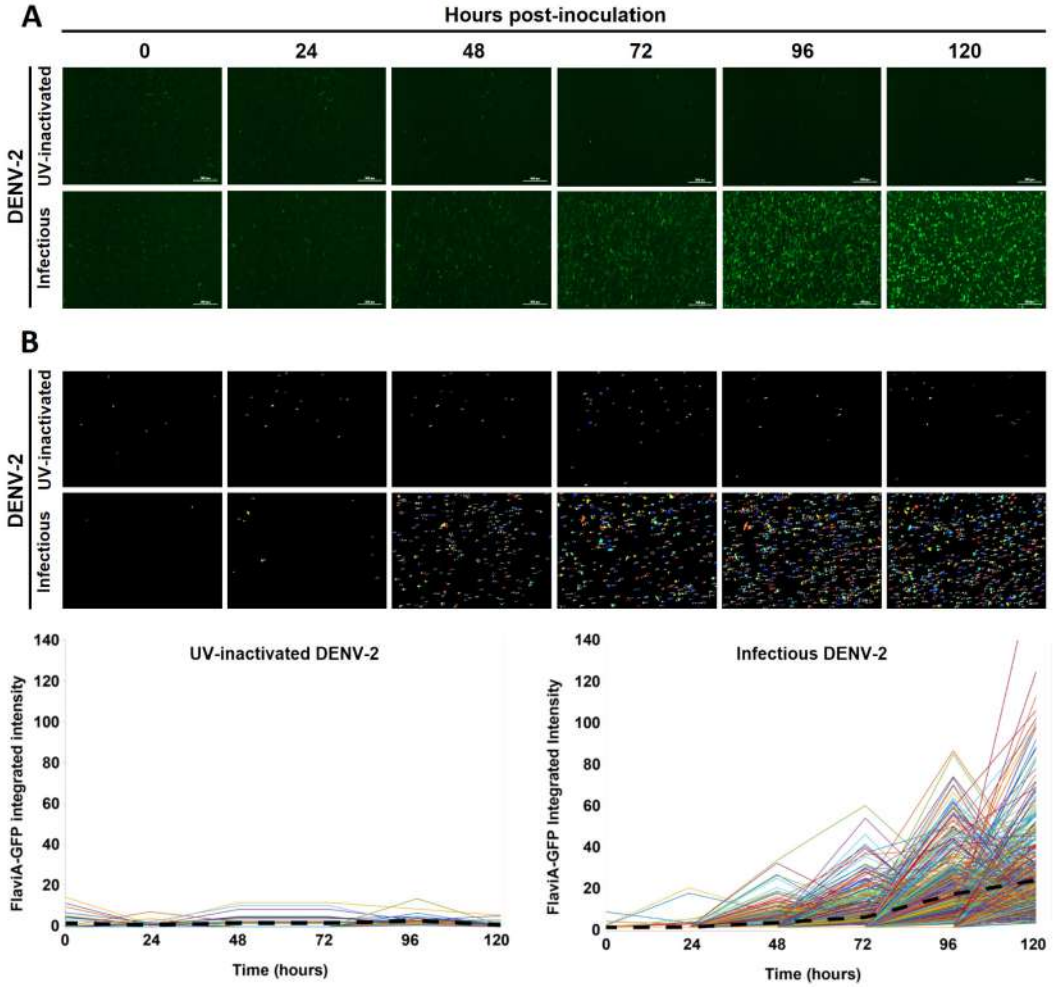

Figure 2. DENV-2 infection kinetics in reporter BHK-21 cells by live-cell imaging. A. Stable BHK-21 cells expressing the FlaviA-GFP reporter were inoculated with either infectious or UV-inactivated DENV-2 13538 at a low MOI of 0.1 and captured by live-cell imaging at the specified time periods. Magnification of 40×, scale bar = 100 µm. B. The image analysis of the infection kinetics with the software CellProfiler 4.0 allowed the tracking of single cells over time based on the reported fluorescence (each colored line in the graphs corresponds to an individual cell). The black dashed lines represent the mean values of cell fluorescence.

D. Kinetic plaque assay in reporter cells by live-cell imaging

1. As described above, seed 25,000 BHK-21/FlaviA-mNeptune stable cells per well in a µClear

Please cite this article as: Arias-Arias and Mora-Rodríguez, (2021). Generation and Implementation of Reporter BHK-21 Cells for Live Imaging of Flavivirus Infection,*Bio-protocol* 11 (5): e3942. DOI: 10.21769/BioProtoc.3942.

black 96-well plate with 100 µl/well of MEM 10% FBS and incubate overnight at 37 °C and 5% CO_2.

2. Prepare 10-fold serial dilutions (10^{-1}-10^{-6}) of the flaviviral seed in 1.5 ml reaction tubes. Start mixing 50 µl of the flaviviral seed in 450 µl of MEM 2% FBS (10^{-1}). Vortex the tube for 5 s and mix 50 µl of the 10^{-1} flaviviral dilution in 450 µl of MEM 2% FBS (10^{-2}). Repeat this procedure for the other dilutions (10^{-3}-10^{-6}). Change the tip between dilutions to avoid cross-contamination. For a detailed and graphical explanation of 10-fold serial dilutions preparation please refer to the bio-protocol paper by Freppel *et al*., 2018 (reference 3).
3. Replace the medium of the cells with 50 µl/well of each serial dilution of the flaviviral seed. Inoculate a control well with 50 µl of UV-inactivated flaviviral seed. Incubate for 2 h at 37 °C and 5% CO_2 for viral adsorption. Using your hands, shake the plate for 5 s every 15 min.
4. Replace the inoculum with 150 µl/well of plaque media 2% FBS (Recipe 8) and incubate for 120 h at 37 °C and 5% CO_2 into the automated fluorescence microscope. Add 200 µl/well of PBS to the surrounding wells to avoid desiccation.
5. Using your microscope's software (*e.g.*, Gen5 Image+), program the image acquisition (a montage of the whole well) with the 4× objective in the far-red/Cy5 channel at the desired post-infection times (Figure 3A).

   Note: The acquisition parameters (excitation intensity, exposure time, and camera gain) of the images are variable according to the particular reporter cell suppopulation isolated by FACS. Always include an extra well of control cells for the adjustment of the acquisition parameters, as the overexposure to the excitation light may harm the cells of the experimental conditions. Our recommendation is to set those parameters to a level where the background signal of the reporter proteins is just perceptible in the first images of the kinetics, in order to increase the dynamic range of the reporter's fluorescence upon activation by flaviviral proteases.

Please cite this article as: Arias-Arias and Mora-Rodríguez, (2021). Generation and Implementation of Reporter BHK-21 Cells for Live Imaging of Flavivirus Infection,*Bio-protocol* 11 (5): e3942. DOI: 10.21769/BioProtoc.3942.

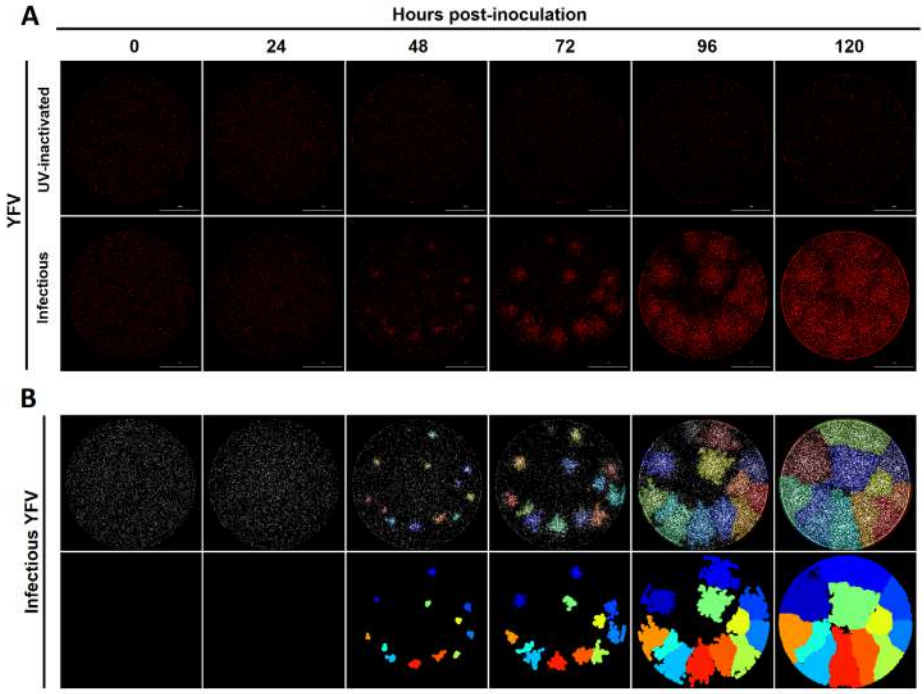

Figure 3. YFV kinetic plaque assay in reporter BHK-21 cells by live-cell imaging. A. Stable BHK-21 cells expressing the FlaviA-mNeptune reporter were inoculated with decimal dilutions (10^{-1}-10^{-6}) of either infectious or UV-inactivated YFV 17D. After addition of plaque media 2% FBS, entire wells of the plate were captured by live-cell imaging at the specified time periods. Magnification of 40×, scale bar = 1,000 µm. B. The image analysis of the kinetic plaque assay with the software CellProfiler 4.0 allowed the identification of single viral plaques (upper panel) and the tracking of those plaques over time (lower panel). For a deeper exemplification of the results obtained with our kinetic plaque assay please watch the live-cell imaging video (Video 1).

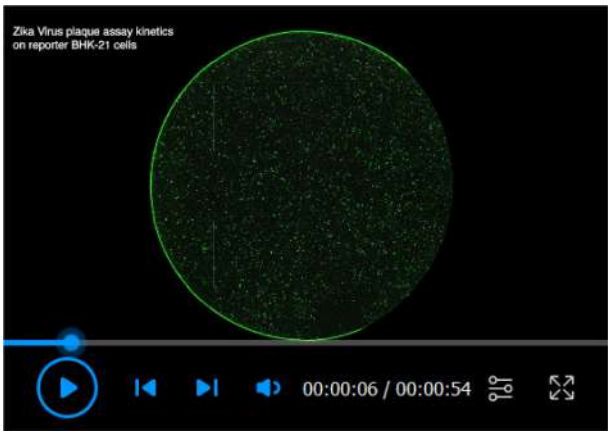

Video 1. ZIKV plaque assay kinetics on reporter BHK-21 cells

Please cite this article as: Arias-Arias and Mora-Rodríguez, (2021). Generation and Implementation of Reporter BHK-21 Cells for Live Imaging of Flavivirus Infection,*Bio-protocol* 11 (5): e3942. DOI: 10.21769/BioProtoc.3942.

Data analysis

A. Infection kinetics in reporter cells

Single cell tracking of infected cells based on its fluorescence (Figure 2B) was performed using our CellProfiler pipeline for single cell analysis ("SingleCellsTracking.cpproj", Figure 4). To perform this analysis just drag and drop the images in the *Images* module and press *Analyze Images*. In order to modify the pipeline for your cells and conditions, go to *Start Test Mode*, adjust the parameters described in the modules (one by one) and press *Step* to see the output of the modifications applied to a particular module. Once all the modifications are ready, press *Exit Test Mode* and go to *Analyze Images*. The modules contained in the single cell analysis pipeline are the following:

1. *Images*: Simply drag and drop the image files of a time series in the *Images* module. Make sure that the name of all the files in the dataset do include the name of the channel where the fluorescence was measured (*e.g.*, GFP) and the increasing consecutive numbers for time-lapse microscopy images (*e.g.*, GFP_72h).
2. *NamesAndTypes*: Select the rule criteria with an expression contained in the name of all the files in the dataset, in this case, indicating the channel of the fluorescence (*e.g.*, GFP). For each file of the dataset it creates an image called "Sensor".

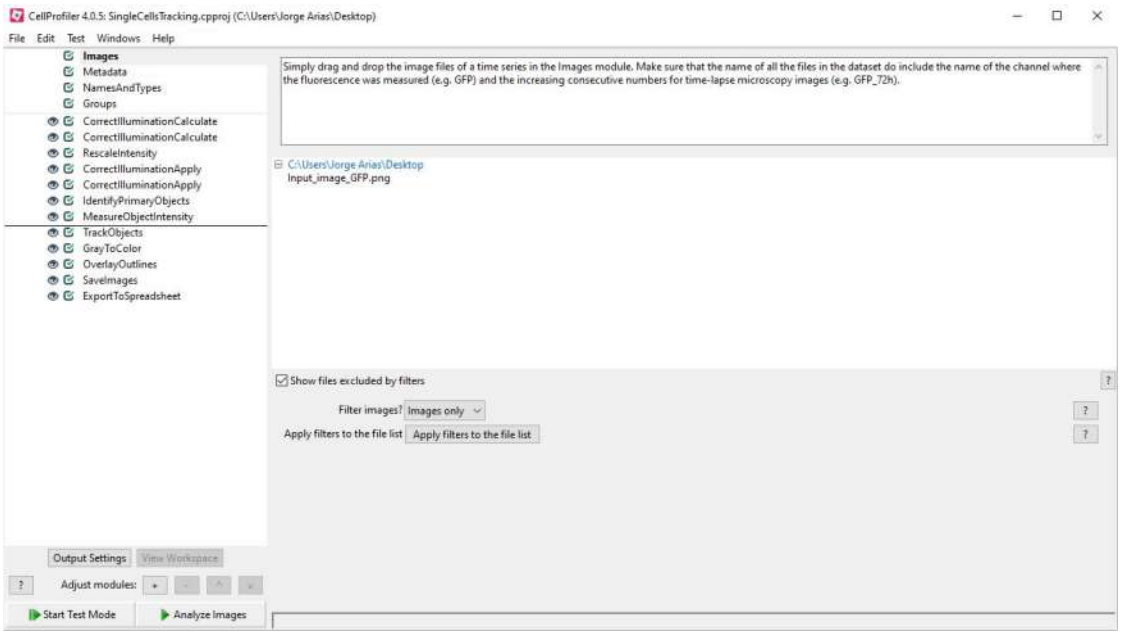

Figure 4. CellProfiler image analysis pipeline for single cell tracking of flavivirus infected BHK-21/FlaviA-GFP reporter cells

3. *CorrectIlluminiationCalculate (Illumination function calculation: Regular):* From the "Sensor" image, this module calculates a regular illumination correction function and creates an image with enhanced contrast, named "IllumSensor".
4. *CorrectIlluminiationCalculate* (*Illumination function calculation: Background*): From the "Sensor"

Please cite this article as: Arias-Arias and Mora-Rodríguez, (2021). Generation and Implementation of Reporter BHK-21 Cells for Live Imaging of Flavivirus Infection,*Bio-protocol* 11 (5): e3942. DOI: 10.21769/BioProtoc.3942.

image, this module calculates a background-based illumination function called "IllumSensorbackground".

5. *RescaleIntensity*: Converts the output image of the regular illumination function ("IllumSensor") to an image with rescaled intensity ("RescaleSensor").
6. *CorrectIlluminationApply*: This module applies the "IllumSensorbackground" correction function to the "RescaleSensor" image and generates an enhanced image named "CorrSensor".
7. *CorrectIlluminationApply*: This second module of correction works on the original "Sensor" image, applies the "IllumSensorbackground" correction function but keeping the original intensity values and generates an output image called "mSensor".
8. *IdentifyPrimaryObjects*: This module works with the enhanced image "CorrSensor" to identify the objects *Cells*. You may modify the *Typical diameter* to obtain the correct cell segmentation with other cell lines or parameters.
9. *MeasureObjectIntensity*: Measures the intensities of the identified objects *Cells* but on the image with the original intensity values only corrected by illumination ("mSensor").
10. *TrackObjects*: This module tracks cells over the time-lapse microscopy and generates an output image called "TrackedCells".
11. *GraytoColor*, *OverlayOutlines*, *SaveImages*: These modules create and save color images with the outlines of the primary objects identification for documentation and validation of the cell segmentation by the researcher's eye and criteria.
12. *ExportToSpreadsheet*: Saves the selected measurements to an excel spreadsheet (*e.g.*, Integrated intensity).

    Note: Together with this protocol we supply the Zip file "SingleCellsTracking pipeline and dataset" which contains the applied pipeline ("SingleCellsTracking.cpproj") and an example dataset composed of a single input image to run the pipeline ("Input_image_GFP") and two output files to corroborate the expected results ("Output_image_GFP" and "Infected_Cells").

B. Kinetic plaque assay in reporter cells

The identification and tracking of viral plaques were performed using two different pipelines programmed in CellProfiler. For single-plaque recognition use our "PlaqueIdentification.cpproj" pipeline (Figure 5) to generate images such as those depicted in the upper panel of Figure 3B. To track the plaques over a time series and determine the cell counts for every recognized plaque, first apply the "PlaqueIdentification.cpproj" pipeline to generate an image with the identified plaques and then use that image and the "PlaqueTracking.cpproj" pipeline (Figure 6) to obtain tracking images such as those showed in the lower panel of Figure 3B. Depending on the cell type and/or density, some modifications to several parameters may be done for an optimal plaque identification using the option *Start Test Mode* and running each module step by step. The modules of the above mentioned pipelines are the following:

Please cite this article as: Arias-Arias and Mora-Rodríguez, (2021). Generation and Implementation of Reporter BHK-21 Cells for Live Imaging of Flavivirus Infection,*Bio-protocol* 11 (5): e3942. DOI: 10.21769/BioProtoc.3942.

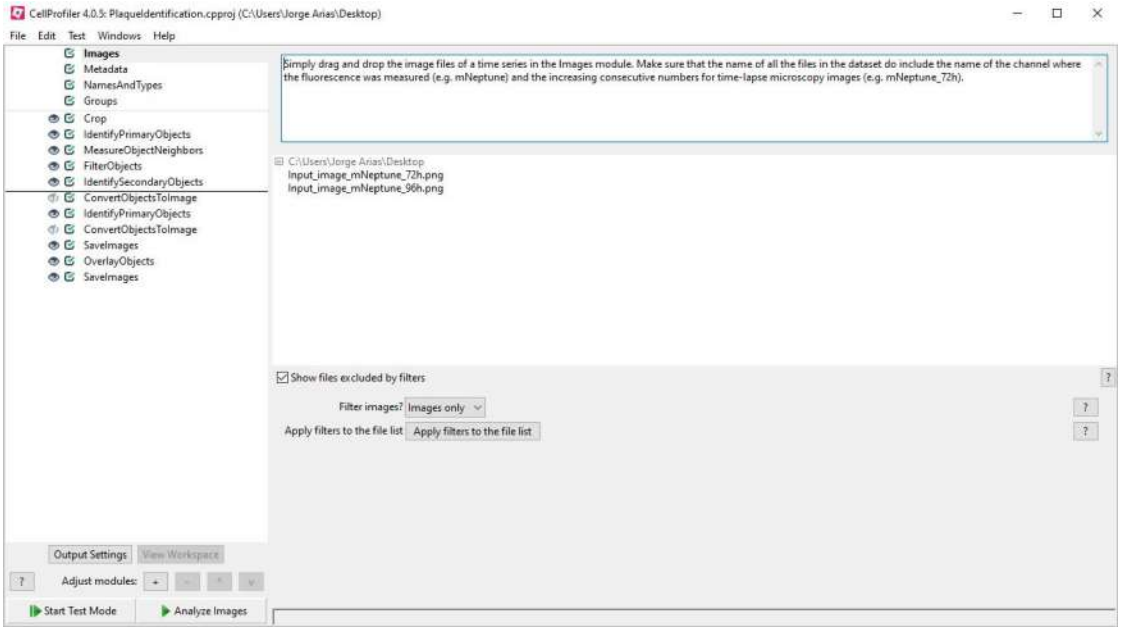

Figure 5. CellProfiler image analysis pipeline for flaviviral plaques identification in BHK-21/mNeptune reporter cells

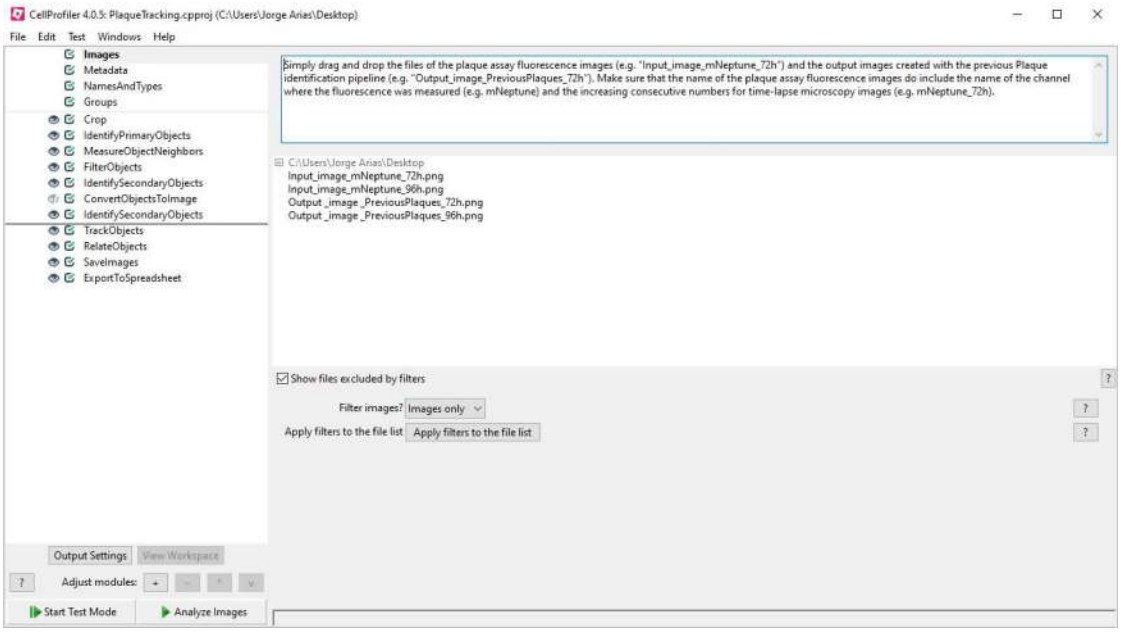

Figure 6. CellProfiler image analysis pipeline for flaviviral plaques tracking in BHK-21/mNeptune reporter cells

Plaque identification pipeline

1. *Images*: Simply drag and drop the image files of a time series in the *Images* module. Make sure that the name of all the files in the dataset do include the name of the channel where the

Please cite this article as: Arias-Arias and Mora-Rodríguez, (2021). Generation and Implementation of Reporter BHK-21 Cells for Live Imaging of Flavivirus Infection,*Bio-protocol* 11 (5): e3942. DOI: 10.21769/BioProtoc.3942.

fluorescence was measured (*e.g.*, mNeptune) and the increasing consecutive numbers for time-lapse microscopy images (*e.g.*, mNeptune_72h).

2. *NamesAndTypes*: Select the rule criteria with an expression contained in the name of all the files in the dataset, in this case, indicating the channel of the fluorescence (*e.g.*, mNeptune). For each file of the dataset it creates an image called “Sensor”.
3. *Crop*: This is an optional module in case you need to remove part of the image (*e.g.*, distance bars). It generates an output image named “CropSensor”.
4. *IdentifyPrimaryObjects*: This module identifies the individual objects *Nuclei* from the “CropSensor” image. You may need to change the *Typical diameter of objects* or the *Threshold strategy* and its parameters to obtain an optimal identification of your cells.
5. *MeasureObjectNeighbors*: Measures the number of neighbors for each *Nuclei* object within a specified *Neighbor distance*. You may need to modify this parameter to obtain a good optimal range of neighbor numbers to differentiate the plaque-belonging cells from the surrounding cells. This module creates an image called “ObjectNeighborCount”.
6. *FilterObjects*: This module sets a threshold to identify plaque-belonging *Nuclei* objects using the range of number of neighbors calculated in the previous module. You may need to set this *Minimum value* according to the range of neighbors for an optimal identification of plaque belonging *Nuclei* objects. It generates the output objects *FilteredNuclei*.
7. *IdentifySecondaryObjects*: Extends the above *FilteredNuclei* by a determined number of pixels to fill the gaps between the plaque-belonging cells in the “CropSensor” image. You may need to modify the *Number of pixels by which to expand the primary objects* in order to fill most of the gaps. This module identifies the output objects *Cells*.
8. *ConvertObjectstoImage*: The expanded *Cells* objects constitute the basis to create a new image named “CellImage”.
9. *IdentifyPrimaryObjects*: Uses the previous “CellImage” to identify the new *Plaque* objects. You may need to modify the range of *Typical diameter of objects* to obtain the correct plaque identification with images from different post-infection times, as shown in the colored frame *Plaque*, within the visual output generated by this module. In such an instance images must be analyzed one by one, like in the case of our example dataset.
10. *ConvertObjectstoImage*: Converts the *Plaque* objects to an image called “PlaqueImage”.
11. *SaveImages*: Uses the “PlaqueImage” to create and save an image called “Output_image_PreviousPlaques”, that constitutes one of the input images for the plaque tracking with the pipeline “PlaqueTracking.cpproj”.
12. *OverlayObjects*: This module fuses the “CropSensor” image with the *Plaque* objects to make a composite image named “OverlayImage”.
13. *SaveImages*: Creates an image called “Output_image_OverlayPlaques” based on the “OverlayImage”.

    Note: Together with this protocol we supply the Zip file “PlaqueIdentification tracking pipeline and dataset” which contains the applied pipeline (“PlaqueIdentification.cpproj”) and an example

Please cite this article as: Arias-Arias and Mora-Rodríguez, (2021). Generation and Implementation of Reporter BHK-21 Cells for Live Imaging of Flavivirus Infection,*Bio-protocol* 11 (5): e3942. DOI: 10.21769/BioProtoc.3942.

dataset composed of two input images to run the pipeline and practice the required adjustments ("Input_image_mNeptune_72h" and "Input_image_mNeptune_96h") and four output files to corroborate the expected results ("Output_image_PreviousPlaques_72h", "Output_image_PreviousPlaques_96h", "Output_image_OverlayPlaques_72h", and "Output_image_OverlayPlaques_96h").

Plaque tracking pipeline

1. *Images*: Simply drag and drop the files of the plaque assay fluorescence images (*e.g.*, "Input_image_mNeptune_72h") and the output images created with the previous *Plaque identification pipeline* (*e.g.*, "Output_image_PreviousPlaques_72h"). Make sure that the name of the plaque assay fluorescence images do include the name of the channel where the fluorescence was measured (*e.g.*, mNeptune) and the increasing consecutive numbers for time-lapse microscopy images (*e.g.*, mNeptune_72h).
2. *NamesAndTypes*: Select the rule criteria with an expression contained in the name of all the plaque assay fluorescence images, in this case, indicating the channel of the fluorescence (*e.g.*, mNeptune). For each fluorescence image it creates an image called "Sensor".
3. The modules 3-8 are the same as those described in the *Plaque identification pipeline*.
4. *IdentifySecondaryObjects*: This module identifies the new *Plaque* objects in the "CellImage" as secondary objects around the previously identified *PreviousPlaques* primary objects.
5. *TrackObjects*: This module tracks the plaques over time using an overlap criteria across the time-resolved images and creates an output image named "TrackedPlaques". You may adjust the *Maximum distance to consider matches* for an optimal plaque tracking.
6. *SaveImages*: Saves the "Tracked_Plaques" image for your validation and final results.
7. *RelateObjects*: This module correlates the new *Plaque* objects with the previously identified *Nuclei* objects.
8. *ExporttoSpreadSheet*: This module exports to an excel spreadsheet the data of the number of cells (*Nuclei* objects) that compose every recognized plaque in all the analyzed images.
   Note: Together with this protocol we supply the Zip file "PlaqueIdentification tracking pipeline and dataset" which contains the applied pipeline ("PlaqueTracking.cpproj") and an example dataset composed of four input images to run the pipeline ("Input_image_mNeptune_72h", "Input_image_mNeptune_96h", "Output_image_Previous Plaques_72h", and "Output_image_PreviousPlaques_96h") and three output files to corroborate the expected results ("Tracked_Plaques_72h", "Tracked_Plaques_96h" and "Viral_Plaque").

Recipes

1. Complete DMEM
   500 ml DMEM (Gibco)
   5 ml Antibiotic-antimycotic 100×

5 ml (for 2%) or 50 ml (for 10%) of FBS

Homogenize by hand rotation (20 times, gently to avoid formation of foam)

Store at 4 °C. Stable for 4 months

2. PEI solution (1 mg/ml)

   1 mg of PEI powder

   1 ml of HCl 0.2 M in distilled water

   Heat and shake at 60 °C, 600 rpm in a ThermoMixer® block

   Sterilize by filtration (0.2 µm pore size)

   Prepare 45 µl aliquots into 2 ml reaction tubes and store at -80° C. Stable for 4 months

3. Polybrene solution (10 mg/ml)

   10.6 mg of hexadimethrine bromide powder

   Dissolve in 1 ml of destilled water

   Sterilize by filtration (0.2 µm pore size)

   Prepare 50 µl single use aliquots into 0.5 ml reaction tubes and store at -20 °C. Stable for 1 year

4. Complete MEM

   500 ml MEM (Gibco)

   5 ml Sodium pyruvate 100 mM

   5 ml Antibiotic-antimycotic 100×

   5 ml (for 2%) or 50 ml (for 10%) of FBS

   Homogenize by hand rotation (20 times, gently to avoid formation of foam)

   Store at 4 °C. Stable for 4 months

5. PBS 1% FBS

   45 ml PBS, pH 7.4

   5 ml complete MEM 10% FBS

   Store at 4 °C. Stable for 4 months

6. Puromycin solution (10 mg/ml)

   10 mg of puromycin

   Dissolve in 1 ml of destilled water

   Sterilize by filtration (0.2 µm pore size)

   Prepare 20 µl single use aliquots into 1.5 ml light protection reaction tubes and store at -20 °C. Stable for 2 years

7. FluoroBrite™ DMEM 2% FBS

   500 ml FluoroBrite™ DMEM (Gibco)

   5 ml GlutaMAX™ supplement

   5 ml Sodium pyruvate 100 mM

   5 ml Antibiotic-antimycotic 100×

   5 ml of FBS

   Homogenize by hand rotation (20 times, gently to avoid formation of foam)

Store at 4 °C. Stable for 4 months

8. Plaque media 2% FBS
   9.4 g MEM (Sigma)
   900 ml Milli-Q water
   Adjust pH to 4.0
   10 g Carboxymethylcellulose sodium salt
   Autoclave (121 °C at 100 kPa for 15 min)
   30 ml 7.5% sodium bicarbonate solution in Milli-Q water (sterilized by filtration – 0.2 µm pore size)
   10 ml GlutaMAX™ supplement
   10 ml Sodium pyruvate 100mM
   10 ml Antibiotic-antimycotic 100×
   20 ml of FBS
   Homogenize by hand rotation (20 times, gently to avoid formation of foam)
   Store at 4 °C. Stable for 4 months

Acknowledgments

We want to thank Dr. Jeanne A. Hardy from the Department of Chemistry, University of Massachusetts, for her kindness and scientific advice during our outstanding collaboration. We also want to acknowledge our funding sources at Universidad de Costa Rica (project VI-803-B9-505) and International Centre for Genetic Engineering and Biotechnology (Grant CRP/CRI18-02).

Competing interests

The authors declare that they do not have any conflicts of interests.

References

1. Arias-Arias, J. L., MacPherson, D. J., Hill, M. E., Hardy, J. A. and Mora-Rodriguez, R. (2020). A fluorescence-activatable reporter of flavivirus NS2B-NS3 protease activity enables live imaging of infection in single cells and viral plaques. *J Biol Chem* 295(8): 2212-2226.
2. Balsitis, S. J., Coloma, J., Castro, G., Alava, A., Flores, D., McKerrow, J. H., Beatty, P. R. and Harris, E. (2009). Tropism of dengue virus in mice and humans defined by viral nonstructural protein 3-specific immunostaining. *Am J Trop Med Hyg* 80(3): 416-424.
3. Freppel, W., Mazeaud, C. and Chatel-Chaix, L. (2018). Production, titration and imaging of Zika virus in mammalian cells. *Bio-protocol* 8(24): e3115.
4. Gould, E. A. and Solomon, T. (2008). Pathogenic flaviviruses. *Lancet* 371(9611): 500-509.
5. Hawley, T. S., Herbert, D. J., Eaker, S. S. and Hawley, R. G. (2004). Multiparameter flow cytometry of fluorescent protein reporters. *Methods Mol Biol* 263: 219-237.

6. Hsieh, M. S., Chen, M. Y., Hsieh, C. H., Pan, C. H., Yu, G. Y. and Chen, H. W. (2017). Detection and quantification of dengue virus using a novel biosensor system based on dengue NS3 protease activity. *PLoS One* 12(11): e0188170.
7. Kümmerer, B. M. (2018). Establishment and application of flavivirus replicons. *Adv Exp Med Biol* 1062: 165-173.
8. Li, S. H., Li, X. F., Zhao, H., Deng, Y. Q., Yu, X. D., Zhu, S. Y., Jiang, T., Ye, Q., Qin, E. D. and Qin, C. F. (2013). Development and characterization of the replicon system of Japanese encephalitis live vaccine virus SA14-14-2. *Virol J* 10: 64.
9. McFadden, M. J., Mitchell-Dick, A., Vazquez, C., Roder, A. E., Labagnara, K. F., McMahon, J. J., Silver, D. L. and Horner, S. M. (2018). A Fluorescent Cell-Based System for Imaging Zika Virus Infection in Real-Time. *Viruses* 10(2).
10. Medin, C. L., Valois, S., Patkar, C. G. and Rothman, A. L. (2015). A plasmid-based reporter system for live cell imaging of dengue virus infected cells. *J Virol Methods* 211: 55-62.
11. Medina, F., Medina, J. F., Colon, C., Vergne, E., Santiago, G. A. and Munoz-Jordan, J. L. (2012). Dengue virus: isolation, propagation, quantification, and storage. *Curr Protoc Microbiol* Chapter 15: Unit 15D 12.
12. Schmid, B., Rinas, M., Ruggieri, A., Acosta, E. G., Bartenschlager, M., Reuter, A., Fischl, W., Harder, N., Bergeest, J. P., Flossdorf, M., Rohr, K., Höfer, T. and Bartenschlager, R. (2015). Live cell analysis and mathematical modeling identify determinants of attenuation of dengue virus 2'-o-methylation mutant. *PLoS Pathog* 11(12): e1005345.
13. Soto-Garita, C., Somogyi, T., Vicente-Santos, A. and Corrales-Aguilar, E. (2016). Molecular Characterization of Two Major Dengue Outbreaks in Costa Rica. *Am J Trop Med Hyg* 95(1): 201-205.
14. Tamura, T., Fukuhara, T., Uchida, T., Ono, C., Mori, H., Sato, A., Fauzyah, Y., Okamoto, T., Kurosu, T., Setoh, Y. X., Imamura, M., Tautz, N., Sakoda, Y., Khromykh, A. A., Chayama, K. and Matsuura, Y. (2018). Characterization of recombinant flaviviridae viruses possessing a small reporter tag. *J Virol* 92(2).
15. Tiscornia, G., Singer, O. and Verma, I. M. (2006). Production and purification of lentiviral vectors. *Nat Protoc* 1(1): 241-245.
16. Xie, X., Zou, J., Shan, C., Yang, Y., Kum, D. B., Dallmeier, K., Neyts, J. and Shi, P. Y. (2016). Zika virus replicons for drug discovery. *EBioMedicine* 12: 156-160.

Protocol. Real-time CPE labeling kinetics in flavivirus infected BHK-21 / Vero cells.

1. Seed 15 000 BHK-21 (ATCC CCL-10) or Vero (ATCC CCL-81) cells per well on a µClear black 96-well plate (Greiner Bio-One 655090) using 100 µL/well of minimum essential medium (MEM, Gibco 41090101) supplemented with 2% fetal bovine serum (FBS, Gibco 10100147) and incubate for 18-24 h at 37 °C -5% CO_2. *Do not use the wells at the plate's periphery as those must be reserved for the addition of PBS to avoid dessication in long-term experiments.*
2. Remove the medium and immediately add 50 µL/well of flavivirus inoculum at the desired MOI in MEM 2% FBS. Likewise, add MEM 2% FBS to a mock-infected control and allow to adsorb for 2 h at 37 °C -5% CO_2. *Work fast and do not handle too many wells at the same time in order to avoid desiccation that could kill and label cells with the dead markers.*
3. Stain cell nuclei by adding over the inoculum 50 µL/well of a 2 µg/mL Hoechst 33342 (Invitrogen H3570, 1:5000 dilution) solution in MEM-2% FBS and incubate for 10 min at 37 °C -5% CO_2.
4. Remove the inoculum and immediately add 100 µL/well PBS-1% FBS to wash and remove unbound viruses and the excess of Hoechst 33342 solution as it results toxic over long incubation periods. *Work fast and do not handle too many wells at the same time in order to avoid desiccation that could kill and label cells with the dead markers.*
5. Remove the washing solution and immediately add 100-300 µL/well of FluoroBrite DMEM (Gibco A1896701) supplemented with 2% FBS and containing one of the following cell dead dyes: 2.5 µg/mL propidium iodide (Invitrogen P3566, 1:400 dilution), 500 nM SYTOX green (Invitrogen S7020, 1:10000 dilution), or 200 nM TO-PRO-3 iodide (Invitrogen T3605, 1:5000 dilution). *Work fast and do not handle too many wells at the same time in order to avoid desiccation that could kill and label cells with the dead markers. The volume of medium to use per well is based on the duration of the experiment: 24 h-100 µL, 48 h-150 µL, 72 h-200 µL, 96 h-250 µL, and ≥ 120 h-300 µL. Add to the wells of the periphery 300 µL/well of PBS in order to reduce the evaporation of media from the other wells with experimental conditions during long-term assays.*

6. Incubate and read out at 37 °C -5% CO_2 into an automated fluorescence microscope (e.g., BioTek Lionheart FX) for the desired incubation period at the preferred magnification and time-lapse imaging acquisition. *To avoid cell toxicity produced by the exposure to the excitation light wavelengths, it is recommended to acquire images at time-lapses ≥ than 30 minutes.*
7. Analyze the images using an image analysis software (e.g., CellProfiler 3.0, Broad Institute, https://www.cellprofiler.org) to quantified the percentages of dead cells and cells with condensed chromatin over time, as read-outs of the CPE.

Note: A similar protocol can be used for real-time kinetic plaque assays by adding the cell dead dyes to a MEM AutoMod (Sigma M0769) supplemented with 2% FBS and 1% carboxymethylcellulose (Sigma C4888).

Concluding remarks

With the current advances in super-resolution microscopy, biological sciences are facing a change in the methodological paradigm, evolving from techniques that rely on indirect inferences to those that allow the direct visualization of the phenomenon of interest in living organisms. Research on emerging diseases, as those caused by flaviviruses, is playing an active role in that revolution, taking advantage of the fluorescence live-cell imaging approaches. These methodologies are pivotal for the deciphering and understanding of the mechanisms involved in virus-host cell interactions, a crucial knowledge for the development of the urgently needed flavivirus antivirals and vaccines in the close future.

For the present work, we developed and validated two live-cell imaging approaches to study the kinetics of flavivirus infection in animal cells based on molecular reporters of the viral NS2B-NS3 protease activity and fluorescent labeling of virus-induced CPE. Such approaches enabled the monitoring of flaviviruses upon time both in single cells and viral plaques, revealing interesting differences in the kinetics of the infection established by DENV-2, ZIKV, and YFV.

We anticipate that future studies of viral infection kinetics with our reporter systems will enable basic investigations of the virus-cell interplay and will also facilitate the screening of antiviral drugs to manage flavivirus infections. For example, our multireporter platform combining the flavivirus-activatable reporters and CPE labeling approaches could be applied in a single experiment for the simultaneous evaluation over time of both the antiviral and cytotoxic effect of candidate drugs against flaviviruses. This and other applications need to be addressed in future works.

References

Agol, V.I., 2012. Cytopathic effects: Virus-modulated manifestations of innate immunity? Trends Microbiol. 20, 570–576. https://doi.org/10.1016/j.tim.2012.09.003

Arias-Arias, J.L., MacPherson, D.J., Hill, M.E., Hardy, J.A., Mora-Rodríguez, R., 2020. A fluorescence-activatable reporter of flavivirus NS2B–NS3 protease activity enables live imaging of infection in single cells and viral plaques. J. Biol. Chem. 295, 2212–2226. https://doi.org/10.1074/jbc.RA119.011319

Arias-Arias J.L., Mora-Rodríguez R., 2021. Generation and implementation of reporter BHK-21 cells for live imaging of flavivirus infection. Bio-protocol XX, X-X.

Arias-Arias, J.L., Vega-Aguilar, F., Corrales-Aguilar, E., Hun, L., Loría, G.D., Mora-Rodríguez, R., 2018. Dengue virus infection of primary human smooth muscle cells. Am. J. Trop. Med. Hyg. 99, 1451–1457. https://doi.org/10.4269/ajtmh.18-0175

Atchison, R.W., Ordonez, J. V., Sather, G.E., Hammon, W.M., 1966. Fluorescent antibody, complement fixation method for detection of dengue viruses in mice. J. Immunol. 96, 936–943.

Bakonyi, T., Lussy, H., Weissenböck, H., Hornyák, Á., Nowotny, N., 2005. In vitro host-cell susceptibility to usutu virus. Emerg. Infect. Dis. 11, 298–301. https://doi.org/10.3201/eid1102.041016

Chiu, C.F., Chu, L.W., Liao, I.C., Simanjuntak, Y., Lin, Y.L., Juan, C.C., Ping, Y.H., 2020. The mechanism of the Zika virus crossing the placental barrier and the blood-brain barrier. Front. Microbiol. 11, 1–15. https://doi.org/10.3389/fmicb.2020.00214

Chong, M.K., Chua, A.J.S., Tan, T.T.T., Tan, S.H., Ng, M.L., 2014. Microscopy techniques in flavivirus research. Micron 59, 33–43. https://doi.org/10.1016/j.micron.2013.12.006

Chu, L.-W., 2013. Single-virus tracking approach to reveal the interaction of Dengue virus with autophagy during the early stage of infection. J. Biomed. Opt. 19, 011018. https://doi.org/10.1117/1.jbo.19.1.011018

Dulbecco, R., 1952. Production of plaques in monolayer tissue cultures by single particles of an animal virus. Proc. Natl. Acad. Sci. 38, 747–752.

Gadea, G., Bos, S., Krejbich-Trotot, P., Clain, E., Viranaicken, W., El-Kalamouni, C., Mavingui, P., Desprès, P., 2016. A robust method for the rapid generation of recombinant Zika virus expressing the GFP reporter gene. Virology 497, 157–162. https://doi.org/10.1016/j.virol.2016.07.015

Garg, H., Mehmetoglu-Gurbuz, T., Joshi, A., 2020. Virus Like Particles (VLP) as multivalent vaccine candidate against Chikungunya, Japanese Encephalitis, Yellow Fever and Zika Virus. Sci. Rep. 10, 1–13. https://doi.org/10.1038/s41598-020-61103-1

Garg, H., Sedano, M., Plata, G., Punke, E.B., Joshi, A., 2017. Development of virus-like-particle vaccine and reporter assay for Zika virus. J. Virol. 91, 1–16. https://doi.org/10.1128/jvi.00834-17

Göertz, G.P., Vogels, C.B.F., Geertsema, C., Koenraadt, C.J.M., Pijlman, G.P., 2017. Mosquito co-infection with Zika and chikungunya virus allows simultaneous transmission without affecting vector competence of Aedes aegypti. PLoS Negl. Trop. Dis. 11, 1–22. https://doi.org/10.1371/journal.pntd.0005654

Gould, E., Solomon, T., 2008. Pathogenic flaviviruses. Lancet 371, 500–509. https://doi.org/https://doi.org/10.1016/S0140-6736(08)60238-X

Hirano, M., Muto, M., Sakai, M., Kondo, H., Kobayashi, S., Kariwa, H., Yoshii, K., 2017. Dendritic transport of tick-borne flavivirus RNA by neuronal granules affects development of neurological disease. Proc. Natl. Acad. Sci. U. S. A. 114, 9960–9965. https://doi.org/10.1073/pnas.1704454114

Hoffmann, A.B., Mazelier, M., Léger, P., Lozach, P.Y., 2018. Deciphering virus entry with fluorescently labeled viral particles. Methods Mol. Biol. 1836, 159–183. https://doi.org/10.1007/978-1-4939-8678-1_8

Hou, W., Armstrong, N., Obwolo, L.A., Thomas, M., Pang, X., Jones, K.S., Tang, Q., 2017. Determination of the cell permissiveness spectrum, mode of RNA replication, and RNA-protein interaction of Zika virus. BMC Infect. Dis. 17, 1–12. https://doi.org/10.1186/s12879-017-2338-4

Hsieh, M.-S., Chen, M.-Y., Hsieh, C.-H., Pan, C.-H., Yu, G.-Y., Chen, H.-W., 2017. Detection and quantification of dengue virus using a novel biosensor system based on dengue

NS3 protease activity. PLoS One 12, 1–19. https://doi.org/https://doi.org/10.1371/journal.pone.0188170

Hung, C.Y., Tsai, M.C., Wu, Y.P., Wang, R.Y.L., 2011. Identification of heat-shock protein 90 beta in Japanese encephalitis virus-induced secretion proteins. J. Gen. Virol. 92, 2803–2809. https://doi.org/10.1099/vir.0.033993-0

Jia, F., Zhu, X., Xu, F., 2016. A single adaptive point mutation in Japanese encephalitis virus capsid is sufficient to render the virus as a stable vector for gene delivery. Virology 490, 109–118. https://doi.org/10.1016/j.virol.2016.01.001

Jones, C.T., Patkar, C.G., Kuhn, R.J., 2005. Construction and applications of yellow fever virus replicons. Virology 331, 247–259. https://doi.org/10.1016/j.virol.2004.10.034

Kato, F., Hishiki, T., 2016. Dengue virus reporter replicon is a valuable tool for antiviral drug discovery and analysis of virus replication mechanisms. Viruses 8, 1–11. https://doi.org/10.3390/v8050122

Kümmerer, B.M., 2018. Establishment and application of flavivirus replicons, in: Caputo, A.T., Alonzi, D.S., Kiappes, J.L., Struwe, W.B., Cross, A., Basu, S., Darlot, B., Roversi, P. (Eds.), Dengue and Zika: Control and Antiviral Treatment Strategies. Springer, pp. 165–173. https://doi.org/https://doi.org/10.1007/978-981-10-8727-1_12

Lai, C.-Y., Tsai, W.-Y., Lin, S.-R., Kao, C.-L., Hu, H.-P., King, C.-C., Wu, H.-C., Chang, G.-J., Wang, W.-K., 2008. Antibodies to envelope glycoprotein of dengue virus during the natural course of infection are predominantly cross-reactive and recognize epitopes containing highly conserved residues at the fusion loop of domain II. J. Virol. 82, 6631–6643. https://doi.org/10.1128/jvi.00316-08

Ledizet, M., Kar, K., Foellmer, H.G., Bonafé, N., Anthony, K.G., Gould, L.H., Bushmich, S.L., Fikrig, E., Koski, R.A., 2007. Antibodies targeting linear determinants of the envelope protein protect mice against West Nile virus. J. Infect. Dis. 196, 1741–1748. https://doi.org/10.1086/523654

Li, S.H., Li, X.F., Zhao, H., Deng, Y.Q., Yu, X.D., Zhu, S.Y., Jiang, T., Ye, Q., Qin, E. De, Qin, C.F., 2013. Development and characterization of the replicon system of Japanese encephalitis live vaccine virus SA14-14-2. Virol. J. 10, 1–6.

https://doi.org/10.1186/1743-422X-10-64

Li, W., Ma, L., Guo, L.P., Wang, X.L., Zhang, J.W., Bu, Z.G., Hua, R.H., 2017. West Nile virus infectious replicon particles generated using a packaging-restricted cell line is a safe reporter system. Sci. Rep. 7, 1–10. https://doi.org/10.1038/s41598-017-03670-4

Lindenbach, B., Thiel, H.-J., Rice, C.M., 2007. Flaviviridae: The viruses and their replication, in: Fields Virology. pp. 1101–1152.

Lindquist, M.E., Schmaljohn, C.S., 2018. Intracellular detection of viral transcription and replication using RNA FISH, in: Salvato, M.S. (Ed.), Hemorrhagic Fever Viruses: Methods and Protocols. Springer, pp. 201–207. https://doi.org/10.1007/978-1-4939-6981-4

Liu, D., Tedbury, P.R., Lan, S., Huber, A.D., Puray-Chavez, M.N., Ji, J., Michailidis, E., Saeed, M., Ndongwe, T.P., Bassit, L.C., Schinazi, R.F., Ralston, R., Rice, C.M., Sarafianos, S.G., 2019. Visualization of positive and negative sense viral RNA for probing the mechanism of direct-acting antivirals against Hepatitis C virus. Viruses 11. https://doi.org/10.3390/v11111039

Lu, C.Y., Hour, M.J., Wang, C.Y., Huang, S.H., Mu, W.X., Chang, Y.C., Lin, C.W., 2017. Single-round infectious particle antiviral screening assays for the Japanese encephalitis virus. Viruses 9, 1–16. https://doi.org/10.3390/v9040076

Makino, Y., Suzuki, T., Hasebe, R., Kimura, T., Maeda, A., Takahashi, H., Sawa, H., 2014. Establishment of tracking system for West Nile virus entry and evidence of microtubule involvement in particle transport. J. Virol. Methods 195, 250–257. https://doi.org/10.1016/j.jviromet.2013.10.002

Martinez-Lopez, A., Persaud, M., Chavez, M.P., Zhang, H., Rong, L., Liu, S., Wang, T.T., Sarafianos, S.G., Diaz-Griffero, F., 2019. Glycosylated diphyllin as a broad-spectrum antiviral agent against Zika virus. EBioMedicine 47, 269–283. https://doi.org/10.1016/j.ebiom.2019.08.060

Martins, L.C., Da Silva, E.V.P., Casseb, L.M.N., Da Silva, S.P., Cruz, A.C.R., De Sousa Pantoja, J.A., De Almeida Medeiros, D.B., Filho, A.J.M., Da Cruz, E.D.R.M., De Araújo, M.T.F., Cardoso, J.F., Da Cunha, M.A.C.R., Almada, G.L., Romano, A.P.M., Santos, M.G.D.P., Rodrigues, G.A.P., Chiang, J.O., Quaresma, J.A.S., Carvalho, V.L., Da Costa Vasconcelos,

P.F., 2019. First isolation of west nile virus in brazil. Mem. Inst. Oswaldo Cruz 114, 1–7. https://doi.org/10.1590/0074-02760180332

Mattia, K., Puffer, B.A., Williams, K.L., Gonzalez, R., Murray, M., Sluzas, E., Pagano, D., Ajith, S., Bower, M., Berdougo, E., Harris, E., Doranz, B.J., 2011. Dengue reporter virus particles for measuring neutralizing antibodies against each of the four dengue serotypes. PLoS One 6. https://doi.org/10.1371/journal.pone.0027252

McFadden, M.J., Mitchell-Dick, A., Vazquez, C., Roder, A.E., Labagnara, K.F., McMahon, J.J., Silver, D.L., Horner, S.M., 2018. A fluorescent cell-based system for imaging zika virus infection in real-time. Viruses 10, 13–18. https://doi.org/10.3390/v10020095

Medin, C.L., Valois, S., Patkar, C.G., Rothman, A.L., 2015. A plasmid-based reporter system for live cell imaging of dengue virus infected cells. J. Virol. Methods 211, 55–62. https://doi.org/10.1016/j.jviromet.2014.10.010

Miorin, L., Romero-Brey, I., Maiuri, P., Hoppe, S., Krijnse-Locker, J., Bartenschlager, R., Marcello, A., 2013. Three-dimensional architecture of Tick-borne encephalitis virus replication sites and trafficking of the replicated RNA. J. Virol. 87, 6469–6481. https://doi.org/10.1128/jvi.03456-12

Mutso, M., Saul, S., Rausalu, K., Susova, O., Žusinaite, E., Mahalingam, S., Merits, A., 2017. Reverse genetic system, genetically stable reporter viruses and packaged subgenomic replicon based on a Brazilian zika virus isolate. J. Gen. Virol. 98, 2712–2724. https://doi.org/10.1099/jgv.0.000938

Nour, A.M., Li, Y., Wolenski, J., Modis, Y., 2013. Viral membrane fusion and nucleocapsid delivery into the cytoplasm are distinct events in some flaviviruses. PLoS Pathog. 9. https://doi.org/10.1371/journal.ppat.1003585

Pang, X., Zhang, M., Dayton, A.I., 2001. Development of Dengue virus type 2 replicons capable of prolonged expression in host cells. BMC Microbiol. 1, 1–7. https://doi.org/10.1186/1471-2180-1-18

Pierson, T.C., Diamond, M.S., 2020. The continued threat of emerging flaviviruses. Nat. Microbiol. 5, 736–812. https://doi.org/10.1038/s41564-020-0714-0

Pierson, T.C., Diamond, M.S., Ahmed, A.A., Valentine, L.E., Davis, C.W., Samuel, M.A.,

Hanna, S.L., Puffer, B.A., Doms, R.W., 2005. An infectious West Nile virus that expresses a GFP reporter gene. Virology 334, 28–40. https://doi.org/10.1016/j.virol.2005.01.021

Pierson, T.C., Sánchez, M.D., Puffer, B.A., Ahmed, A.A., Geiss, B.J., Valentine, L.E., Altamura, L.A., Diamond, M.S., Doms, R.W., 2006. A rapid and quantitative assay for measuring antibody-mediated neutralization of West Nile virus infection. Virology 346, 53–65. https://doi.org/10.1016/j.virol.2005.10.030

Raquin, V., Wannagat, M., Zouache, K., Legras-Lachuer, C., Moro, C.V., Mavingui, P., 2012. Detection of dengue group viruses by fluorescence in situ hybridization. Parasites and Vectors 5, 1. https://doi.org/10.1186/1756-3305-5-243

Ricciardi-Jorge, T., Bordignon, J., Koishi, A., Zanluca, C., Mosimann, A.L., Duarte Dos Santos, C.N., 2017. Development of a quantitative NS1-capture enzyme-linked immunosorbent assay for early detection of yellow fever virus infection. Sci. Rep. 7, 1–9. https://doi.org/10.1038/s41598-017-16231-6

Roby, J.A., Pijlman, G.P., Wilusz, J., Khromykh, A.A., 2014. Noncoding subgenomic flavivirus RNA: Multiple functions in West Nile virus pathogenesis and modulation of host responses. Viruses 6, 404–427. https://doi.org/10.3390/v6020404

Rothan, H.A., Kumar, M., 2019. Role of endoplasmic reticulum-associated proteins in flavivirus replication and assembly complexes. Pathogens 8. https://doi.org/10.3390/pathogens8030148

Rudkin, G.T., Stollar, B.D., 1977. High resolution detection of DNA-RNA hybrids in situ by indirect immunofluorescence. Nature 265, 472–473. https://doi.org/10.1038/265472a0

Růžek, D., Vancová, M., Tesařová, M., Ahantarig, A., Kopecký, J., Grubhoffer, L., 2009. Morphological changes in human neural cells following Tick-borne encephalitis virus infection. J. Gen. Virol. 90, 1649–1658. https://doi.org/10.1099/vir.0.010058-0

Sakin, V., Paci, G., Lemke, E.A., Müller, B., 2016. Labeling of virus components for advanced, quantitative imaging analyses. FEBS Lett. 590, 1896–1914. https://doi.org/10.1002/1873-3468.12131

Schmid, B., Rinas, M., Ruggieri, A., Acosta, E.G., Bartenschlager, M., Reuter, A., Fischl, W.,

Harder, N., Bergeest, J.P., Flossdorf, M., Rohr, K., Höfer, T., Bartenschlager, R., 2015. Live cell analysis and mathematical modeling identify determinants of attenuation of dengue virus 2'-O-methylation mutant. PLoS Pathog. 11, 1–36.

Schoggins, J.W., Dorner, M., Feulner, M., Imanaka, N., Murphy, M.Y., Ploss, A., Rice, C.M., 2012. Dengue reporter viruses reveal viral dynamics in interferon receptor-deficient mice and sensitivity to interferon effectors in vitro. Proc. Natl. Acad. Sci. U. S. A. 109, 14610–14615. https://doi.org/10.1073/pnas.1212379109

Sheng, Z.Y., Gao, N., Wang, Z.Y., Cui, X.Y., Zhou, D.S., Fan, D.Y., Chen, H., Wang, P.G., An, J., 2017. Sertoli cells are susceptible to ZIKV infection in mouse testis. Front. Cell. Infect. Microbiol. 7, 1–13. https://doi.org/10.3389/fcimb.2017.00272

Shi, P.Y., Tilgner, M., Lo, M.K., 2002. Construction and characterization of subgenomic replicons of New York strain of West Nile virus. Virology 296, 219–233. https://doi.org/10.1006/viro.2002.1453

Sinigaglia, L., Gracias, S., Décembre, E., Fritz, M., Bruni, D., Smith, N., Herbeuval, J.P., Martin, A., Dreux, M., Tangy, F., Jouvenet, N., 2018. Immature particles and capsid-free viral RNA produced by Yellow fever virus-infected cells stimulate plasmacytoid dendritic cells to secrete interferons. Sci. Rep. 8, 1–15. https://doi.org/10.1038/s41598-018-29235-7

Slon Campos, J.L., Poggianella, M., Marchese, S., Mossenta, M., Rana, J., Arnoldi, F., Bestagno, M., Burrone, O.R., 2017. DNA-immunisation with dengue virus E protein domains I/II, but not domain III, enhances Zika, West Nile and yellow fever virus infection. PLoS One 12, 1–19. https://doi.org/10.1371/journal.pone.0181734

Suphatrakul, A., Duangchinda, T., Jupatanakul, N., Prasittisa, K., Onnome, S., Pengon, J., Siridechadilok, B., 2018. Multi-color fluorescent reporter dengue viruses with improved stability for analysis of a multi-virus infection. PLoS One 13, 1–19. https://doi.org/10.1371/journal.pone.0194399

Usme-Ciro, J.A., Lopera, J.A., Alvarez, D.A., Enjuanes, L., Almazán, F., 2017. Generation of a DNA-launched reporter replicon based on Dengue virus type 2 as a multipurpose platform. Intervirology 59, 275–282. https://doi.org/10.1159/000476066

Velado Fernández, I., Okamoto, N., Ito, A., Fukuda, M., Someya, A., Nishino, Y., Sasaki, N., Maeda, A., 2014. Development of a novel protocol for generating flavivirus reporter particles. J. Virol. Methods 208, 96–101. https://doi.org/10.1016/j.jviromet.2014.08.002

Vyboh, K., Ajamian, L., Mouland, A.J., 2012. Detection of viral RNA by fluorescence in situ hybridization (FISH). J. Vis. Exp. 2–6. https://doi.org/10.3791/4002

Westaway, E.G., Mackenzie, J.M., Kenney, M.T., Jones, M.K., Khromykh, A.A., 1997. Ultrastructure of Kunjin virus-infected cells: colocalization of NS1 and NS3 with double-stranded RNA, and of NS2B with NS3, in virus-induced membrane structures. J. Virol. 71, 6650–6661. https://doi.org/10.1128/jvi.71.9.6650-6661.1997

Wu, P., Nicholls, S.B., Hardy, J.A., 2013. A Tunable, modular approach to fluorescent protease-activated reporters. Biophys. J. 104, 1605–1614. https://doi.org/10.1016/j.bpj.2013.01.058

Yoshii, K., Ikawa, A., Chiba, Y., Omori, Y., Maeda, J., Murata, R., Kariwa, H., Takashima, I., 2009. Establishment of a neutralization test involving reporter gene-expressing virus-like particles of tick-borne encephalitis virus. J. Virol. Methods 161, 173–176. https://doi.org/10.1016/j.jviromet.2009.05.016

Zhang, S., Tan, C., Ooi, E., 2011. Visualizing dengue virus through Alexa Fluor labeling. J. Vis. Exp. 8–11. https://doi.org/10.3791/3168

Zhang, S.L.X., Tan, H.C., Hanson, B.J., Ooi, E.E., 2010. A simple method for Alexa Fluor dye labelling of dengue virus. J. Virol. Methods 167, 172–177. https://doi.org/10.1016/j.jviromet.2010.04.001

Zuza, A.L., Barros, H.L.S., de Mattos Silva Oliveira, T.F., Chávez-Pavoni, J.H., Zanon, R.G., 2016. Astrocyte response to St. Louis encephalitis virus. Virus Res. 217, 92–100. https://doi.org/10.1016/j.virusres.2016.03.005